STRESS AND STRAIN CONCENTRATION FACTORS

OF

WELDED MULTIPLANAR TUBULAR JOINTS

STRESS AND STRAIN CONCENTRATION FACTORS

OF

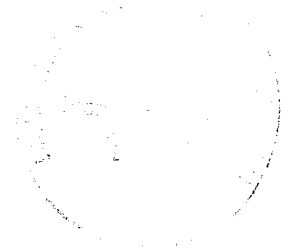# WELDED MULTIPLANAR TUBULAR JOINTS

PROEFSCHRIFT

ter verkrijging van de graad van doctor
aan de Technische Universiteit Delft,
op gezag van de Rector Magnificus Prof. Ir. K.F. Wakker,
in het openbaar te verdedigen ten overstaan van een commissie,
door het College van Dekanen aangewezen,
op maandag 14 november 1994 te 13.30 uur

door

Arie ROMEIJN

HBO-ingenieur (weg- en waterbouwkunde)

geboren te Hardinxveld-Giessendam

Dit proefschrift is goedgekeurd door de promotor:
Prof.dr.ir. J. Wardenier

NON-UNIFORM STRESS DISTRIBUTION: axial force on horizontal brace member

STRESS : VON MISES

ACKNOWLEDGEMENTS

KEYWORDS

Welded tubular joint, Joint flexibility, Lattice girder, Numerical modelling, Fatigue, Hot spot stress, Uniplanar, Multiplanar, Stress (strain) concentration factor.

CONTENTS

ABSTRACT

Circular hollow sections are frequently used in structures subjected to fatigue loading such as bridges, offshore structures and cranes. These sections are generally connected by direct welding of the sections to each other. For the design of these welded connections, information is required on the fatigue behaviour. Especially for multiplanar connections, insufficient data is available regarding stress concentration factors (SCFs) which affect the fatigue life.

Also, there is no standard for determining the fatigue strength of welded tubular joints. This has led to a divergence in the methods being used both experimentally as well as numerically.

This thesis presents the results of experimental and numerical research on the fatigue strength of welded tubular joints. Also, results on tubular joint flexibility behaviour, which affects the load distribution (hot spot stresses) and deflection is presented.

The work has been carried out in the framework of:

-   A STW sponsored numerical research project entitled:

    "Numerical and experimental investigation for the stress concentration factors of welded tubular joints". (STW Nr. DCT 80-1457).

For the calibration of the numerical models, use is made of:

-   An ECSC sponsored experimental research project entitled:

    "Fatigue behaviour of multiplanar welded hollow section joints and reinforcements measures for repair". (CECA Convention Nr. 7210-SA/114).

Additional work is sponsored by Cidect in the programme entitled:

    "7A: Fatigue strength of multiplanar welded unstiffened CHS and RHS joints".

The research projects aim to provide guidelines and design recommendations on the fatigue strength of welded tubular joints, to be proposed for inclusion in international codes of practice such as Eurocode 3.
The numerical work mainly consist of an investigation on:

-   *Modelling of tubular joint flexibility.*
-   *Modelling of tubular joints for the determination of stress concentration factors.*
-   *Modelling of multiplanar triangular lattice structures.*
-   *Calibration of numerical results with experimental results.*

- *The development of a standard for determining stress concentration factors.*
- *Determination of SCFs and SNCFs at weld toes for a large range of joint parameters on T, Y, K, X, TT, KK and XX joints. Because of the enormous amount of data obtained, the results of SCFs and SNCFs are stored in data files. SCF and SNCF results for reference as well as carry-over effects, independent of the boundary conditions used, are given for both brace and chord member loads using FE models with the weld shape included.*
- *The influence of the presence of a carry-over brace member on SCFs due to reference loading.*
- *The importance of carry-over effects on SCFs.*
- *The relationship between SCF and SNCF.*

The experimental work consist of an investigation on:

- *The load distribution, hot spot stresses and deflection of multiplanar triangular lattice girders.*
- *The fatigue behaviour of multiplanar KK joints which form part of the multiplanar triangular lattice girders tested.*

5

NOTATION

$$\alpha = \frac{2 \cdot L_{chord}}{d_0}$$

$$\beta = \frac{d_1}{d_0}$$

$$\gamma = \frac{d_0}{2 \cdot t_0}$$

$$\tau = \frac{t_1}{t_0}$$
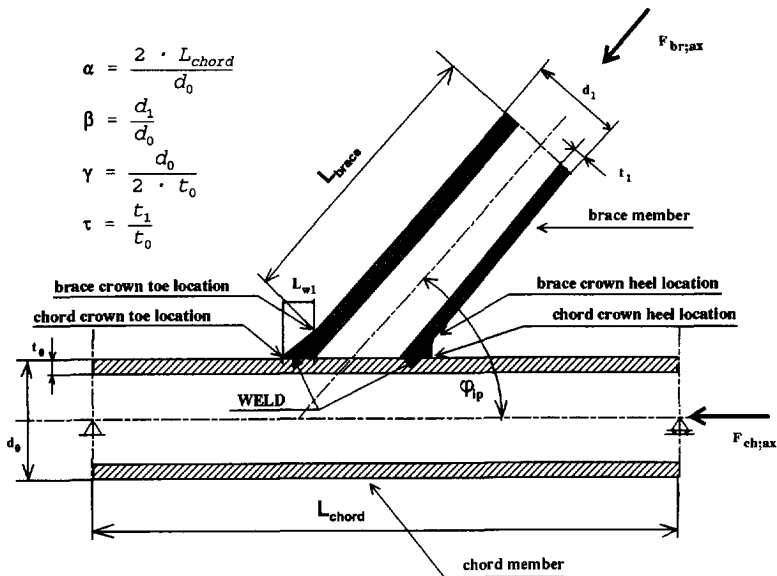
Figure 1.   Welded tubular joint.

A	Cross sectional area of member considered.
D_d	Linear damage calculation by "Palmgren-Miner" summation.
E	Youngs modulus of elasticity (E_{steel} = 2.068·10^5 N/mm^2).
F	Girder load or axial load on a member.
$F_{br;ax;a}$	Axial load on brace member 'a'.
$F_{br;ax;a,b}$	Axial load on brace members 'a' and *b* .
$F_{ch;ax}$	Axial load on chord member.
F_r	Girder load range.
I	Moment of inertia of member or girder considered.
$K_{br;ax}$	Brace member stiffness: axial stiffness term.
$K_{m;ax}$	Member stiffness: axial stiffness term.
K_{ii}	Joint stiffness: spring diagonal term.
K_{ij}	Joint stiffness: spring diagonal or cross term.
$K_{ii;ax}$	Joint stiffness: axial spring diagonal term.
L	Length of member considered.
L_{w1}	Length of weld footprint on chord member: *weld footprint length alternative 1.*
M	Bending moment or torsional moment on a member.
$M_{br;ip;a}$	In-plane bending moment on brace member 'a'.
$M_{br;ip;a,b}$	In-plane bending moment on brace members 'a' and *b* .
$M_{br;t;a}$	Torsional moment on brace member 'a'.
$M_{ch;ip}$	In-plane bending moment on chord member.

M_1	Numerical idealization of a lattice girder: *idealization method 1*.
N	Number of cycles.
N_f	Number of cycles to failure (through-thickness cracking).
N_f^*	Number of cycles to failure (through-thickness cracking) after repairing determined by inspection.
N_{ini}	Number of cycles to initiation of cracks determined by strain gauge measurements.
N_i	Number of cycles of design stress range causing failure in the design fatigue resistance S-N curve.
R	Stress ratio $\sigma_{min} / \sigma_{max}$ in a cycle for constant amplitude loading.
$SCF_{ch;ax}$	Stress concentration factor for an axial load on the chord member.
$S_{r_{h.s.}}$	Hot spot stress range: $S_{r_{h.s.}} = SCF \cdot \sigma_r = SCF \cdot (\sigma_{max} - \sigma_{min})$.
S_1	Lattice girder: *analysed girder 1*.
SR_{ax}	Joint stiffness ratio: $SR_{ax} = K_{ii;ax} / K_{m;ax}$.
W	Elastic section modulus of member considered.
a	Weld throat thickness.
bdc_1	Boundary condition of an isolated joint: *boundary condition method 1*.
cpu	Computation time.
ds	Disk space occupied.
d_0	External diameter of chord member.
d_{1-4}	External diameter of brace members 1-4.
e	Eccentricity in uniplanar plane.
$e_{m.p.}$	Eccentricity in multiplanar plane.
f_u	Ultimate stress of member considered.
f_y	Yield stress of member considered.
g	Gap in uniplanar plane between individual braces.
g^*	Gap in uniplanar plane between the weld toes of individual braces.
$g_{m.p.}$	Gap in multiplanar plane between individual braces.
$g_{m.p.}^*$	Gap in multiplanar plane between the weld toes of individual braces.
i	Radius of gyration.
int_1	Integration scheme of an element: *integration scheme method 1*.
l_k	Buckling length.
$l_{r;min}$	Extrapolation region: minimum distance from the weld toe.
$l_{r;max}$	Extrapolation region: maximum distance from the weld toe.
mf_1	Mesh refinement: *alternative 1*.
n_i	Number of cycles of design stress range in load spectrum block i.
o_v	Overlap in uniplanar plane.
snf	Conversion factor: *snf* = SCF/SNCF.
r_0	External radius of chord member.
r_{1-4}	External radius of brace members 1-4.
t_0	Wall thickness of chord member.
t_{1-4}	Wall thickness of brace members 1-4.
α	Chord length to half chord diameter ratio: $\alpha = 2L / d_0$.
α_M	Multiplication factor: $\alpha_M = \delta_{tot} / \delta_i$.
α_{br}	Brace strain ratio: $\alpha_{br} = \epsilon_{h.s.;tot} / \epsilon_{h.s.;ax}$.
β	Brace to chord diameter ratio: $\beta = d_1 / d_0$.

ΔK	Stress intensity factor.
τ	Brace to chord wall thickness ratio: $\tau = t_1 / t_0$.
γ	Radius to wall thickness ratio of chord member: $\gamma = d_0 / (2 \cdot t_0)$.
γ_m	Partial safety factor.
δ_i	Initial deflection (excl. contribution caused by joint flexibility).
δ_{tot}	Total deflection (incl. contribution caused by joint flexibility).
$\epsilon_{ch;ax}$	Nominal axial strain in chord member.
$\epsilon_{h.s.;tot}$	Total hot spot strain (at a fixed weld toe location).
ϵ_r	Nominal strain range.
ϵ_{tot}	Total nominal strain: $\epsilon_{tot} = \epsilon_{extrap;nom} = \epsilon_{axial;nom} \pm \sqrt{\epsilon^2_{extrap;ipb} + \epsilon^2_{extrap;opb}}$.
$\epsilon_{tot;num}$	Total nominal strain obtained from numerical work.
ϵ_y	Strain measured in a direction parallel to the weld toe (chord outerwall surface), or along the brace member perpendicular to the axis of the brace member (brace outerwall surface).
λ	Slenderness of member considered: $\lambda = l_k / i$.
σ	Standard deviation.
$\sigma_{ch;ax}$	Nominal axial stress in chord member.
$\sigma_{h.s.tot}$	Total hot spot stress (or geometric stress).
σ_{max}	Maximum nominal stress in a constant amplitude loading cycle.
σ_{min}	Minimum nominal stress in a constant amplitude loading cycle.
σ_{nom}	Nominal stress.
σ_r	Nominal stress range.
φ_{ip}	Smallest in-plane angle between chord and brace member. (Measured along the chord axis: uniplanar plane).
φ_{op}	Smallest out-of-plane angle between two brace members. (Measured perpendicular to the chord axis: multiplanar plane).
v	Poison ratio: $v_{steel} = 0.30$.

SUBSCRIPTS

ax	Axial.
b(e)	Joint modelled with beam elements.
br	Brace member.
ch	Chord member.
exp	Experimental.
extrap	Extrapolation along a specified distance.
h.s.	Hot spot.
i	Row number of the matrix considered.
ip(b)	In-plane (bending).
j	Column number of the matrix considered.
nom	Nominal.
num	Numerical.
op(b)	Out-of-plane (bending).
s	Joint modelled with shell and/or solid elements.
x,y,z	Specified directions related to a given coordinate system.

8

chord saddle: cs;7

chord inbetween: ci;6

chord outer wall surface

chord inbetween: ci;8

chord crown heel: cc;1

chord crown toe: cc;5

chord inbetween: ci;2

chord inbetween: ci;4

chord saddle: cs;3

chord member

brace member

brace saddle: bs;7

brace inbetween: bi;6

brace inbetween: bi;8

brace crown heel: bc;1

brace crown toe: bc;5

brace outer wall surface

brace inbetween: bi;2

brace inbetween: bi;4

brace saddle: bs;3

Figure 2. Locations of interest on stress and strain concentration factors.
          Top figure: chord member locations; bottom figure: brace member locations.

9

Fixed weld toe locations (see figure 2).

cc;1   Chord crown heel.
ci;2   Chord inbetween crown heel and saddle (largest out-of-plane gap region).
cs;3   Chord saddle (largest out-of-plane gap region).
ci;4   Chord inbetween saddle and crown toe (largest out-of-plane gap region).
cc;5   Chord crown toe.
ci;6   Chord inbetween crown heel and saddle (smallest out-of-plane gap region).
cs;7   Chord saddle (smallest out-of-plane gap region).
ci;8   Chord inbetween saddle and crown toe (smallest out-of-plane gap region).

Brace members (see also figures 6 and 7).

'a' or (1)   Reference brace member.
 b or (2)   Out-of-plane carry-over brace member.
 c or (3)   In-plane carry-over brace member.
 d or (4)   Out-of-plane carry-over brace member.

ACRONYMS

API   American Petroleum Institute.
AWS   American Welding Society.
CHS   Circular (Tubular) Hollow Section.
CIDECT   Comité International pour le Développement et l'Étude de la Construction Tubulaire.
CISC   Canadian Institute of Steel Construction.
DEn   Department of Energy (UK).
ECSC   European Coal and Steel Community.
EC3   Eurocode No. 3.
FE   Finite Element.
FM   Fracture Mechanics.
HSE   Health and Safety Executive.
IIW   International Institute of Welding.
NAFEMS   National Agency for Finite Element Methods and Standards.
RHS   Rectangular Hollow Section.
SCF   Stress concentration factor.
SNCF   Strain concentration factor.
STW   Netherlands Technology Foundation.
UEG   Underwater Engineering Group.

10

1.   INTRODUCTION

1.1   *The use of circular hollow sections*

In nature it is shown that circular hollow sections are excellent structural elements. Their use offer many advantages over open structural sections such as I-beams because of:

- *Equal bending strength and stiffness in all directions.*
- *High strength-to-weight ratio.*
- *Low drag coefficient and shape factor.*
- *Possible use of internal void (buoyancy, transport, filling with concrete, etc.).*

Furthermore, compared to the open structural sections, the circular hollow sections offer an excellent profile for:

- *Resistance against buckling in all directions.*
- *Environmental corrosion protection.*
- *Fire resistance (water or concrete filling).*
- *Composite steel-concrete members.*
- *An economical construction (direct welded connection of members avoiding expensive stiffeners or gusset plates).*

In addition, the closed curved shape of circular hollow sections offers architecturally pleasing features making them increasingly popular, and for the near future, it is expected that the use of circular hollow sections will increase also because of robot welding, which makes the fabrication of the joints less labour intensive.

Circular hollow sections are frequently used in *bridges, offshore structures, cranes, amusement parks, agriculture* and *mechanical engineering.*
These types of structures however, are generally subjected to fatigue loading, which requires knowledge on the fatigue strength of the joints between the tubular members in the structure.

The welded circular joints constitute the structural elements in a lattice girder, formed by the hollow sections identified as brace and chord members.
The non-uniform stiffness around the perimeter of the brace to chord intersection results in a geometrical non-uniform stress distribution, which may be unfavourable in case of fatigue loading. The non-uniform stress distribution depends on the type of loading (axial, bending in plane, bending out of plane and torsion) and the connection (types and geometry). Thus many cases exist.
Therefore, the fatigue behaviour of welded tubular joints is treated in a different way than for example for welded connections between plates.

11

1.2   *Research objectives*

The fatigue behaviour of welded tubular joints can be determined either by σ_r - N methods or with a fracture mechanics (FM) approach.

- The various σ_r - N methods are based on experiments, resulting in $S_{r_{h.s.}}$ - N_f curves with a defined hot spot stress range also called geometric stress range on the vertical axis and the number of cycles N_f to a specified failure criterion on the horizontal axis.
The advantage of a σ_r - N method, so-called hot spot stress method, is that all types of welded tubular joints are related to the same $S_{r_{h.s.}}$ - N_f curve by the stress concentration factors (SCFs), which depend on the global connection geometry and loading.

- The FM approach is based on a fatigue crack growth model. The material crack growth parameters of the model can be determined from standardized small specimens and the influence of the connection geometry is incorporated in the stress intensity factor ΔK.

This thesis deals with the σ_r - N methods

The design of welded uniplanar tubular joints by means of $S_{r_{h.s.}}$ - N_f curves and parametric formulae for determining SCFs is implemented in the different design codes like API [F1], AWS [F2], IIW [F22], DEn [F9] and EC3 [F12].
However, the work carried out so far on uniplanar joints has some major drawbacks. This is because of:

- *Fairly "open" guidelines on how the hot spot stresses should be determined.*
- *Assumptions are made for converting experimentally measured hot spot strains into hot spot stresses for use in fatigue design $S_{r_{h.s.}}$ - N_f curves, by the use of a constant average conversion factor of snf = 1.2 .*
- *Large variations in the predicted SCFs can occur depending on the parametric formulae adopted [F26], and many design codes do not specify which formulae to use.*

Furthermore, SCF parametric formulae for uniplanar joints obtained from numerical work, mainly cover:

- *The use of FE models where the shape of the weld is not included. This has been found to give large differences, particularly for the brace member locations. (This problem also exists for SCF parametric formulae obtained from experimentally*

*tested small acrylic models where the weld shape is not inclu-
ded).*

- *The use of principal stresses instead of stresses in a direction
  perpendicular to the weld toe (chord member locations) and
  parallel to the axis of the brace member (brace member locati-
  ons), which is found to be more realistic.*
- *SCFs for limited locations around the perimeter of the brace to
  chord intersection.*
- *SCFs caused by brace member loads, so that no information
  on SCFs caused by chord member loads exist. Also, no infor-
  mation exists on SCFs caused by torsional moments.*
- *SCFs, which are dependent upon the combination of boundary
  and loading conditions used. Therefore, the hot spot stresses
  caused, for instance by brace member loads in a T joint incor-
  porate the effect of bending in the chord member (the so-called
  α influence).*

For multiplanar tubular joints, which are more frequently encountered in compari-
son to uniplanar joints, only limited numerical information [*F13*] and limited experi-
mental information [*F3, F30, F47, F63*] is available.
No recommendations on fatigue design $S_{h.s.}$ - N_f curves and SCFs specifically for
these types of joints in codes exist.

The above mentioned lack of information on fatigue strength of welded tubular
joints has been the reason for setting up two projects, namely:

• A STW sponsored numerical research project entitled:

   *"Numerical and experimental investigation for the stress concentration
   factors of tubular joints"*, carried out at Delft University of Technology,
   The Netherlands.

• An ECSC sponsored experimental research project entitled:

   *"Fatigue behaviour of multiplanar welded hollow section joints and reinfor-
   cement measures for repair"*, carried out by the following partners:

The Netherlands:	-	Delft University of Technology.
	-	TNO Building and Construction Research.
Germany:	-	Mannesmannröhren-Werke A.G.
	-	Universität Karlsruhe.

Additional work is sponsored by Cidect in the programme entitled:

   *"7A: Fatigue strength of multiplanar welded unstiffened CHS and RHS
   joints"*.

The projects aim at providing guidelines and design recommendations on fatigue
strength of (unstiffened) welded tubular joints, and information on joint flexibility
behaviour. Information on joint flexibility behaviour is found to be necessary to

13

determine the correct load distribution, so that the hot spot stress range can be accurately determined.

This thesis, which mainly concerns the numerical work, contains the following four topics:

1   _**Numerical modelling of welded tubular joints.**_

-      Numerical modelling of tubular joint flexibility.
-      Numerical modelling of tubular joint stress concentration factors.

2   _**Numerical modelling of lattice structures containing welded tubular joints.**_

-      Numerical idealization of lattice structures incorporating multiplanar tubular joints with gaps and overlaps along the chord axis.
-      Calibration of numerical results with experimental results. (Deflection and load distribution).

3   _**Fatigue behaviour of multiplanar welded tubular joints in lattice girders.**_

-      Experimental investigation.
-      Calibration of numerical results with experimental results.

4   _**Parameter study on SCFs and SNCFs.**_

-      Method of SCF and SNCF determination.
-      Numerical determination of stress and strain concentration factors of unstiffened uniplanar and multiplanar welded tubular joints with a gap and having no eccentricity.
-      Calibration of numerical results with experimental results.
-      Comparison between numerical results from the parameter study and existing parametric formulae on SCFs.
-      The influence of the presence of a carry-over brace member on SCFs due to reference loading.
-      The importance of carry-over effects.
-      The relationship between SCF and SNCF.

1.3   _Definitions_

In this work, several existing as well as new definitions particularly relating to multiplanar joints are used.

14

1.3.1 Definitions related to joint stiffness

Finite Element (FE) modelled joint
The translation of a joint and its loading into a mathematical model which can be solved numerically by the use of finite elements (shell, solid, etc.), and which have geometrical and material properties and load and boundary conditions which correspond to the real behaviour of the joint in an acceptable manner.

Joint stiffness coefficient (K_{ij})
Joint stiffness coefficient (K_{ij}) is the term of a joint stiffness matrix **K** which is used as stiffness property of a spring element to be placed at the joints of structures modelled by beam elements only.
The joint stiffness (flexibility) behaviour, which affects the load distribution and deflection of such structures is taken into account by the use of these spring elements.
The joint stiffness coefficient, defined as the difference in displacements of a member end for a joint modelled with beam elements and a joint modelled with shell/solid elements, is given by the following equations:

$$K_{ij;axial} = \frac{F_i}{\delta_{i;axial,s} - \delta_{i;axial,b}} \qquad \text{and}$$

$$K_{ij;bending} = \frac{M_i}{\varphi_{i;bending;s} - \varphi_{i;bending;b}} \quad ;$$

in which the subscripts are:

i	=	The row number of the corresponding matrix.
j	=	The column number of the corresponding matrix.
b	=	A joint modelled with beam elements, which does not take the joint stiffness behaviour into account.
s	=	A joint modelled with shell and/or solid elements, which takes the joint stiffness behaviour into account.

Spring pivot term and spring cross term
The spring pivot term is a main diagonal term of the joint stiffness matrix **K**, so that i=j of K_{ij}, whereas the spring cross term is a non diagonal term with i≠j.

Stiffness ratio (SR)
The significance of joint stiffness (spring pivot terms only) on the aspects of load distribution and deflection of lattice girders is investigated by comparison of joint stiffness coefficients (K_{ij}) with stiffness coefficients K_m of the connecting brace member itself.
The stiffness ratio *SR* is defined as:

$$SR_{axial} = \frac{K_{ii;axial}}{K_{m;axial}} \qquad \text{and} \qquad SR_{bending} = \frac{K_{ii;bending}}{K_{m;bending}} \quad .$$

15

1.3.2 Definitions related to fatigue

Fatigue
For a structure subjected to fluctuating loads, because of:

- geometric peak stresses caused by the non-uniform stiffness of the welded tubular joint;
- the geometry of the weld;
- the condition at the weld toe;

micro structural changes resulting in the development of cracks are likely to occur at the weld toe locations of the joint.
The development of such cracks is identified as a fatigue phenomenon.

Fatigue life
The fatigue life of a structural component (joint) is defined as the number of load cycles N of stress or strain up to which a failure of a specified nature occurs [F58]. Various modes like *first visible crack, certain crack length, crack through the wall* and *end of test* (because of complete loss of strength) can be considered.
Nowadays, a crack through the wall so-called first through-thickness cracking is adopted as the failure criterion for welded tubular joints.

Nominal stress
The nominal stress σ_{nom} is defined as the maximum stress (linear-elastic behaviour) in a cross section of a loaded chord or brace member according to the equations:

$$\sigma_{axial,nom} = \frac{F_{axial}}{A_x} \quad , \quad \sigma_{ipb,nom} = \frac{M_{ipb}}{W_y} \quad \text{and} \quad \sigma_{opb,nom} = \frac{M_{opb}}{W_z} .$$

For the fatigue loaded multiplanar KK joints in the triangular lattice structures tested (described in chapter 5), extrapolated nominal stresses for the braces under axial tension loading are used as illustrated in figure 3, for which:

$$\sigma_{extrap,nom} = \sigma_{axial,nom} + \sqrt{\sigma^2_{extrap;ipb} + \sigma^2_{extrap,opb}}$$

16

direction extrapolation

brace under axial
tension loading

100% overlap joint

50% overlap joint

gap joint

↘ location stress measurement

● extrapolated nominal stress

● location of extrapolation
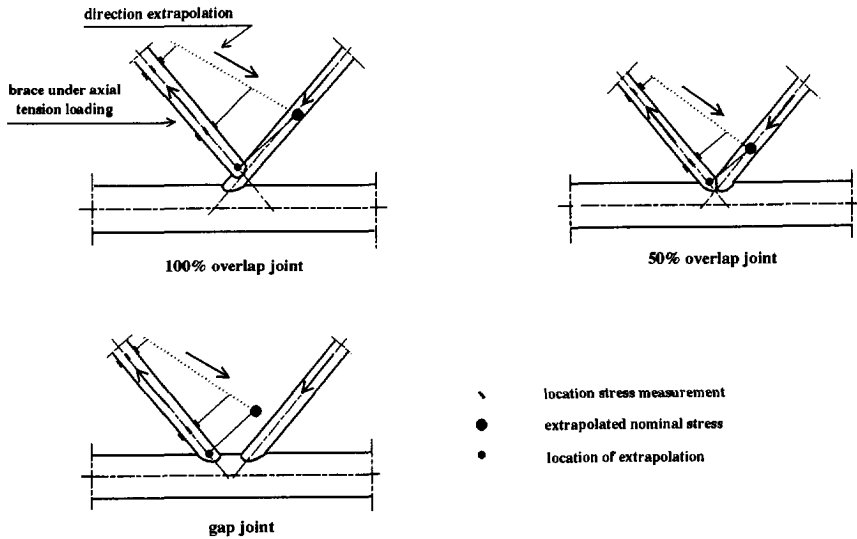
Figure 3.   Definitions of extrapolated nominal stresses $\sigma_{extrap.;nom}$ for the tested multiplanar KK joints placed inside a structure.

Stress range

The stress range σ_r, is the main parameter to be determined for fatigue analysis. In case of constant amplitude loading (see figure 4), the stress range is defined as $\sigma_r = \sigma_{max} - \sigma_{min}$.
The nominal stress range σ_r is based on nominal stresses, while the hot spot stress range $S_{r_{h.s.}}$ is based on hot spot stresses.
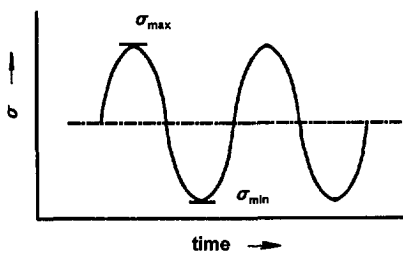
Figure 4.   Stress range for constant amplitude loading.

Stress ratio

The stress ratio R, is defined as the ratio between the minimum and maximum stress for constant amplitude loading (see also figure 4).
$R = \sigma_{min} / \sigma_{max}$:   tension is taken positive and compression as negative.

17

Hot spot stress or also called geometric stress

A hot spot is a critical point at a discontinuity, usually a weld toe location, where fatigue crack initiation is expected and joint failure starts.

The hot spot stress $\sigma_{h.s.}$ is the extrapolated stress to the weld toe, which takes the global joint geometrical effects into account only.

The definition of the hot spot stress is closely related to the choice of the fatigue design $S_{r_{h.s.}}$ - N_f curve.

A standard procedure for the determination of the hot spot stress is an extrapolation of stresses from a defined distance to the weld toe (see figure 5).

On the basis of this procedure, S-N data for tubular joints within a large range of geometries, fall within a common $S_{r_{h.s.}}$ - N_f scatterband.
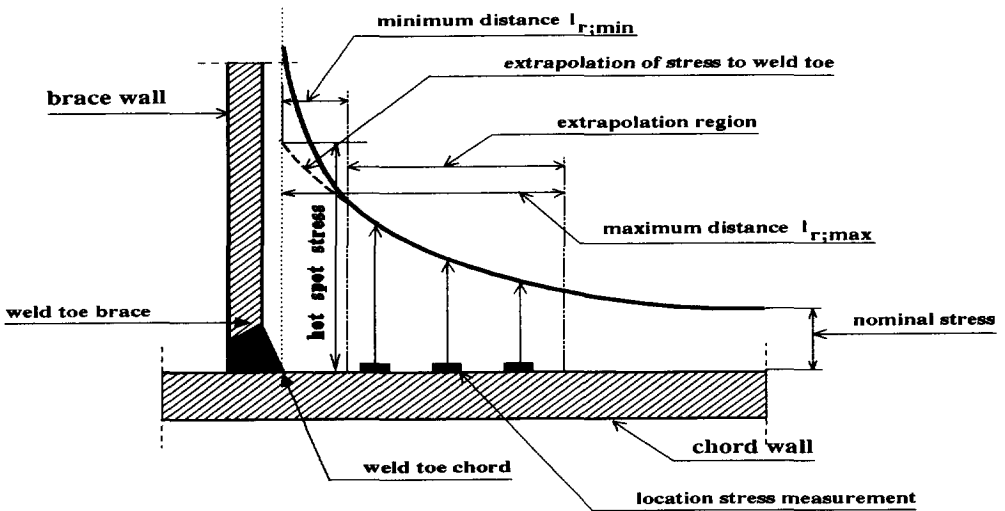
Figure 5. Definition on hot spot stress.

Extrapolation region

The extrapolation region is defined by a specified minimum and maximum distance from the weld toe of the joint (see figure 5). The region is defined in such a way that the effects of the global geometry of the weld (flat, concave, convex) and the condition at the weld toe (angle, undercut) are not included in the hot spot stress. Therefore, the first point of extrapolation should be outside the influence area of the weld.

The extrapolation region depends on the location of interest on hot spot stresses for which SCFs are determined as shown in figure 2.

The extrapolation region according to the recommendations given by ECSC WG III are summarized in table 1.

18

Table 1.   Extrapolation region (with linear extrapolation of the stresses to the weld toe) recommended by ECSC WG III [F3]. Distance l_r measured from the weld toe location in a direction perpendicular to the weld toe (chord member locations) and parallel to the axis of the brace member (brace member locations).

Chord member		Brace member
crown location (cc)	saddle location (cs)	crown location (bc) and saddle location (bs)
$l_{r;min} = 0.4 \cdot t_o$ $l_{r;min} \geq 4$ mm*		$l_{r;min} = 0.4 \cdot t_1$ $l_{r;min} \geq 4$ mm*
$l_{r;max} = 0.4 \cdot (r_1 \cdot t_1 \cdot r_0 \cdot t_0)^{1/4}$	$l_{r;max} = 5°$	$l_{r;max} = 0.65 \cdot (r_1 \cdot t_1)^{1/2}$

*   Minimum distance given by IIW.

Stress concentration factor: *(parameter study on isolated joints)*
The hot spot stresses are determined around the connection of the reference brace member '*a*' to the chord member (see figures 6 and 7). The stress concentration factor (SCF) for an isolated joint loaded individually by separate chord member loads $F_{ch;ax}$, $M_{ch;ip}$ and $M_{ch;op}$ and brace member loads $F_{br;ax}$, $M_{br;ip}$ and $M_{br;op}$ is defined as:

for the chord member loads:

$$SCF_{m.n.o} = \frac{\sigma_{h.s.;m.n.o}}{\sigma_{ch;nom;o}}$$ and

for the brace member loads:

$$SCF_{m.n.o} = \frac{\sigma_{h.s.;m.n.o}}{\sigma_{br;nom;o}}$$ with:

m   =   Chord member at the connection of brace '*a*', or brace '*a*' member.
n   =   Location around the perimeter of the brace '*a*' to chord intersection, e.g. crown, saddle or inbetween.
o   =   Type of loading (axial, in plane bending or out of plane bending).

SCFs obtained from a parameter study should be independent of the boundary condition used. Therefore, in case of brace member loads which causes bending in the chord member, to obtain the effect of brace member load only, compensating moment(s) on the chord member end(s) needs to be incorporated (see chapter 7.2.7).

19

Stress concentration factor: *(numerical calibration of tested joints placed inside a structure)*

For the multiplanar KK joints in the triangular lattice girders tested (described in chapter 5), the stress concentration factor (SCF) includes the influence of all chord and brace member loads as follows:

$$SCF_{m.n.o} = \frac{\sigma_{h.s.;m.n.o}}{\sigma_{extrap;nom}} \qquad \text{with:}$$

m	=	Chord member or a brace member.
n	=	Location around the perimeter of a brace to chord intersection, e.g. crown, saddle or inbetween.
o	=	Combination of all chord and brace member loads.
$\sigma_{extrap.;nom}$	=	Extrapolated nominal stress of the in-plane axial tensile loaded brace member (see figure 3).

Total hot spot stress based on stress concentration factors

The total hot spot stress $\sigma_{h.s.;m.n_{total}}$ for an isolated joint under combined loads at a particular location around the brace to chord connection, is defined as the superposition of the individual hot spot stress components $\sigma_{h.s.}$ according to the following equations:

$$\sigma_{h.s.;m.n_{total}} = \sigma_{h.s.;m.n_{chord\ loads}} + \sigma_{h.s.;m.n_{brace\ loads}}$$

with for the chord member loads (reference loads exist <u>only</u>):

$$\sigma_{h.s.;m.n_{chord\ loads}} = SCF_{m.n;F_{ch;ax}} \cdot \sigma_{nom;F_{ch;ax}} + SCF_{m.n;M_{ch;ip}} \cdot \sigma_{nom;M_{ch;ip}} +$$
$$SCF_{m.n;M_{ch;op}} \cdot \sigma_{nom;M_{ch;op}}$$

and for the brace member loads (reference loads and carry-over loads exist):

$$\sigma_{h.s.;m.n_{brace\ loads}} = \sum_{i=1}^{p} SCF_{m.n;F_{br;ax;i}} \cdot \sigma_{nom;F_{br;ax;i}} + SCF_{m.n;M_{br;ip;i}} \cdot \sigma_{nom;M_{br;ip;i}} +$$
$$SCF_{m.n;M_{br;op;i}} \cdot \sigma_{nom;M_{br;op;i}}$$

with:	i	=	The brace number (defined as 'a', b, c, d etc. shown in figures 6 and 7).
	p	=	The total number of connecting braces.

Joint type

Different types of welded tubular uniplanar and multiplanar gap joints are conside-
red in the parameter study on SCFs and SNCFs (chapter 7).
The joints are grouped into two parts, namely:

- *Joints with braces perpendicular to the chord axis (T, X, TT and XX joints). (See figure 6).*
- *Joints with braces inclined to the chord axis (Y, K and KK joints). (See figure 7).*
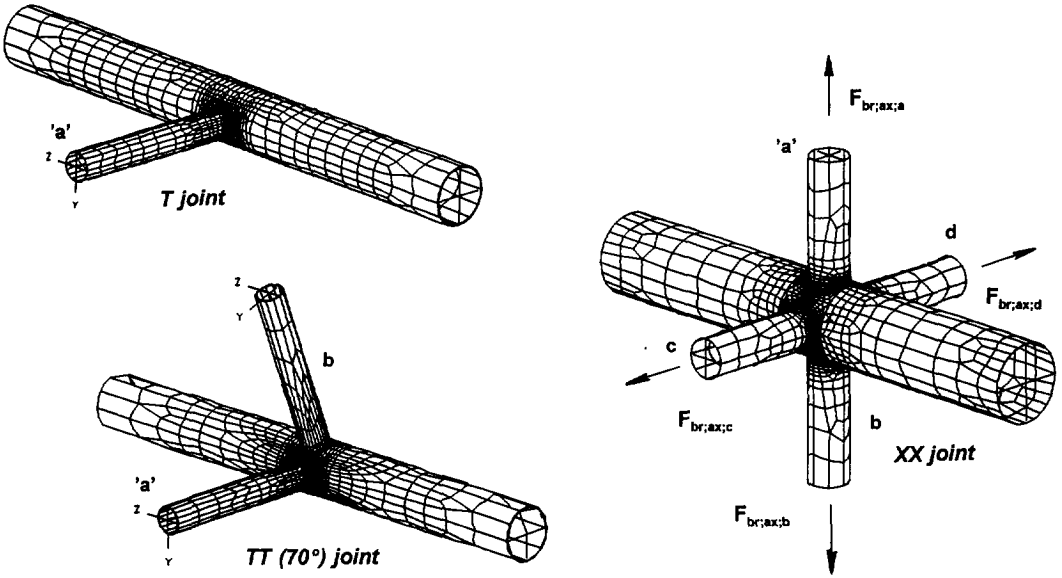
Figure 6. Joints with braces perpendicular to the chord axis.
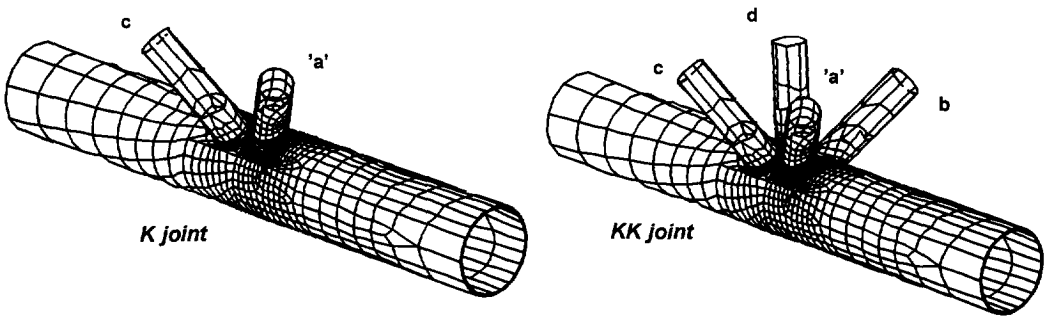
Figure 7. Joints with braces inclined to the chord axis.

21

Uniplanar joint

A uniplanar joint is a type of joint with braces lying in the same plane along the chord axis. The considered uniplanar joints are: T, Y, X also called TT (180°), K and KK (180°) joints.

The angle (180°) for the TT and KK joints given, is defined as the out-of-plane angle φ_{op}.

Multiplanar joint

A multiplanar joint is a type of joint with braces lying in different planes along the chord axis.

The considered multiplanar joints are: TT (45°, 70°, 90°, 135°), KK (60°, 90°) and XX (90°-180°-270°) joints.

Reference effect

The reference effect on SCFs is caused by:

- *Loads on the reference brace, identified as brace member 'a', i.e. SCFs due to $F_{br;ax;a}$, $M_{br;ip;a}$ and $M_{br;op;a}$.*
- *Loads on the chord member, i.e. SCFs due to $F_{ch;ax}$, $M_{ch;ip}$ and $M_{ch;op}$.*

The reference brace shown in figures 6 and 7, is the brace for which SCFs around the connection to the chord member for all load cases considered are determined.

Carry-over effect

The carry-over effect on SCFs around the connection of brace member 'a' to the chord member is caused by loads on the other (carry-over) brace members, identified as brace member *b, c, d* etc., i.e. SCFs caused by:

- *Axial forces:* $F_{br;ax;b}$, $F_{br;ax;c}$, $F_{br;ax;d}$ *etc.;*
- *In-plane bending moments:* $M_{br;ip;b}$, $M_{br;ip;c}$, $M_{br;ip;d}$ *etc.;*
- *Out-of-plane bending moments:* $M_{br;op;b}$, $M_{br;op;c}$, $M_{br;op;d}$ *etc.*

Locations of interest on SCFs

The locations of interest for the SCF determination (around the connection of brace member 'a' to the chord member) are shown in figure 2. For the parameter study, a total of 16 locations for the SCF determination are considered; namely 8 locations on the chord member and 8 locations on the reference brace 'a' member.

$S_{r_{h.s.}}$ - N_f curve

The $S_{r_{h.s.}}$ - N_f curve gives for a specified probability of failure, the hot spot stress range to the number of cycles to fatigue failure. The hot spot stress range is given on the vertical axis and the number of cycles to fatigue failure on the horizontal axis, both on a logarithmic scale as illustrated in figure 8.

1	EC3:	class 112;
		t = 16 mm (based on DEn)
2	IIW:	line A;
		t = 16 mm
3	API:	line X;
		welds with profil controle
4	API:	line X';
		weld profile requirements for
		the wall thickness of the brace
		are not met
5	AWS:	line X_1;
		welds with profil controle
6	AWS:	line X_2;
		weld profile requirements are
		not met
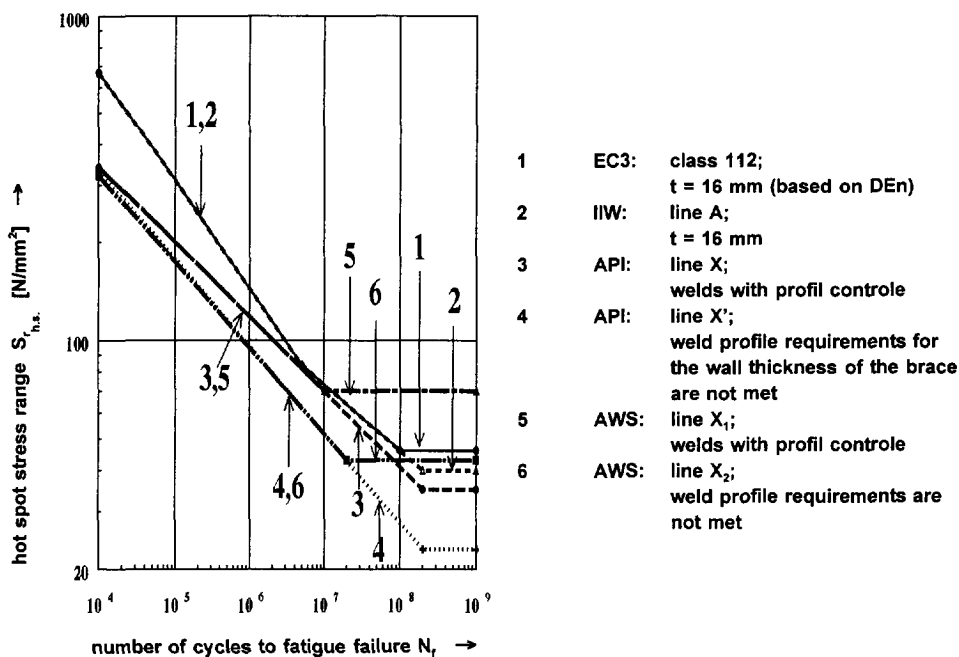
Figure 8.   Major $S_{r_{h.s.}}$ - N_f curves for hollow section joints. (Butt weld).

Thickness effect

The fatigue strength is dependent upon the wall thickness of the member conside-red, and tends to decrease with increasing wall thickness. This is called the thickness effect.

The thickness effect is attributed to three sources, namely *geometrical effects*, *statistical effects* and *technological effects* [F58].

Based on results of ECSC and CIDECT sponsored research programmes, the following thickness corrections for hollow section joints have been proposed for uniplanar joints [F12]:

-    For wall thicknesses of 4 to 16 mm:

$$S_{r_{h.s.;t = 4-16}} = S_{r_{h.s.;t = 16}} \cdot (16/t)^{0.11 \cdot \log N_f}$$

-    For wall thicknesses of 16 mm and more:

$$S_{r_{h.s.;t \geq 16}} = S_{r_{h.s.;t = 16}} \cdot (16/t)^{0.30}$$

For thicknesses below 4 mm, no guidance is given, since the fatigue behaviour may be adversely affected by the welding imperfections at the root of the weld.

23

2. LITERATURE REVIEW

Literature studies have been carried out on the following main aspects:

    1   *Analysis by using FE packages.*
    2   *Flexibility (stiffness) behaviour of welded tubular joints.*
    3   *Fatigue behaviour of welded uniplanar and multiplanar tubular joints.*
    4   *Design codes and recommendations on the fatigue behaviour of welded tubular joints.*

The literature study on fatigue behaviour of uniplanar and multiplanar joints is reported in [*F40*].
A full list of the publications is summarized in chapter 10, and only a brief overview of publications of particular interest for the present work, is given below.

2.1 Analysis by using FE packages

Bathe [*N2*]
Provides a basis for the understanding on the basic FE procedures, such as the formulation of a problem in variational form, the FE discretization of this formulation and the effective solution of the resulting FE equations.

NAFEMS (National agency for finite element methods and standards) [*N4*]
Fundamentals behind the finite element method such as use of different element types, mesh densities and integration schemes are discussed.

2.2 Flexibility (stiffness) behaviour of welded tubular joints

Buitrago [*S1*]
Parametric equations to calculate the local joint flexibility of tubular joints are presented, and the practical implementation of joint flexibility in conventional frame analysis of offshore structures is discussed.

Ueda [*S13*]
Publications are made on various topics, such as "improved joint model and equations for flexibility of tubular joints".

UEG report UR 22 [*S14*]
This report presents an investigation of the tubular joint flexibility on the behaviour of offshore jacket structures.

2.3 *Fatigue behaviour of welded uniplanar and multiplanar tubular joints*

d. Back [*F3, F4, F5, F6*]
Data on SCFs (or hot spot stresses) and fatigue life for uniplanar as well as multiplanar joints are published. The data is mainly obtained from tested steel models.
Furthermore, based on a large number of tested steel specimens, results on the influence of weld improvement techniques, plate thickness and environmental conditions on the fatigue behaviour of joints are published.

Efthymiou [*F13*]
SCF formulae and generalised influence functions based on FE analysis for use in fatigue analysis of tubular joints are given.

Irvine [*F20*]
Different approaches on the determination of SCFs are compared. This includes work carried out on steel models, acrylic models (using gauges and photoelastic technique) and numerical FE models using shell elements without the weld shape included.

Lalani [*F26*]
Data on the fatigue behaviour is reviewed and assessed. The data have been generated by steel companies and research laboratories in eight countries. An extensive reliability assessment of various SCF equations using test results from large scale steel model tests is carried out. The SCF equations given by Kuang et al [*F24*], Gibstein [*F15*], Wordsworth and Smedley [*F62*], UEG [*F56*], Efthymiou [*F13*] and Marshall [*F30*] have been screened, which shows that the SCF formulae giving the best correlation to test data are those given by Wordsworth and Smedley and Efthymiou. Attention on the correlation between numerical and experimental work is mainly given to the chord saddle locations only.

Kurobane [*F25*]
A large number of reports on various topics are published, such as fatigue design of welded joints in trussed legs of offshore jack-up platforms, research on fatigue strength of thin walled tubular joints, criteria for ductility design of joints based on complete CHS truss tests, ultimate limit state criteria for design of tubular K joints, investigation into estimation of fatigue crack initiation life in tubular joints, fatigue tests of tubular T and K joints and developments in the fatigue design rules in Japan.

Marshall [*F30, F31, F32*]
Work on the fatigue design of welded tubular connections, which is implemented in the American API and AWS codes is presented. Topics covered are failure modes for offshore structures, problems in long-life fatigue assessment for fixed offshore structures, fatigue analysis of dynamically loaded offshore structures and recent developments in the fatigue design rules in the USA .

25

Niemi [F34]
Published recommendations concerning stress determination for fatigue analysis of welded components .

Packer [F35]
A "*Design guide for hollow structural section connections*" is published together with Henderson, which is a compendium of current design information directed to practising structural engineers, on the topic of Hollow Structural Section (HSS) connections.

Puthli [F36]
Some publications, which have formed a basis for the present work are: "*Numerical and experimental determination of strain (stress) concentration factors of welded joints between square hollow sections*" and "*Geometrical non-linearity in collapse analysis of thick walled shells with application to tubular steel joints*" .

Wardenier [F58, F59]
Papers, reports and design guides on a large number of topics are used for the present work. These include "*Fatigue design of tubular joints*", and the "*Design guide for circular hollow section (CHS) joints under predominantly static loading*", which is published together with Kurobane, Packer, Dutta and Yeomans.

v. Wingerde [F60, F61]
Based on knowledge gained from experimental and numerical work on square hollow sections, design recommendations and comments regarding the fatigue behaviour of hollow section joints are given.

Wordsworth and Smedley [F64]
SCF formulae for the chord crown and saddle locations are developed on the basis of tested small scale acrylic models and FE analyses. The formulae cover uniplanar gap joints. The SCFs for the brace side are related to the SCFs for the chord side by means of a function: $SCF_{brace} = 1 + 0.63 \cdot SCF_{chord}$.
The SCFs obtained from the SCF formulae, are the values at the toe and heel of the intersecting tubular members. For T and TT (180°) joints, they recommended that the SCF for the chord member locations is corrected for the leg length of the weld as follows:

$$SCF_{corrected} = \frac{SCF_{formulae}}{(1 + \frac{x}{T})^{0.33}}$$

with:

x = The leg length of the weld on the chord side;
T = The wall thickness of the chord member.

2.4 Design codes and recommendations on fatigue behaviour of welded tubular joints

The developments of fatigue research on welded tubular joints are reflected in design codes, such as IIW [F22], DEn [F9], EC3 [F12], AWS [F2] and API [F1]. For the mentioned design codes, recommendations on how hot spot stresses should be determined, which parametric SCF formulae to use, weld profile effect on the fatigue strength, and the influence of secondary bending moments on fatigue strength are summarized in table 2.

Table 2.   Design codes: recommendations on fatigue of welded tubular joints.

Recommendations	IIW	DEn	EC3	AWS	API
Determining hot spot stresses. *Type of stress:* - principal stresses; - stresses perpendicular to the weld toe.	x	x	x	x	x
Determining hot spot stresses. *Extrapolation method:* - no extrapolation procedure; - linear extrapolation; - non-linear extrapolation.	*(1)	*(2) *(2)	*(1)	*(3)	*(3)
Parametric SCF formulae: - uniplanar joints; - multiplanar joints.	*(4)			*(5)	*(5)
Weld type and profile effect on the fatigue behaviour.		30%[6]	classes[7]	*(8)	*(8)
Secondary bending moments.			coefficients [9]		

(1)   No clear guidance is given on the location of the extrapolation region and the type of extrapolation method.

(2)   A linear extrapolation is used for T and X joints, and a non-linear extrapolation is recommended for Y and K joints.

(3)   The hot spot stress is taken as the stress adjacent and perpendicular to the weld toe. Therefore, no extrapolation is carried out.

(4)   SCF graphs are given for uniplanar T, Y, X, K and N joints. These formulae are fairly provisional.

(5)   The AWS and API codes recommend using the formulae given by Marshall [F30], which are based on an analogy of the behaviour of a circular cylinder subjected to uniform circumferential loads established by Kellogg.

(6)   A 30% higher fatigue strength is allowed for a grounded weld toe.

(7)   The influence of weld type and profile on the fatigue behaviour is included using classes. (Comments on this are among others given by [F60, F61]).

(8)   In the AWS and API codes the hot spot stress at $N_f=2\cdot10^6$ range from 79 N/mm^2 to 100 N/mm^2 for an improved weld profile.

(9)   EC3 gives factors to account for the secondary bending effects if these are not calculated. The stress ranges obtained for axial loading should be multiplied by these factors if the secondary bending moments are not included in the analysis.

As shown in table 2, no systematic recommendations exist, which results in different values particularly for SCFs.

Inconsistency in determining hot spot stresses exists. For instance according to AWS and API, the SCFs should be based on hot spot stresses adjacent and perpendicular to the weld toe locations, without the use of an extrapolation method. The IIW and EC3 specify that hot spot stresses should be based on the use of an extrapolation method perpendicular to the weld toe. However, no clear guidance is given on the location of the extrapolation region and the type of extrapolation method. It is also not always clear to which location the extrapolation needs to be carried out. Some identified locations to which extrapolation of stresses take place are:

- *The intersection of the outer surface of the connecting member walls. (For tested small scale acrylic models without the weld shape included);*
- *The fictitious intersection of the midplanes of the connecting member walls. (Numerical investigation without the weld shape included in the FE model);*
- *The weld toe location.*

3. NUMERICAL MODELLING OF WELDED TUBULAR JOINTS

3.1 General

The fatigue design of structures containing welded tubular joints requires knowledge of the joint stiffness (flexibility) behaviour and the stress concentration factors. These can be obtained experimentally by the use of test specimens, or by numerical work using finite element (FE) analyses.
However, because of high costs using solely experimental methods, investigations based on numerical work together with experimental calibration are more widely accepted nowadays.
The numerical modelling of welded tubular joints puts certain obligations on the use of finite element programs, because results can be obtained without having an insight of the actual behaviour. Also, for the problem to be solved, in case of inexperienced use, the analysis results can have either a low accuracy or e.g. high computer costs.
As no systematic guidance concerning the numerical modelling of welded tubular joint flexibility behaviour and welded tubular joint stress concentration factors exists, a study is carried out on several main aspects which affect the numerical results and computer costs.

General purpose FE programs being used

For the numerical modelling of tubular joints, a (pre-processing) FE package is essential. Several of such packages are available around the world, like *Diana*, *Marc*, *I-Deas*, *Patran*, *Ansys*, *Sesam* and *Abaqus*. Each of them have their own specific (dis)advantages, like conditions of use, hardware required, user-friendliness, available types of finite elements and element generation of joints. After comparison of the (dis)advantages of the above mentioned packages, the decision was made to use the module *Pretube* of the Norwegian *Sesam* package and the module *Supertab* of the American *I-Deas* package for the numerical modelling of welded tubular joints.
The analysis was carried out on a Sun Sparc station and using the general purpose finite element computer program *Diana* and the solver module of the *I-Deas* package. There is an interface linking *Diana* to *I-Deas*. However, as no link exist between *Pretube* (*Sesam*) and *I-Deas*, an interface program was developed between the *Sesam* and *I-Deas* package.

3.2 Aspects of importance for modelling

For numerical modelling, correct choices have to be made on the use of *element type*, *mesh refinement*, *integration scheme*, *weld shape* modelling and *boundary conditions*. No standard answer exists, because it entirely depends on the combination of geometry (thin walled, thick walled), type of forces (membrane,

29

plate bending), analysis (linear, non-linear) and the desired accuracy (global load distribution, local stress pattern).

A study has been carried out on the effect of numerical modelling on tubular joint flexibility behaviour [N5] and tubular joint stress concentration factors [F46].

From this study, several conclusions have been made (chapters 3.3.2 and 3.4.2), which should be considered when linear-elastic flexibility and stress concentration factors of tubular joints are analysed numerically.

Computational aspects of finite element (FE) modelling

The aim here is not to discuss theoretical aspects that can be obtained from textbooks [N1-N4]. However, brief details are given as background information.

Element types
Depending on the FE package used, various types of elements, such as membrane elements, plate bending elements and solid elements, are available. For each type of element, differences in topology (triangular, quadrilateral) and order (linear, parabolic, cubic) exist. Using the same number of elements, a joint modelled with elements having midside node(s) gives generally much more accurate analytical results compared to a joint modelled with elements having corner nodes only.

Mesh refinement
Generally, increasing the number of elements (mesh density), in which the elements meet all compatibility and equilibrium conditions, gives more accurate analytical results. However, computer costs also increase. It is assumed that computational time is proportional to $N \cdot B^2$, where N is the number of nodes and B the maximum optimized bandwidth [N3].

Integration scheme
In the practical use of the numerical integration procedures, for finite element analyses, basically two questions arise. Namely, what kind of integration scheme is to be used and what order of integration is to be selected. The correct choice for the problem to be solved is important, because firstly, the cost of analysis might increase when a high order integration is employed, and, secondly, using a different integration order, the results can be greatly affected. These considerations are particularly important for the complex three dimensional behaviour of welded tubular joints.

3.3   Numerical modelling of tubular joint flexibility

The tubular joint flexibility behaviour affects the load distribution and deflection of a structure [S14]. The designer should be aware of this, because it may affect several aspects, such as fatigue life, buckling behaviour and natural frequencies.

Very little information is available on the numerical modelling of joint flexibility. In the past, the main concern has been to investigate the static and fatigue strength,

including stress concentration factors of uniplanar joints.

The influence of various aspects like the type of element, mesh refinement, integration scheme and weld shape on numerical modelling for tubular joint flexibility are considered in this chapter. For the influence of boundary conditions on joint flexibility behaviour, reference is made to the results given in chapter 4.2.

3.3.1 *Effect of modelling on tubular joint flexibility*

A comparison on the use of different element types, mesh density, integration scheme and weld shape modelling on the joint flexibility behaviour and computer costs has been carried out for an XX joint, with joint parameters $\beta=0.30$, $\gamma = 20$ and $\tau = 1.00$ and a chord dimension ø $406.4 \cdot 10$ [$N5$]. The load case and boundary conditions used are shown in figure 9, and table 3 gives an overview of the investigated combinations of computational aspects of FE modelling. Five different main types of FE models have been considered, namely:

FE model 1: Joint modelled with 4-n quadrilateral linear shell elements, excluding the weld shape.
FE model 2: Joint modelled with 8-n quadrilateral quadratic shell elements, excluding the weld shape.
FE model 3: Joint modelled with 20-n hexahedral quadratic solid elements, including the weld shape (see figure 9).
FE model 4: Joint modelled with 8-n quadrilateral quadratic shell elements, including the weld shape by 20-n hexahedral quadratic solid elements. Between the shell and solid elements, 13-n quadrilateral quadratic transition elements are used.
FE model 5: Joint modelled with 2-n beam elements, and all member ends rigidly connected. The fictitious part (brace member inside the chord member) is assumed to be infinitely stiff [S11].

For FE models 3 and 4, the weld has been modelled according to the AWS specifications [$F2$]. For FE models 1 to 4, different mesh refinements are used, and the mesh refinements are classified as mf_1, mf_2, mf_3, and mf_4, in which mf_1 is a fine mesh and mf_4 is a coarse mesh. As an example, figure 10 shows FE model 2 with mesh refinements mf_1 and mf_4.
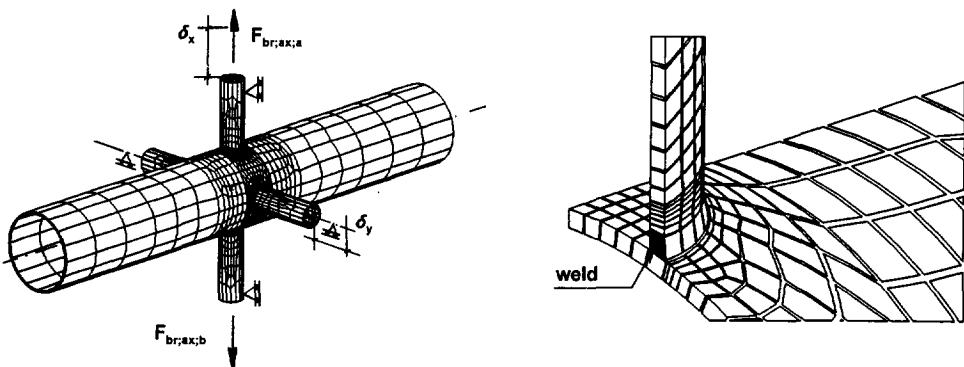
Figure 9.   FE model 3, using 20-n solid elements.
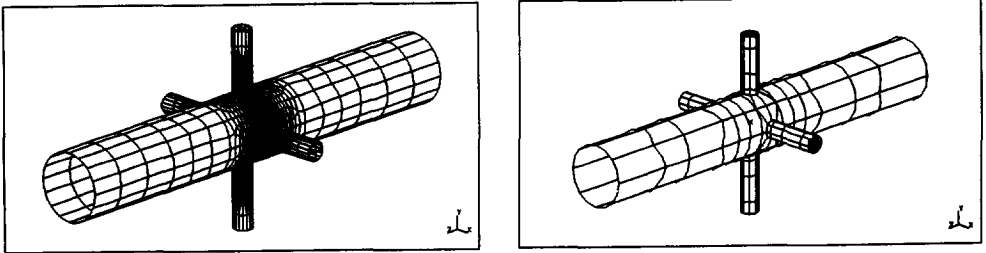
Figure 10. FE model 2, using 8-n shell elements.
Mesh refinements mf_1 (left figure) and mf_4 (right figure) shown.

Table 3. Investigated combinations of computational aspects of FE modelling regarding joint flexibility, CPU-time and disk space.

XX joint	Joint parameters: $\beta = 0.30$; $\gamma = 20$; $\tau = 1.00$: Chord ø 406.4 · 10				
FE model	1	2	3	4	5
Element type	4-n shell	8-n shell	20-n solid	8-n shell + 20-n solid + 13-n transition	2-n beam
Diana-code	CQ20S	CQ40S	CHX60	CQ40S + CHX60 + CQT49	L12BE
Integration scheme	2x2x2 (int_1); 2x2x3 (int_2); 2x2x5 (int_3); 3x3x3 (int_4)				-
Mesh refinement	Nodes	Elements	Nodes	Elements	Nodes	Elements	Nodes	Elements	Nodes/ Elements

Mesh refinement	Nodes	Elements	Nodes	Elements	Nodes	Elements	Nodes	Elements	Nodes/Elements
mf_1	5972	6064	17732	6064	29940	4576	15162	4448	10
mf_2	2452	2528	7156	2528	18036	2848	5249	1408	
mf_3	1188	1248	3348	1248	8708	1472	1952	512	
mf_4	348	432	932	432	2620	592			

The variation of mesh refinement is considered to have the highest influence in the intersection area between the brace and chord member, so that more attention is paid to modelling in this area.

For FE models 1 to 4, alternative integration schemes classified as int_1, int_2, int_3 and int_4 are used. The integration schemes are explained in table 4 and figure 11.

Table 4.   Investigated integration schemes int_{1-4} (see also figure 11).

Integration scheme	ξ	η	ζ
int_1	2	2	2
int_2	2	2	3
int_3	2	2	5
int_4	3	3	3

Integration schemes
4-n shell element.

(a) Nodes and isoparametric axes   (b) 2×2×2 integration   (c) 2×2×3 integration

Integration schemes
8-n shell element.

(a) Nodes and isoparametric axes   (b) 2×2×2 integration   (c) 2×2×3 integration

Integration schemes
20-n solid element.

(a) Nodes and isoparametric axes   (b) Integration points 2×2×2   (c) Integration points 3×3×3
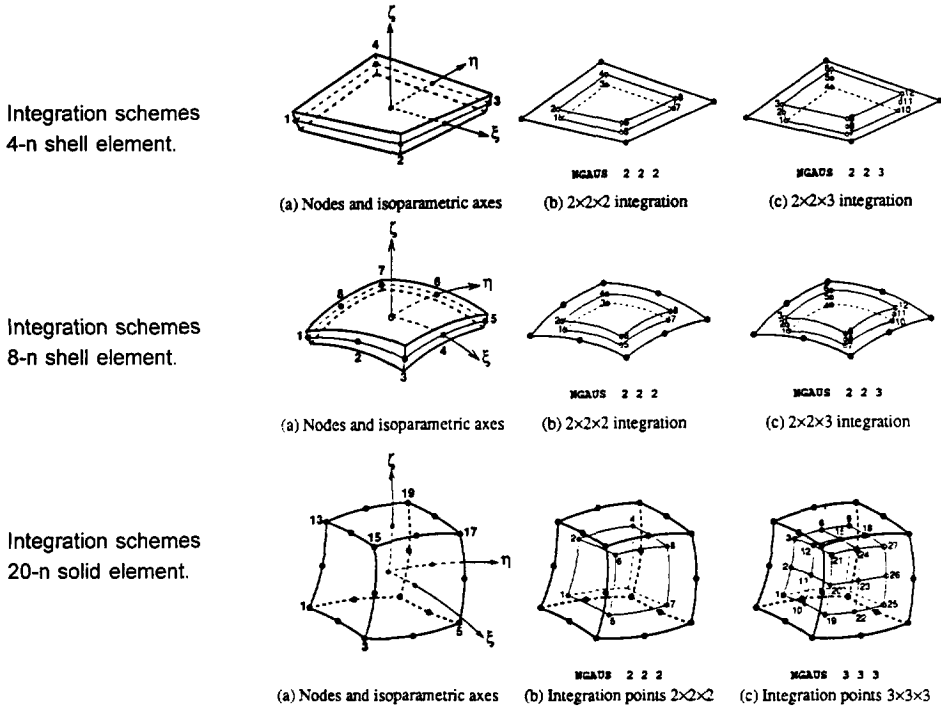
Figure 11.   Explanation on integration schemes int_{1-4} given in table 4.

Schemes int_1, int_2 and int_4 can each have an influence on the flexibility behaviour of the element. Scheme int_3, which is normally used only for non-linear work, is chosen to compare computer costs (CPU-time and disk-space). It is well known that due to spurious shear energy, the 3x3x3 integration scheme int_4 could exhibit a less flexible behaviour of the element. However, it is applied not only to compare the costs of this integration scheme, but also to compare the accuracy for joint flexibility.

The effect of weld shape using FE model 3 on the joint flexibility has been studied using three types of weld shapes, as shown in figure 12. The first weld shape with

33

a weld footprint L_{w1} ($\approx$ 1.3 · t_1) is modelled according to the AWS specifications for a weld accessible from one side. For the second and the third weld shape, only increases in length of the chord weld footprint have been made, so that L_{w2} = 1.5 · L_{w1} and L_{w3} = 2.0 · L_{w1}.

Also, an investigation have been carried out on the difference in joint flexibility for the whole range of joint parameters β (0.30-0.60), γ (8-32) and τ (0.25-1.00) for an XX joint when such a joint is modelled according to FE models 2 and 3. For the results of this investigation, reference is made to [N5].
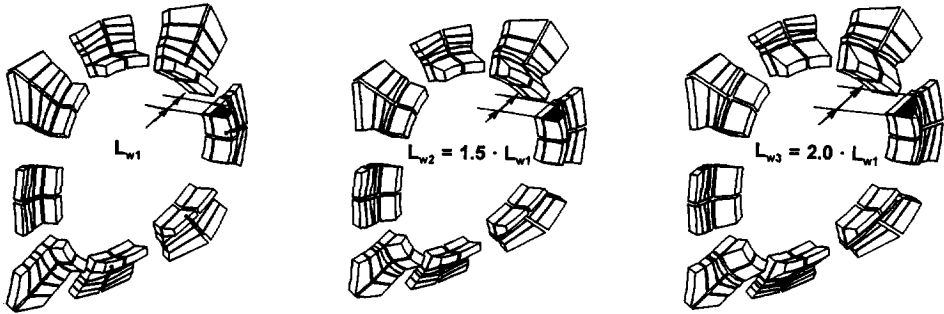
Figure 12. Different types of weld shapes considered.

Some FE results on joint flexibility and computer costs, for the different element types, mesh refinement, integration schemes and weld shape modelling, are grouped as follows:

Tables 5 and 6 : -   Member end displacements δ_x (braces 'a', b) and δ_y (braces c, d).
                  -   CPU-time required.
                  -   Disk space occupied.
Figures 13 to 16 : - Show some of the results of tables 5 and 6.
Figure 17   : - The effect of weld shape using FE model 3 (solid elements only) on the joint flexibility behaviour.

Table 5. Results on the influence of FE models with alternative integration schemes on cpu-time (sec) and disk space (ds in mega bytes) using mesh refinement mf_1.
(Because of symmetry ¼ XX-joint analysed).

FE model	1		2		3		4	
Integration scheme	cpu	ds	cpu	ds	cpu	ds	cpu	ds
int_1 (2x2x2)	337	76	1094	166	2162	162	3194	173
int_2 (2x2x3)	374	90	1156	186	2162	159	3237	186
int_3 (2x2x5)	450	118	1273	225	2202	165	3275	199
int_4 (3x3x3)	520	148	>1400	>270	2263	177	3420	243

34

Table 6.   Influence of computational aspects on joint flexibility (δ_x, δ_y), calculation time (cpu) and disk space (ds). (Because of symmetry ⅛ XX joint considered).

FE model	1 4-n shell				2 8-n shell				3 20-n solid				4 8-n shell + 20-n solid + 13-n connectivity			5 2-n beam
Mesh refinement	mf_1	mf_2	mf_3	mf_4	mf_1	mf_2	mf_3	mf_4	mf_1	mf_2	mf_3	mf_4	mf_1	mf_2	mf_3	
Integration scheme int_1 (2x2x2)																
δ_x [mm]	6.41	6.33	5.75	3.06	7.19	7.16	7.09	5.66	6.81	6.70	6.62	5.21	6.82	6.73	6.04	1.65
δ_y [mm]	5.29	5.25	4.84	2.69	5.98	5.96	5.93	4.72	5.69	5.67	5.64	4.44	5.77	5.71	5.28	0.00
cpu [sec]	131	56	33	22	290	111	53	25	342	197	76	32	508	91	29	< 1
ds [Mb]	37	17	9	4	73	30	14	6	64	37	17	7	65	18	6	< 1
Integration scheme int_2 (2x2x3)																
δ_x [mm]	6.41	6.33	5.75	3.06	7.19	7.15	7.09	5.66	6.46	6.01	5.74	2.74	6.80	6.72	6.03	
δ_y [mm]	5.29	5.25	4.84	2.69	5.98	5.96	5.93	4.72	5.33	5.01	4.80	2.04	5.75	5.71	5.27	
cpu [sec]	149	64	37	23	319	123	60	27	343	200	77	32	527	97	31	
ds [Mb]	44	19	10	5	83	34	16	7	64	35	16	6	71	20	7	
Integration scheme int_3 (2x2x5)																
δ_x [mm]	6.41	6.33	5.75	3.06	7.19	7.15	7.09	5.66	6.46	6.01	5.73	2.74	6.81	6.72	6.03	
δ_y [mm]	5.29	5.25	4.84	2.69	5.98	5.96	5.93	4.72	5.33	5.01	4.80	2.03	5.76	5.72	5.27	
cpu [sec]	185	78	44	24	379	147	70	31	383	223	87	35	584	109	34	
ds [Mb]	58	25	12	5	103	42	20	7	67	39	18	7	85	23	8	
Integration scheme int_4 (3x3x3)																
δ_x [mm]	6.39	6.31	5.71	3.04	6.12	5.98	5.49	1.83	5.69	5.58	4.81	1.68	5.78	5.72	1.73	
δ_y [mm]	5.28	5.24	4.80	2.64	4.94	4.85	4.48	1.30	4.67	4.60	4.02	1.19	4.77	4.33	1.24	
cpu [sec]	220	92	50	27	435	169	81	33	447	261	106	41	615	123	38	
ds [Mb]	73	31	15	6	123	50	24	8	79	46	21	8	99	28	9	
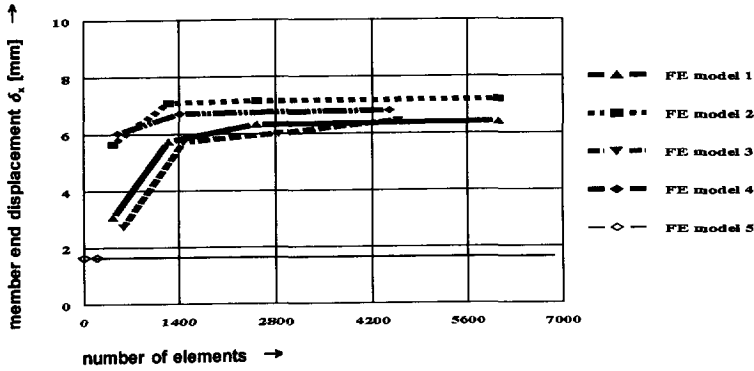
Figure 13.   Relation between mesh refinement (mf_{1-4}) and joint flexibility behaviour (displacement δ_x) for the different FE models investigated using integration scheme int_2 (2x2x3).
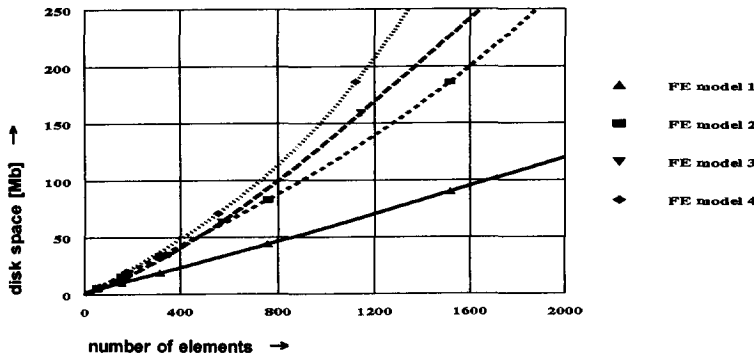
Figure 14.   Relation between mesh refinement (mf_{1-4}) and required disk space for the different FE models investigated using integration scheme int_2 (2x2x3).
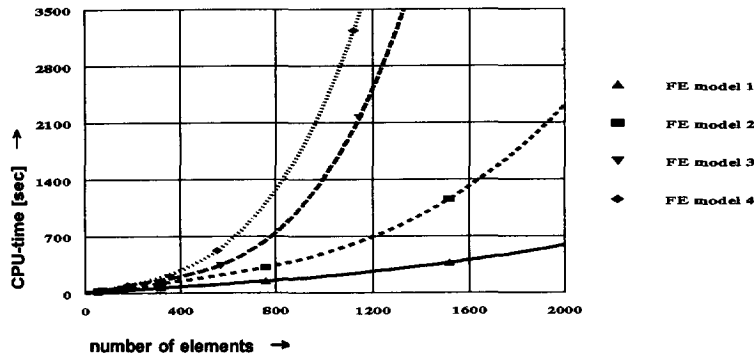
Figure 15.   Relation between mesh refinement (mf_{1-4}) and required cpu-time for the different FE models investigated using integration scheme int_2 (2x2x3).

36
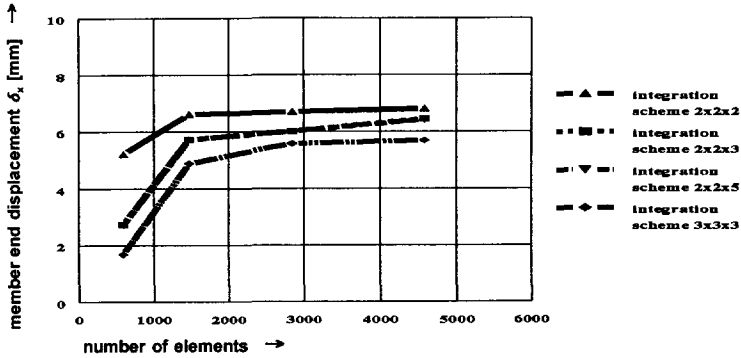
Figure 16.   Relation between mesh refinement (mf_{1-4}) and joint flexibility behaviour (displacement δ_x) for the different integration schemes (int_{1-4}) investigated using FE model 3.
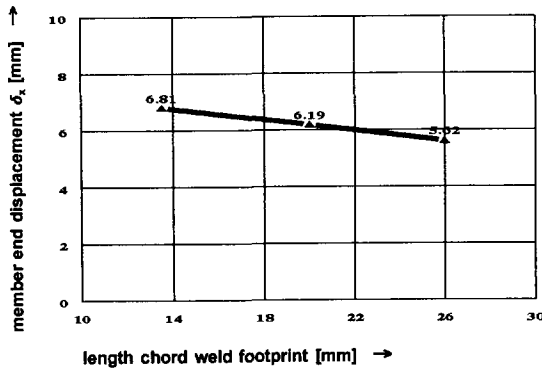
Figure 17.   Influence of weld shape (L_{w1-3}) on joint flexibility behaviour (displacement δ_x) for integration scheme int_2 (2x2x2) using FE model 3.

3.3.2   Conclusions of modelling on tubular joint flexibility

It is found that the results of the investigation on numerical modelling for tubular joint flexibility largely depends on the type of element, mesh refinement, integration scheme and the weld shape considered.
Some difference is expected, because:

- Differences in element displacement field, described by interpolation polynominals.
- Shortcomings in the element formulation regarding transverse shear stresses, termed shear locking, and singularities in case of reduced integration option.
- Shell elements ignore the 6th d.o.f. (rotation about the normal to the mid-plane).

37

From the results given in tables 5 and 6, figures 13 to 17 and [N1-5, S11], the following conclusions are made:

Flexibility behaviour δ_x of welded tubular joints:

Element type:
- When using shell or solid elements, the elements having midside node(s) exhibit a more flexible behaviour than elements with corner nodes only, and they are considered to be more accurate. Therefore, the use of elements having a midside node (8-n shell and 20-n solid), is recommended.

Mesh refinement:
- For FE models 1-4, the joint flexibility increases with mesh refinement (mf_{1-4}) and converges to an optimum value, beyond which refinement is not necessary (see figure 13). Even after convergence, differences (up to 20%) exist for the FE models 1-4 investigated. The use of mesh refinement mf_2 is recommended. For mf_2, the length of the element having midside node(s) measured along the intersection area is approximately 1/12 of the total length of the intersection area.

Integration scheme:
- For 4-n shell elements, the joint flexibility remains the same for all integration schemes considered.
- When 8-n shell elements are used, no difference in joint flexibility has been found using integration schemes 2x2x2, 2x2x3 and 2x2x5. However, as expected [N2], integration scheme 3x3x3 results in a remarkable decrease in the joint flexibility.
- Figure 16 shows that, when 20-n solid elements are used (apart from the fact that 2x2x3 and 2x2x5 integration schemes are expected to give the same result), comparison of the other integration schemes results in differences of joint flexibility, especially when integration scheme 3x3x3 is used.
- When using the reduced integration scheme 2x2x2, small differences (up to 8%) in joint flexibility exist between a joint modelled with 8-n shell elements (without the weld shape included) and a joint modelled with 20-n solid elements (with a weld shape according to AWS included).
- For the recommended types of elements, the use of a reduced numerical integration (integration scheme 2x2x2) which results into the largest joint flexibility behaviour, is preferable. This because, provided the convergence criteria are satisfied, the displacement formulation of FE analysis yields a lower bound on the "exact" strain energy of the system considered; i.e., physically, a displacement formulation results in overestimating the system stiffness. Therefore, by not evaluating the element stiffness matrices exactly in the numerical integration, in fact, better results can be obtained provided that the error in the numerical integration compensates approximately for the overestimation of structural stiffness due to the FE discretization. In other words, a reduction of the numerical integration order from the order that is required to

38

evaluate the element stiffness matrix exactly should lead generally to improved results.

Weld shape:
- Figure 17 shows that increasing the length of the weld footprint on the chord member surface results in a substantial decrease of joint flexibility.
- The difference in joint flexibility between a joint modelled with 8-n shell elements (without the weld shape included) and a joint modelled with 20-n solid elements (with the weld shape included) becomes larger when β and γ decrease and τ increase.
  For load case $F_{br;ax;a,b}$, the joint flexibility when including the weld shape (AWS-code) is 16% (maximum difference) lower than without the weld shape included.

Required cpu-time and disk space (ds):

- When a joint is modelled with 8-n shell elements, 13-n transition elements and 20-n solid elements only in the region of the weld, the required disk space and cpu-time increases, rather than decreases, when compared to the use of solid elements only (see figures 14 and 15).
  Therefore, the use of transition elements is not advised.
- For the investigated integration schemes (int_{1-4}), the 4-n and 8-n shell elements show a large difference in required disk space and cpu-time.
- For 4-n shell elements, all investigated integration schemes int_{1-4} exhibit an almost linear behaviour between the mesh refinement mf_{1-4} and the required disk space and CPU-time.
- Using 20-n solid elements only, or a combination of 8-n shell elements, 20-n solid elements and 13-n transition elements, a parabolic relation between the mesh refinements mf_{1-4} and the required disk space and CPU-time for all investigated integration schemes int_{1-4} is found.

Note! The use of other FE packages might give some small changes in results. However, the conclusions are not likely to change.

3.4   *Numerical modelling of tubular joint SCFs*

From literature studies, it has been found that recommendations for the numerical SCF determination of uniplanar as well as multiplanar tubular joints are limited [F34].
There is no standard guidance, which has led to a divergence in the numerical methods in SCF determination being used. Differences on the effect of numerical modelling on tubular joint SCFs exist, because of:

- *The use of different types of elements, mesh refinements and boundary conditions.*

39

- *FE modelling with and without the weld shape included.*
- *Disregarding the effect of a chosen integration scheme for the numerical integration procedures on SCFs.*

The effect of various aspects like the type of element, mesh refinement, integration scheme and weld shape on numerical modelling for tubular joint SCFs are considered in this chapter.

3.4.1 Effect of modelling on tubular joint SCFs

For the determination of SCFs, various methods of numerical modelling are applied. For a proper understanding of the effects of the various methods of numerical modelling on SCFs, knowledge regarding the definition of hot spot stress from which SCFs are obtained, is necessary. Chapter 1.3.2 explains the definition on hot spot stress.

A comparison of the various methods of numerical modelling on SCFs has been carried out for a multiplanar KK and XX joint with joint parameters as summarized in table 7.

Table 7.   Joints considered for a comparison of the various methods of numerical modelling on SCFs.

Joint	Joint parameters						Chord dimension [mm]
	γ	β	τ	α	φ_{ip}	φ_{op}	
KK	24	0.40	1.00	8.5	60°	180°	ø 400.0 · 8.33
XX	20	0.30	1.00	10.0	90°	90°-180°-270°	ø 406.4 · 10.00

Since the results of the comparisons were found to be the same for the KK and XX joints investigated, the results are presented for one type of joint, either KK or XX.

Influence of element type on SCFs

The following four types of FE models have been compared:

FE model a: *4-n thin shell elements; weld shape not included and SCFs defined at the intersection of the midplanes of the connecting walls.*

FE model b_1:   *8-n thin shell elements; weld shape not included and SCFs defined at the intersection of the midplanes of the connecting walls.*

FE model b_2:   *8-n thin shell elements; weld shape not included and SCFs defined at the fictitious weld toe location.*

FE model c: *8-n solid elements; weld shape included and SCFs defined at weld toe position.*

FE model d: *20-n solid elements; weld shape included and SCFs defined at weld toe position.*

40

The SCFs are determined using the extrapolation method and region as described in chapter 7.2. Because FE model d can be regarded as the most accurate FE model (as the weld shape is included and the element type has a high degree of accuracy [$N2$, $N4$]), the results of FE models a, b_1, b_2 and c have been compared to those of FE model d using the same mesh refinement. For the investigated KK joint with the reference brace 'a' (see figure 7) loaded by a nominal stress of 1 N/mm^2 and bending moments in the chord compensated, the stress pattern at the crown (heel) and saddle positions of the chord and brace member are given in figures 18 and 19. For the influence of the investigated types of elements on the stress distribution (SCFs) it is found that small differences on SCFs for the brace member locations and large differences on SCFs for the chord member locations exist. Especially for the chord crown location large differences in the stress gradient to the weld toe position occurs. The reason for the different influence of the element types on the SCF results for the chord and brace member locations is caused by the numerical formulation of the element types, especially in case of shear deformation and bending stresses, which are more prevalent in the chord member.

Figure 18.   Stress distribution perpendicular to the weld toe for the cc;1 location (top figure) and cs;3,7 location (bottom figure) of a KK joint.
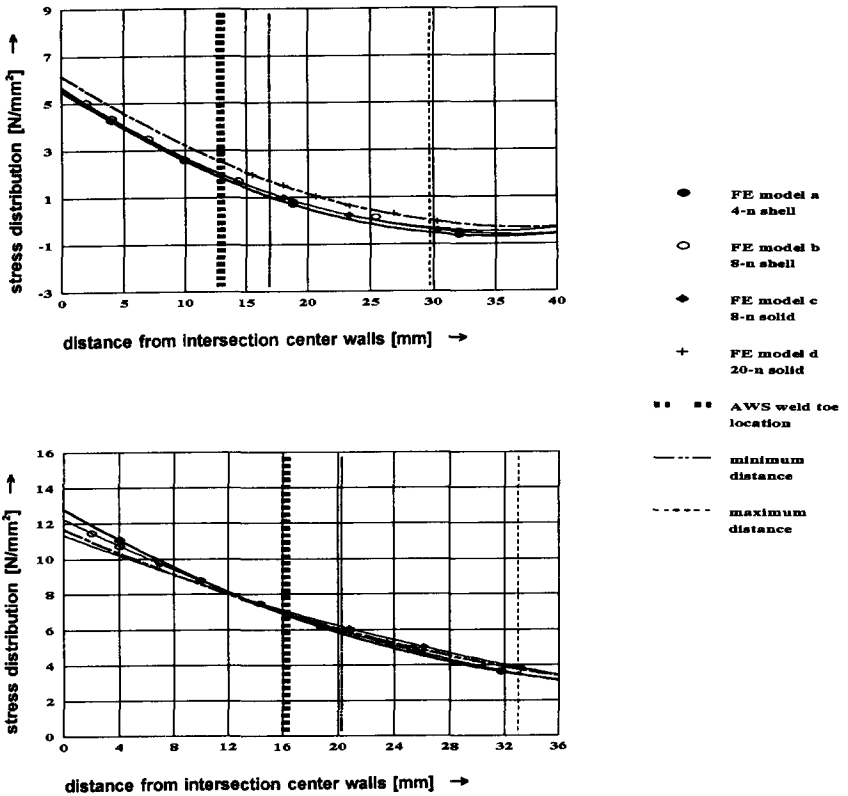
Figure 19.   Stress distribution in the vicinity of the weld toe, in a direction parallel to the brace axis, for the bc;1 location (top figure) and bs;3,7 location (bottom figure) of a KK joint.

Generally, for the FE models investigated, the lowest SCFs are found using FE model *c* (8-n solid elements), and the highest SCFs are found using FE model *d* (20-n solid elements).

From figures 18 and 19, it is also obvious that ignoring the weld and defining SCFs at the intersection of the midplanes of the member walls leads to entirely different results (especially for the brace member differences up to 300% are expected). This is because although the distance between this intersection point and the weld toe position is small, the stress gradients are high. If this distance is taken into account, in other words, if the SCFs are calculated at the fictitious weld toe locations, a considerable improvement, especially for the brace member, arises.

42

Considering the degree of element accuracy (using the same number of elements, 20-n solid elements gives much more accurate results compared to 8-n solid elements), the results on SCFs for the investigated element types and the information given by [N1-3], the use of 20-n solid elements with the weld shape included and determining the SCFs at the weld toe location is recommended.

Influence of mesh refinement on SCFs

For the influence of changes in mesh refinement on SCFs, the variation is mainly concentrated at the locations where SCFs are defined. As an illustration of this, figure 20 shows the mesh refinements considered for the KK joint investigated, using FE model d.
The corresponding number of nodes and elements are given in table 8.

Table 8. Investigated mesh refinements regarding SCFs (see also figure 20).

Mesh refinement : KK joint	Nodes	Elements
mf_1	15171	2227
mf_2	10323	1557
mf_3	8238	1330

mf_1 mf_2

mf_3
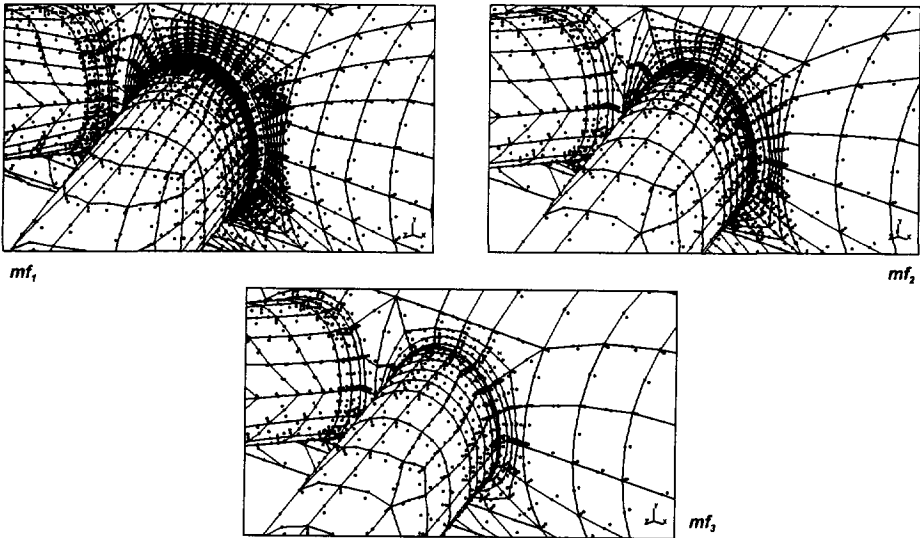
Figure 20. Investigated mesh refinements mf_1-mf_3 for the determination of SCFs of a KK joint.

For the mesh refinements mf_1-mf_3 as shown in figure 20, the analysed SCFs for the chord member and brace 'a' member of the KK-joint using FE model d are shown in figures 21 and 22. The SCFs are given for fifteen load cases (with

compensating moments as described in chapter 7.2.7), namely:
Three chord member loads : $F_{ch;ax}$; $M_{ch;ip}$ and $M_{ch;op}$.
Twelve brace member loads : $F_{br;ax;a-d}$; $M_{br;ip;a-d}$ and $M_{br;op;a-d}$.
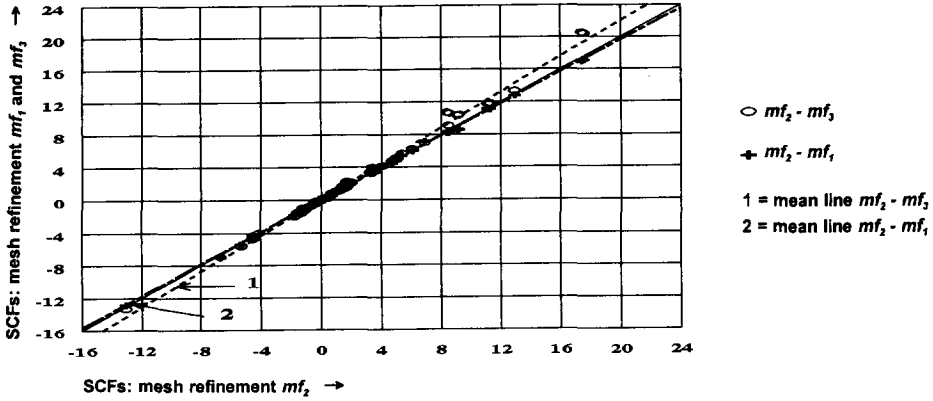
Figure 21.   Influence of mesh refinement on SCFs for the chord member locations 1-8 of a KK joint. (The chord member locations are shown in figure 2).
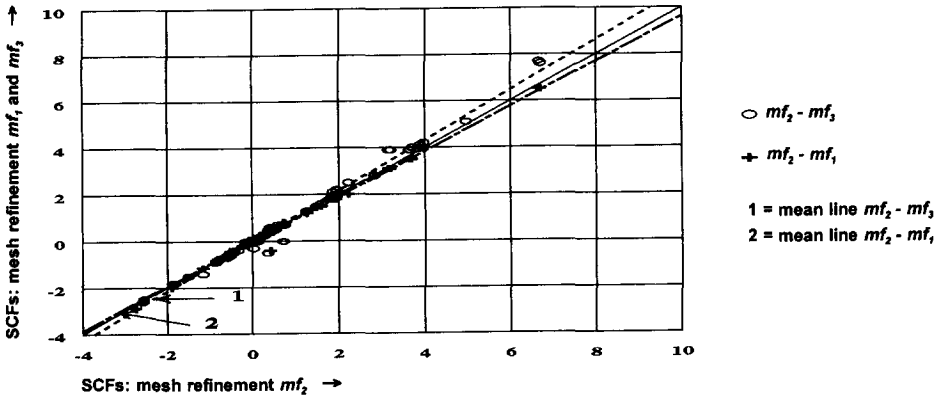
Figure 22.   Influence of mesh refinement on SCFs for the brace member locations 1-8 of a KK joint. (The brace member locations are shown in figure 2).

Generally, an increase of mesh refinement, when the element type meets all consistency criteria (this is the case for 20-n solid elements), results in a convergence of deformation, stresses and strains to an optimum value [N1].

44

Therefore, refinement of the mesh should be such that any further refinement does not result in a substantial change of the stress distribution (outside the notch effect area). Comparison of the SCF results for the three analysed mesh refinements justifies the use of mesh refinement mf_2. Using mf_2, the length of the 20-n solid element measured along the intersection area is approximately 1/16 of the total length of the intersection area.

Influence of the integration scheme on SCFs

Regarding the effect of the integration scheme on the SCFs, two types of FE models have been studied, namely:

FE model d: Joint modelled with 20-n solid elements, and the weld shape included. Variations in integration scheme are: int_1 (2x2x2) and int_4 (3x3x3).

FE model e: Joint modelled with 8-n shell elements and the weld shape included by 20-n solid elements. Between the shell and solid elements, 13-n transition elements have been used. The variations in integration scheme for the shell elements are int_1 (2x2x2); int_2 (2x2x3); int_3 (2x2x5) and int_4 (3x3x3).

The SCFs for balanced axial loads on the vertical brace members 'a' and b (load case $F_{br;ax;a,b}$ as shown in figure 6), and balanced loads on the horizontal brace members c and d (load case $F_{br;ax;c,d}$) of the XX joint, using the various integration schemes int_{1-4} are together with test results [F47] summarized in table 9. The test results used are described in chapter 7.5.5.

Table 9. The effect of integration schemes int_{1-4} on SCFs.

XX joint $\gamma = 20$ $\beta = 0.50$ $\tau = 1.00$	SCFs						
	20-n solid + 8-n shell + 13-n transition				20-n solid		test results [F47]
FE model	Load case: vertical braces 'a' and b balanced axial loaded ($F_{br;ax;a,b}$)						
Integration scheme	int_1 2x2x2	int_2 2x2x3	int_3 2x2x5	int_4 3x3x3	int_1 2x2x2	int_4 3x3x3	
cs;3,7	20.7	35.7	35.7	33.0	33.7	33.3	30.7
cc;1,5	1.7	1.6	1.6	2.0	1.9	2.0	2.2
bs;3,7	9.8	14.1	14.1	14.1	14.7	16.0	14.2
bc;1,5	-0.4	0.0	0.0	0.0	0.0	- 0.1	0.4
	Load case: horizontal braces c and d balanced axial loaded ($F_{br;ax;c,d}$)						
cs;3,7	-15.3	-25.7	-25.7	-23.2	-24.0	-23.7	-25.6
cc;1,5	0.3	1.5	1.5	0.9	0.8	0.8	0.8
bs;3,7	-7.1	-10.6	-10.6	-10.3	-11.2	-12.2	-13.6
bc;1,5	1.0	0.7	0.7	0.7	0.6	0.7	0.1

Using the recommended 20-n solid elements, table 9 shows small differences in SCFs for the alternative integration schemes and a reasonable agreement with the

45

test results. Therefore, the use of integration scheme 2x2x2 is recommended. For shell elements the reduced integration scheme 2x2x2 gives much lower SCFs compared to other integration schemes, and seems to be inaccurate.

Influence of weld shape on SCFs

The effect of various types of weld shapes (see figure 12) on SCFs has been considered for the three alternatives as described in paragraph 3.3.1. In an identical way as described for the influence of element type on SCFs caused by a brace member load $F_{br;ax;a}$ (with compensating moments), the stress pattern using FE model d for the three alternative types of weld shapes considered is given in figures 23 and 24. Figures 23 and 24 show, that an increase of the chord weld footprint for the geometry and joint parameters considered leads to a substantial increase of the SCFs for the brace member and decrease for the chord member. As illustrated by the SCFs for the brace member locations (constant weld toe location for the three types of weld shapes considered), the SCF differences are mainly caused by differences in the shape of the weld toe (angle between the weld and the member).
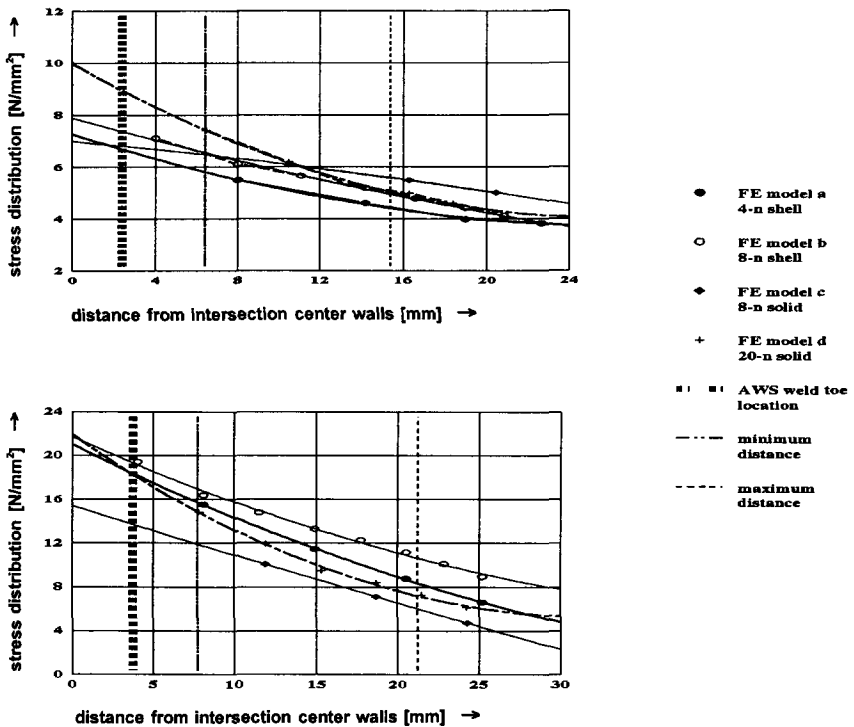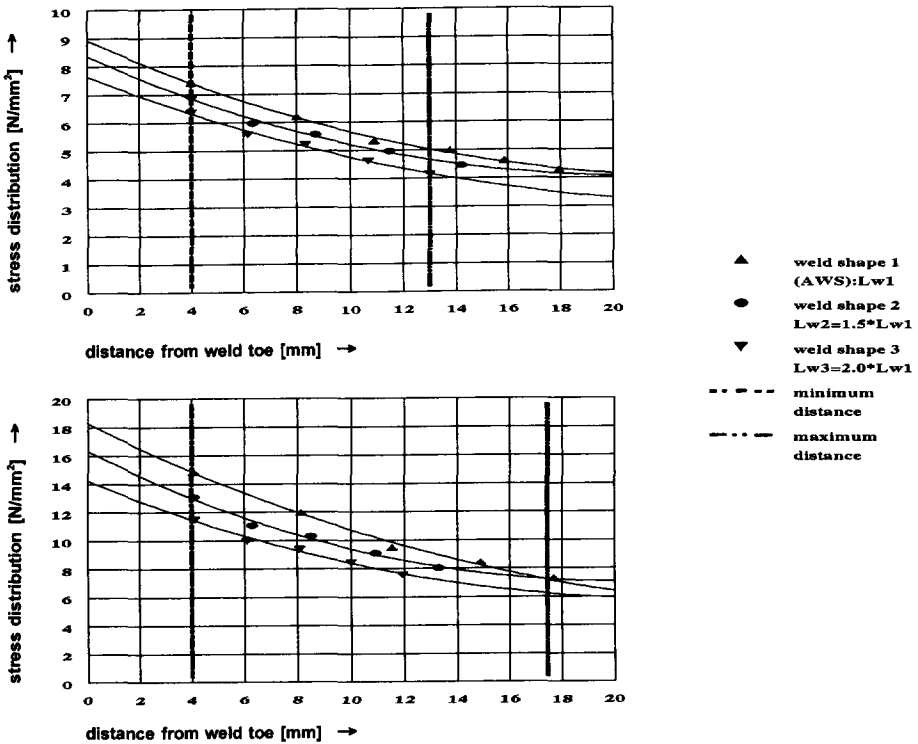

Figure 23. Influence of weld shape on the stress distribution perpendicular to the weld toe for the cc;5 location (top figure) and cs;3,7 location (bottom figure) of a KK joint.

46
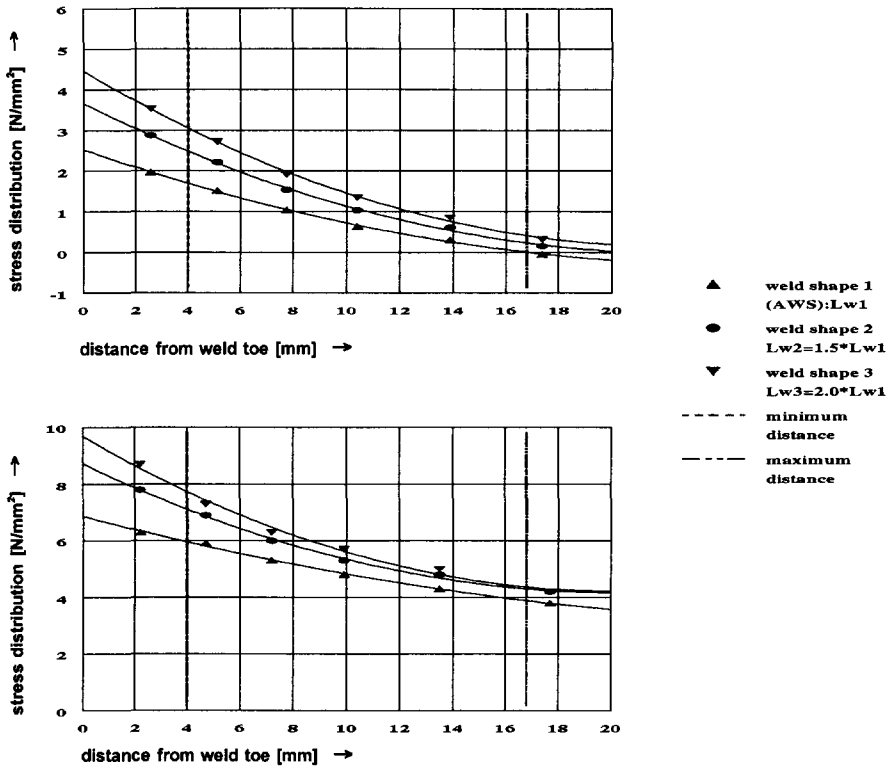
Figure 24. Influence of weld shape on the stress distribution in the vicinity of the weld toe, in a direction parallel to the brace axis, for the bc;5 location (top figure) and bs;3,7 location (bottom figure) of a KK joint.

Influence of boundary condition on SCFs

For the sake of equilibrium the (chord) member(s) should be adequately supported. This is particularly true for unbalanced load cases. At the supports, boundary conditions arise, which cause reaction forces and moments in the members.
The effect of boundary conditions (*bdc*) on SCFs has been studied using three alternatives, namely:

bdc_1. *SCFs determined with chord member ends pin-ended.*
bdc_2. *SCFs determined with chord member ends fully-clamped.*
bdc_3. *SCFs determined with chord member ends pin-ended and a correction applied to the SCFs to account for the forces and moments introduced. A method on this is given in chapter 7.2.7.*

Using FE model *d*, for the three alternative boundary conditions bdc_{1-3} considered, results on SCFs for the chord member locations of a KK joint loaded by the load

47

cases $F_{br;ax;a}$, $F_{br;ax;b}$, $F_{br;ax;c}$ and $F_{br;ax;d}$ are given in figure 25. Large differences in SCFs are found for the three alternative boundary conditions bdc_{1-3} considered. The magnitude of the differences depends on the load case and joint considered and on the relevant location between crown and saddle. The influence of the boundary conditions on the SCFs from the carry-over effects (SCFs caused by brace member loads $F_{br;ax;b,c,d}$) is much larger than for the reference effects (SCFs caused by brace member load $F_{br;ax;a}$), because the former effect is smaller than the latter, while the effect due to moments from boundary conditions can be the same.
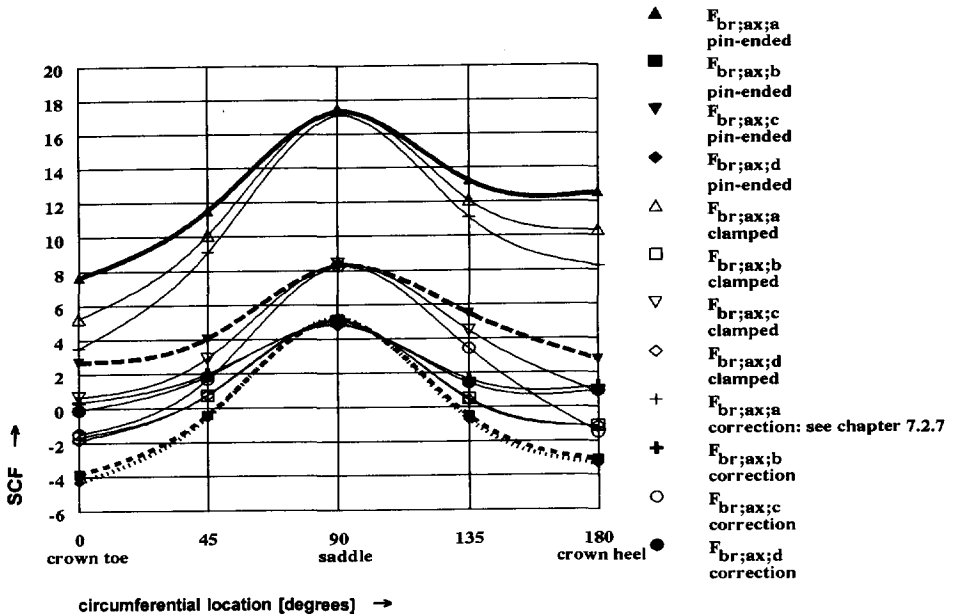
Figure 25. Influence of boundary conditions on SCFs for the chord member of a KK joint.

3.4.2 *Conclusions on modelling for tubular joint SCFs*

It is found that the results of numerical models of tubular joint SCFs are greatly influenced by the method used, which causes problems in the interpretation of numerical FE results (as well as experimental results).
From the observations obtained, the following conclusions are made:

Position SCF determination:
- SCFs should always be determined at the weld toe position and not at the intersection of the member wall midplanes or at the intersection of the member wall outer surfaces.

48

Element type:
- Modelling the weld shape improves the accuracy of SCFs largely.
- Using solid elements to model the weld area is recommended, as it is a more realistic representation compared to model the weld area using shell elements.
- Because of high accuracy requirements, the use of 20-n solid elements is recommended above 8-n solid elements.
- The use of transition elements is disadvised. Because these types of elements increase rather than decrease computer costs. Thus a combination of solid and shell elements should not be used.

Mesh refinement:
- The length of the 20-n solid element, measured along the intersection area, should be less than 1/16 of the total length of the intersection area.

Integration scheme:
- When using 20-n solid elements, the integration scheme 2x2x2 is preferred to 3x3x3. This because the investigation on numerical modelling for tubular joint flexibility shows that the 3x3x3 integration scheme underestimates the joint flexibility behaviour largely.

Boundary condition:
- It is preferable to compensate for the influence of boundary conditions when determining SCFs. This is particularly true in case of multiplanar joints (having carry-over effects). However, such an approach is not always possible to simulate experimental work, so that SCFs particularly at crown locations include the influence of boundary conditions.

49

4. NUMERICAL IDEALIZATION OF MULTIPLANAR LATTICE TUBULAR STRUCTURES

4.1 *Introduction*

The influence of welded tubular joint flexibility upon the behaviour of lattice structures (load distribution: secondary bending moments) is generally ignored for predominantly statically loaded structures, which is allowed if there is adequate deformation and rotation capacity in the critical connections or members to allow redistribution of stresses after local yielding of the connection [F12].

For structures loaded in fatigue, however, the correct force and moment distribution should be calculated, so that hot spot stresses required for fatigue strength calculations can be accurately determined. As an example, according to Eurocode 3 for a fatigue loaded tubular lattice structure:

>   - *The axial load distribution may be determined on the assumption that the members are connected by pinned joints.*
>   *The secondary moments in the joints, caused by the actual joint flexibility and joint eccentricities should always be taken into account in the fatigue design of the joints.*
>   *To avoid complicated analysis, Eurocode 3 [F12] gives factors to account for the secondary bending moment effects. The stress range obtained for axial loading should be multiplied by these factors if the secondary bending moments are not included in the analysis. Chapter 6 show some examples using such a method.*

Including the flexible behaviour of the joints by the use of flexible brace member ends or springs provides a more accurate load and moment distribution.

Using such a method, a database or formulae on joint stiffness coefficients (K_{ij}) is required, which is based on the difference in linear-elastic behaviour between a joint modelled with beam elements and a joint modelled with shell / solid elements. The values of K_{ij} determined by the proposed method can be used in stress analysis for determining the correct load distribution, since fatigue problems occur under serviceability loading, which is assumed to be in the linear elastic stage.

Because of lack of sufficient information on tubular joint flexibility behaviour, a (limited) study on the flexibility of uniplanar and multiplanar tubular joints by means of K_{ij} has been carried out. Detailed results of this study are given in [S11], and chapter 4.2 summarizes some results.

Different methods of numerical idealization of multiplanar lattice structures as summarized in chapter 4.3 are identified. The influence of the methods of numerical idealization on the deflection and load distribution has been investigated for several analysed multiplanar lattice girders, from which the results together with test results [F23] are given in chapter 4.4. The numerical results and the test results regarding the contribution of bending strains on the total strain are also discussed in this chapter.

4.2 Flexibility of uniplanar and multiplanar tubular joints

In this chapter, results of a study on the flexibility of uniplanar and multiplanar tubular joints are given on the following topics:

- Methods for defining values of K_{ij}.
- Influence of the joint geometry and joint parameters on values of K_{ij}.
- The significance of spring pivot terms $K_{ii;ax}$.
- The significance of spring cross terms $K_{ij;ax}$.

Methods for defining values of K_{ij}

Different existing methods for defining joint stiffness coefficients K_{ij} are identified [S1, S4, S5, S13], and especially for the bending joint stiffness coefficients $K_{ij,bending}$, results entirely depend on the method (approach) used. The main differences are due to the influence of boundary conditions used when determining K_{ij}.

The correct method in determining K_{ij} is found to be complicated and very cumbersome in use. This because of all matrix handling (inverse calculations) on the stiffness and flexibility matrices for the beam as well as shell / solid modelled joint, and determining all the terms of the joint stiffness matrix. As an example, to obtain the whole stiffness matrix for a multiplanar KK joint, because of the differences in restraint conditions, the FE modelled joint must be analysed 36 times (= the total number of degrees of freedom for all member ends).

As an approach, for an axially loaded brace member, the difference in axial displacement of a joint modelled with shell / solid elements and a joint modelled with rigid ended beam elements only produce the spring value on $K_{ii;ax}$, namely:

$$K_{ii;axial} = \frac{F_i}{\delta_{i;axial;s} - \delta_{i;axial;b}}$$

Influence of the joint parameters and joint geometry on values of K_{ij}

The values on K_{ij} of the tubular joints depends on the type of joint geometry considered and on the joint parameters β, γ, τ, φ_{ip}, and φ_{op}. The influence of β and γ is most dominant on the joint flexibility behaviour, whereas the influence of τ is found to be small compared to the influence of other parameters. Increasing β and decreasing γ results in a decrease of the joint flexibility. Also, in general the flexibility decreases with increase in the number of connecting braces, and joints without overlapping braces (gap joints) behave more flexible compared to joints with overlapping braces (partly-fully overlap joints).

As an example, results on axial joint flexibility for T, Y, K and KK gap and KK overlap joints with joint parameters $\tau = 0.50$, $\varphi_{ip} = 45°$ and $\varphi_{op} = 90°$ are shown in figures 26 and 27.
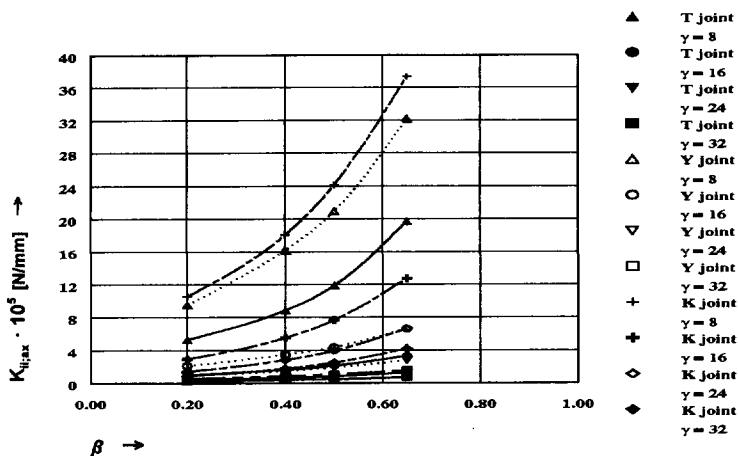
Figure 26. Uniplanar joints: influence of joint parameters β and γ and joint geometry on the axial joint flexibility behaviour. Y and K joints: $\varphi_{ip} = 45°$ and $\tau = 0.50$.
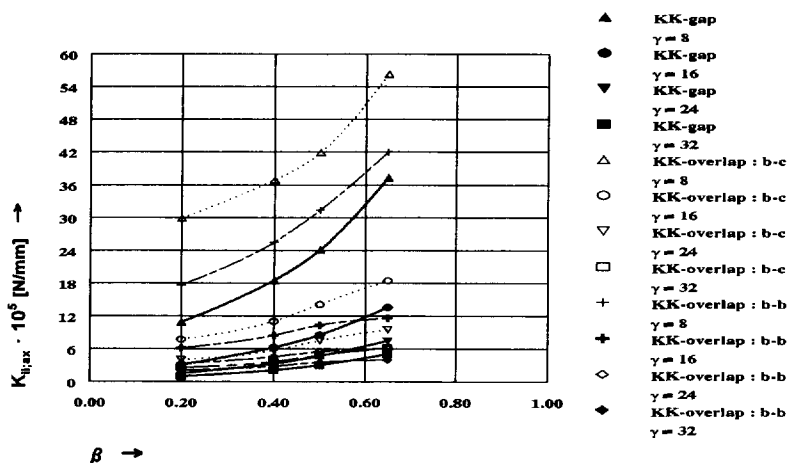
Figure 27. Multiplanar joints: influence of joint parameters β and γ and joint geometry on the axial joint flexibility behaviour. KK joints: $\varphi_{ip} = 45°$ and $\varphi_{op} = 90°$. $\tau = 0.50$.
(b-b = brace to brace connection and b-c = brace to chord connection).

The significance of spring pivot terms $K_{ii;ax}$

The significance of $K_{ii;ax}$ of a lattice girder is investigated by comparison of $K_{ii;ax}$ with the member stiffness coefficient $K_{br;ax}$. To enable this comparison, the term stiffness ratio (SR_{ax}) is introduced as:

52

$$SR_{ax} = \frac{K_{ii;ax}}{K_{br;ax}} \qquad \text{with} \qquad K_{br;ax} = \frac{2 \cdot E \cdot A_{br}}{L_{br}}$$

A decrease of the stiffness ratio SR_{ax} results in an increase of the significance of joint flexibility behaviour $K_{ii;ax}$ on the load distribution and deflection compared to rigidly connected.

As an example, results on SR_{ax} for a T joint are given in figure 28. For the comparison, the relation between brace length and brace dimensions is based on values commonly used in offshore design, i.e. the brace slenderness is taken λ=80, and the buckling length is taken $L_k = 0.80 \cdot L$.
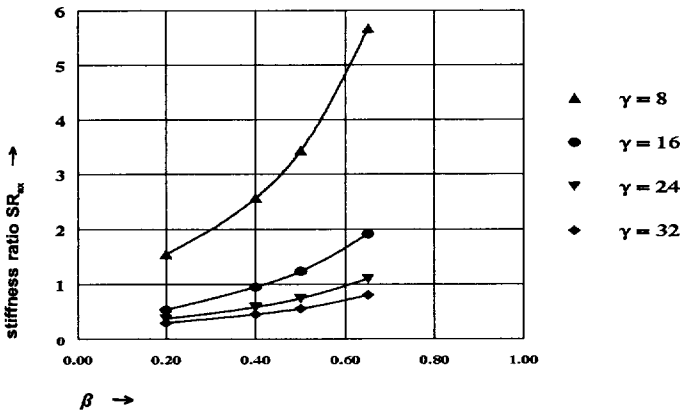
Figure 28. Stiffness ratio (SR_{ax}) for T joints (chord $d_0 = 300$; $r = 0.50$).

It is concluded that:

- The axial joint flexibility is significant in comparison to the axial brace member flexibility.
- The value of $K_{ii;ax}$ depends on the type of joint (uniplanar-multiplanar; gap-overlap), the number of connecting braces and the joint parameters β, γ, τ, φ_{ip} and φ_{op}.
  Generally, uniplanar joints with a low number of connecting braces, a small β ratio, a large γ ratio and a large value of φ_{ip} results in a small value of $K_{ii;ax}$.

The significance of spring cross terms $K_{ij;ax}$

For certain types of joints, especially multiplanar XX joints, the influence of cross terms in case of axially loaded multiplanar brace members cannot be neglected if the horizontal members cannot translate horizontally free. This undermines the

53

accepted philosophy that pin ended or fixed member ends and ignoring the joint flexibility gives correct axial forces in the members of lattice structures.

Figure 29 shows the ratio R/F for a multiplanar XX joint, in which F is the (balanced) axial force on the vertical brace members ($F_{br;ax;a,b}$), and R is the (balanced) reaction force on the horizontal brace members ($R_{br;ax;c,d}$). For the investigated range of joint parameters, with:

γ = 8; 14; 20; 26 and 32 : β = 0.3; 0.4; 0.5 and 0.6 : τ = 0.25; 0.50 and 1.00,
the largest variation in the ratio R/F is:

R/F = 0.46   for γ = 8 ; β = 0.60 and τ = 0.25 .
R/F = 0.92   for γ = 32 ; β = 0.60 and τ = 1.00 .

In case of a beam modelled multiplanar XX joint the ratio R/F is always zero, because the horizontal deflection of the joint is assumed to be zero.
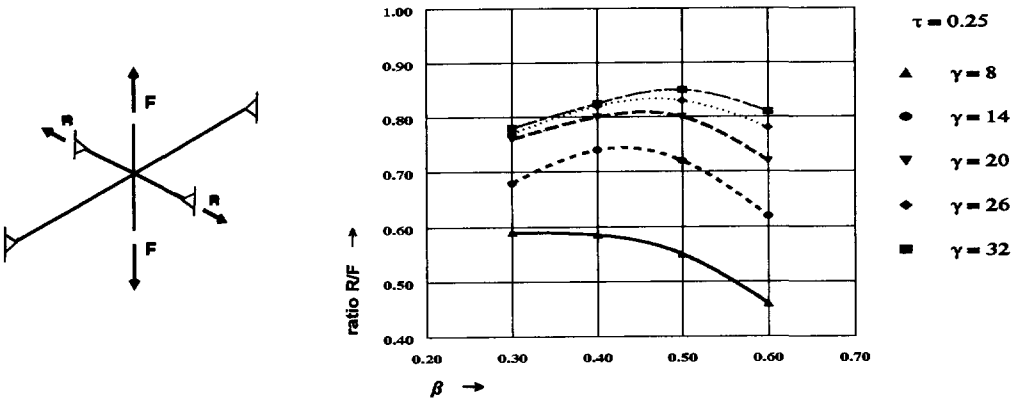
Figure 29.   XX joint: axial carry-over effect due to joint flexibility.

4.3   *Methods of numerical idealization of lattice girders*

For analysing the deflections and load distribution of a tubular lattice girder in the linear elastic range, different methods of numerical idealizations M_j are identified (see also figures 30 and 31), namely:

M_1   *Girder modelled with beam elements and rigid joints.*
M_2   *Girder modelled with beam elements, where braces are pin ended*
       and the chords are continuous.
M_3   *Girder modelled with beam elements, where brace and chord member ends are pin ended (as far as no mechanisms are formed).*

M_4 Girder modelled with beam elements and springs (or flexible brace member ends) representing the joint flexibility.

M_5 Girder modelled with beam elements for the member parts only, and a shell / solid element mesh for the joints.

M_6 Girder modelled with beam elements for the member parts only, and a substructure technique applied for the joint stiffness matrices.

For the idealization method M_4, joint stiffness coefficients K_{ij} (spring pivot terms) based on the difference in displacement between a joint modelled with beam elements and a joint modelled with shell elements have been included.

For the idealization methods M_{1-4}, the fictitious brace member parts inside the chord member are taken infinitely stiff.
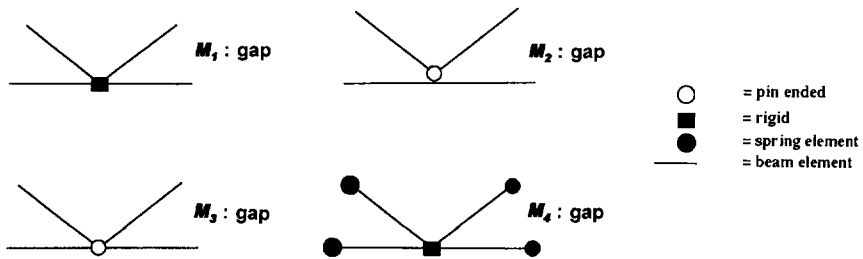
Figure 30. Investigated methods of numerical idealizations M_{1-4} of lattice girders.
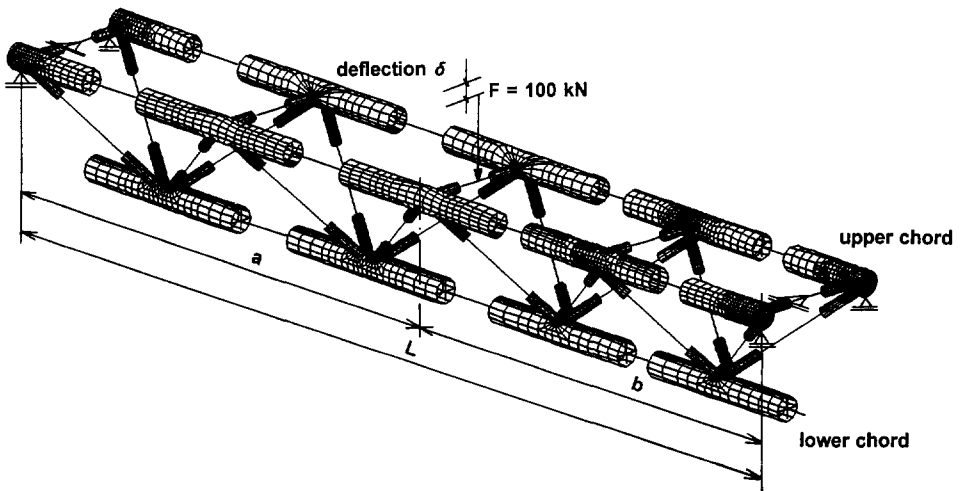
Figure 31. Investigated method of numerical idealization M_5 of lattice girders.

55

The (dis)advantages of using a certain numerical idealization M_j on the required experience and the computer costs are summarized in table 10.

Table 10.   (Dis)advantages for various methods of numerical idealization for tubular lattice girders.

Aspects considered	- = low o = average + = above average ++ = high +++ = extreme	Numerical idealization [M_j]					
		M_1	M_2	M_3	M_4	M_5	M_6
Experience required		-	-	-	o	+++	+++

Costs
   - software/hardware
   - preprocessing time
   - CPU-time
   - disk space (ds)
		-
		-
		-
		-
			-
			-
			-
			-
				-
				-
				-
				-
					+
					++
					-
					-
						++
						+++
						+++
						+++
							++
							+++
							+++
							+++

4.4   Influence of different methods of numerical idealization of lattice girders on deflection and load distribution

4.4.1   Type of lattice girders analysed

For calibration purposes, tubular multiplanar triangular girders tested in the framework of the ECSC research programme [F23] have been studied to investigate the influence of the different methods of numerical idealization as summarized in chapter 4.3. Also, alternative girders have been studied, which are similar to the girders that have been tested.
The main configuration (FE model shown in figure 31) and dimensions of the girders S_i analysed are given in figure 41 (chapter 5) and table 11.

Table 11. Girders analysed to study the influence of methods of numerical idealizations
            of tubular lattice girders on the deflections and load distribution.

Analysed girders [S_i]	Type of multiplanar joint	Joint parameters chord ⌀193.7; $\tau = 0.50$		Remark: for tested girders see also chapter 5
		γ	β	
S_1 S_2 S_3	gap gap + 100% overlap 100% overlap	12 12 12	0.40 0.40 0.40	tested girder 5
S_4 S_5 S_6	gap gap + 100% overlap 100% overlap	6 6 6	0.40 0.40 0.40	tested girder 6
S_7	gap + 50% overlap	12	0.60	tested girder 7
S_8	gap + 50% overlap	6	0.60	tested girder 8

56

Within the framework of this research, as shown in table 12, a restricted number of combinations, so-called S_i - M_j have been carried out.

Table 12. Analysed girders S_i for numerical analysis methods M_j.

* = done - = not done	M_1	M_2	M_3	M_4	M_5	M_6
S_1 S_2 S_3	* * *	* * *	* * -	* * *	* * *	- - -
S_4 S_5 S_6	* * *	* * *	* * -	* * *	* * *	- - -
S_7	*	*	-	-	-	-
S_8	*	-	-	-	-	-

For the numerical work, only half of the girder is considered because of symmetrical geometry, loading and boundary conditions.

Using numerical idealization M_5, in spite of using a shell element type and not modelling the weld shape, a minimum disk space of 700 Mb (carried out in 1992) is required for analysing half of the girder.

4.4.2 Results of different methods of numerical idealization of lattice girders on the deflection

The numerical results for the analysed combinations S_i - M_j and the experimental results [F23], for the maximum deflection of the upper chord (as shown figure 31) and various comparisons are given in table 13.

Table 13. Numerically and experimentally obtained maximum deflection δ ($\cdot 10^{-1}$ mm) for the upper chord. (Load case F=100kN as shown in figure 31).

Analysed girder	Numerical calculated deflection					Deflection in test	Ratios				
	M_1	M_2	M_3	M_4	M_5		M_2/M_1	M_4/M_1	M_5/M_3	M_3/M_4	test/M_1
S1	38.6	38.7	40.7	45.9	45.6		1.00	1.18	1.12	0.99	
S2	32.1	32.3	34.3	37.2	36.3	37.5	1.01	1.13	1.06	0.98	1.17
S3	26.2	26.4		32.0	31.9		1.01	1.22		1.00	
S4	20.3	20.4	21.4	23.5	22.4		1.00	1.10	1.05	0.96	
S5	17.0	17.2	18.1	19.5	18.6	17.8	1.01	1.09	1.03	0.96	1.05
S6	13.9	14.1		15.9	15.7		1.01	1.13		0.99	
S7	29.5	29.8				34.4	1.01				1.17
S8	15.4					17.3					1.12

57

From table 13, the following conclusions on the maximum deflection are made:

- The difference in deflection between M_1 (beam elements with rigid joints) and M_2 (beam elements with pin ended brace members) is negligible. Both idealizations underestimate the real deflection, and the size of underestimation grows with increasing γ.
  This supports the significance of joint flexibility on the structural behaviour of lattice girders ($K_{ii;ax}$) as mentioned in chapter 4.2.
  For the girders considered, a relatively low brace member slenderness (assuming $L_k = 0.8L$, the slenderness varies between $25 < \lambda < 40$) is used compared to offshore structures ($\lambda \approx 80$), which results in a small stiffness ratio SR_{ax} as explained in chapter 4.2. Therefore, for the girders analysed, there is a relatively large contribution of joint flexibility on the deflection.
- A good agreement between M_4 (beam elements with springs) and M_5 (beam elements with FE modelled joints) is found, which shows for the structures analysed the (expected) small influence of the cross terms of axial joint stiffness coefficients $K_{ij;ax}$ ($i \neq j$) on the deflection.
- When comparing M_3 (pin ended beam elements) with M_5, the use of pin connections still underestimates the deflection.
  Identical conclusions are given by Frater and Packer [s7], namely that the idealizations M_{1-3} underestimate the real deflection by 12% to 15% for gap connected uniplanar rectangular lattice girders.
- Because of their higher stiffness, overlap joints give smaller deviations than the gap joints.
- For practical situations, when using idealization method M_1, a multiplication factor α_M to account for the influence of joint flexibility on the total deflection is proposed, so that $\delta_{tot} = \alpha_M \cdot \delta_i$.
  The value of α_M depends on the stiffness ratio SR_{ax}, and the limits of this factor are expected to be $1.05 < \alpha_M < 1.20$ for girders with K or KK joints.

It is also worthwhile mentioning that:

- When comparing the deflection of the upper and lower chord, considering idealization M_5, a ratio up to $\dfrac{\delta_{upperchord}}{\delta_{lowerchord}} = 1.30$ has been found, which indicates the large effect of joint flexibility $K_{ii;ax}$ due to the low brace slenderness.

- A comparison of the fictitious moment of inertia $I_{fic.}$ for the tested girders obtained from the equation $I_{fic.} = \dfrac{F \cdot a^2 \cdot b^2}{3 \cdot E \cdot \delta_{test} \cdot L}$ (see also figure 31) with the theoretical moment of inertia $I_{gird.}$ (centre of the girder) has been carried out.
  Results of the comparison as given in table 14, show a variation of $0.44 < I_{fic.} / I_{gird.} < 0.57$ (caused by joint flexibility + member shear deformation).
  An increase of β gives an increase of the ratio $I_{fic.} / I_{gird.}$.

58

Table 14. Comparison of the moments of inertia for the girders that have been tested.

Tested girder	$I_{gird.} \cdot 10^5$ [mm⁴]	$I_{fic.} \cdot 10^5$ [mm⁴]	Ratio $I_{fic.} / I_{gird.}$
S2: girder 5; β=0.40	2.394	1.047	0.44
S5: girder 6; β=0.40	4.573	2.206	0.48
S7: girder 7; β=0.60	2.394	1.321	0.55
S8: girder 8; β=0.60	4.573	2.627	0.57

4.4.3 Results of different methods of numerical idealization of lattice girders on the load distribution

The four tested girders are provided with strain gauges at two cross sections of all members (chord and braces), to determine the axial strains ϵ_{ax} and bending strains ϵ_{ip} and ϵ_{op}. The distance between the strain gauges and the joints is $3d_{1-4}$ for the braces and $3d_0$ for the chord to avoid end effects on the measurements.
The measured axial and bending strains in the braces and chord have been linearly extrapolated to the intersection of the brace centre line and chord outer wall surface for determining the nominal strains (see also figure 3).
For the lattice girders S_2 - M_{1-5} (girder 5) and S_5 - M_{1-5} (girder 6) with S_i the analysed girder according to table 11 and M_j the method of numerical idealization as described in chapter 4.3, the analysed and measured results of the load distribution by means of (extrapolated) nominal strains ϵ_{ax}, ϵ_{ipb}, ϵ_{opb} and total nominal strains ϵ_{tot} with $\epsilon_{tot} = \epsilon_{ax} \pm \sqrt{\epsilon^2_{ipb} + \epsilon^2_{opb}}$ are given in tables 15 and 16.
The strains are given for the upper chord (member CA), lower chord (member CC) and braces (members A, C, E, G, I, K, M, O), and are analysed for a boundary and load condition as shown in figure 31. The location of the members inside the girders is explained in figure 32.
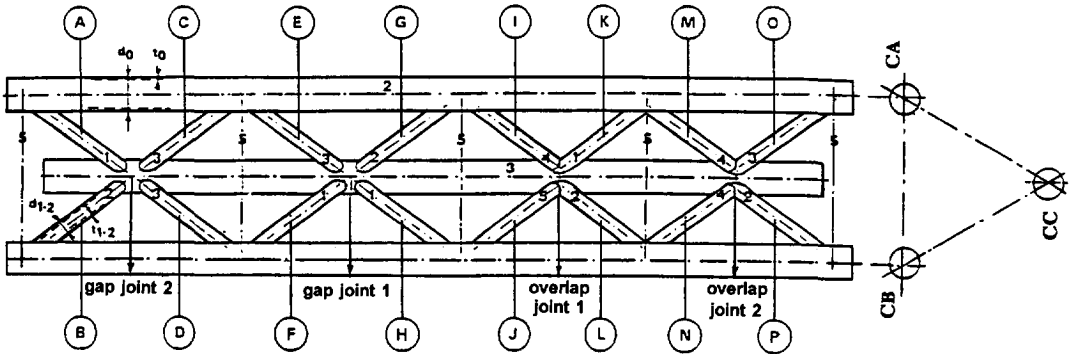
Figure 32. Location of members inside the girders S_i.

Some results of comparison of the numerical and experimental results on ϵ_{tot} as given in tables 15 and 16 are shown in figures 33 and 34.

For the comparison given in figures 33 and 34, the test results on ϵ_{tot} are given on the horizontal axis, and the numerical results on ϵ_{tot} are given on the vertical axis.
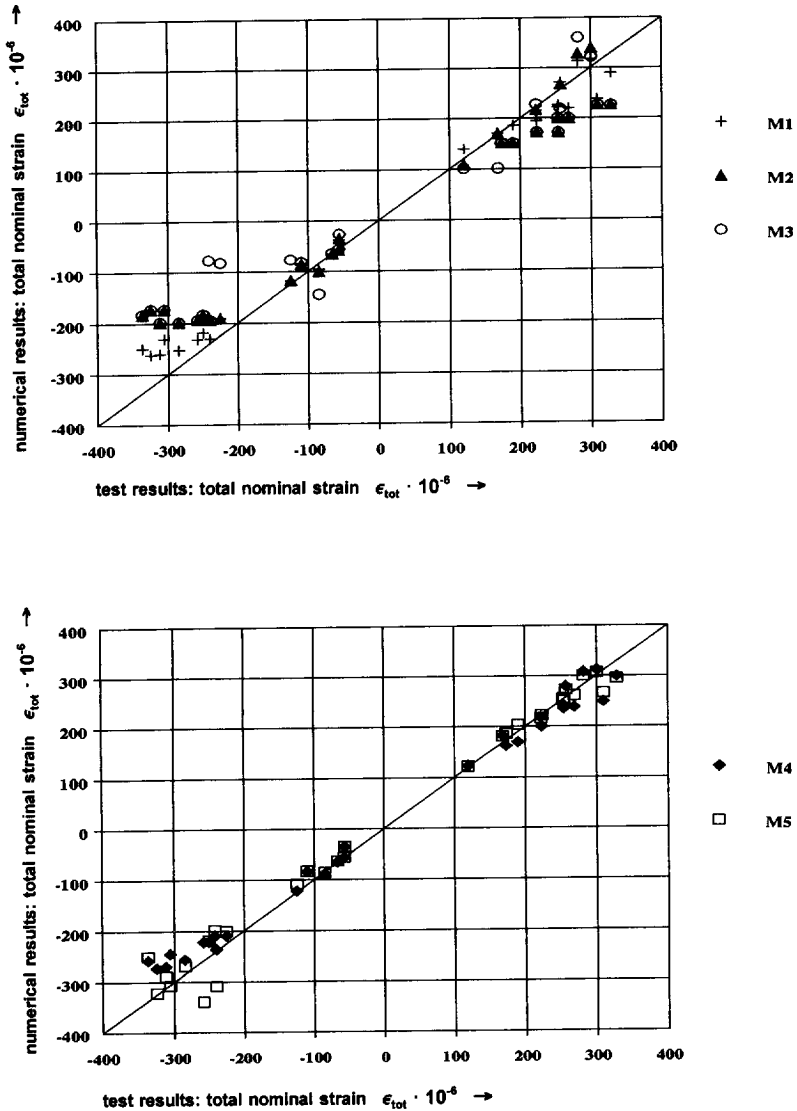
Figure 33. Comparison of experimental and numerical M_{1-5} results on ϵ_{tot} for girder 5. (Idealizations M_{1-3} top figure and idealizations M_{4-5} bottom figure).
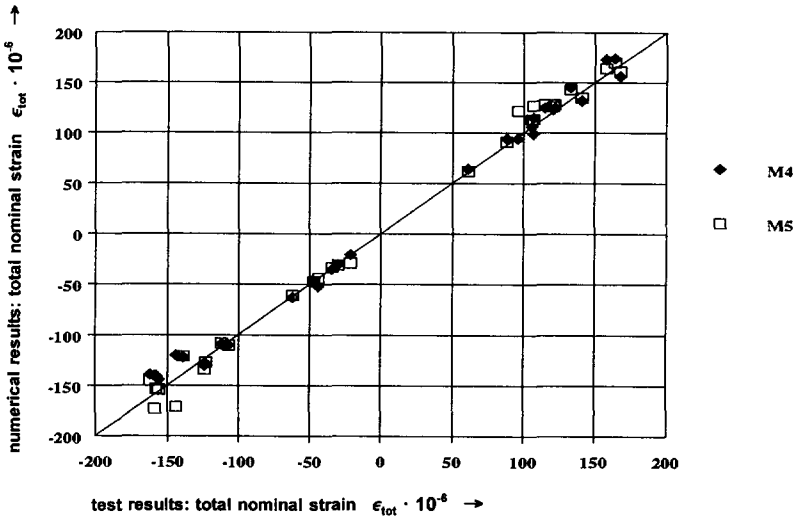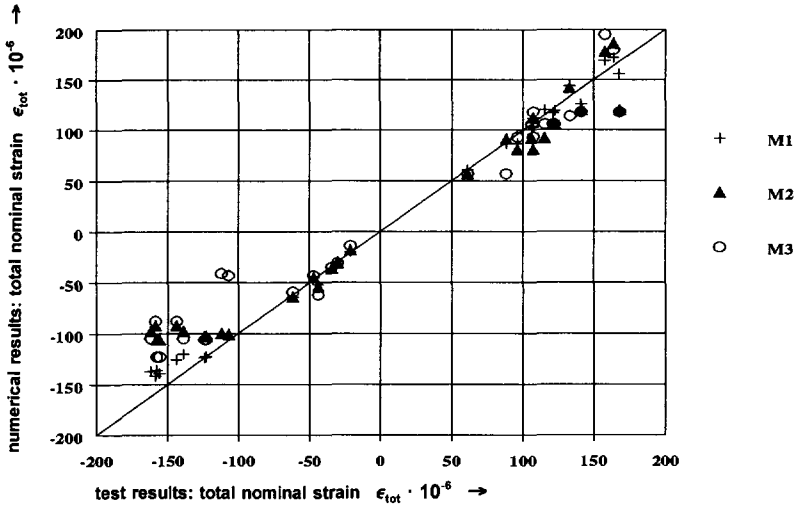
Figure 34. Comparison of experimental and numerical M_{1-5} results on ϵ_{tot} for girder 6.
(Idealizations M_{1-3} top figure and idealizations M_{4-5} bottom figure).

61

Table 15a: Analysed nominal strains $\epsilon \cdot 10^{-6}$ for numerical idealizations M_{1-3} of girder 5 (S_2 - M_{1-3}).

S_2	M_1					M_2					M_3				
member	ax.	ipb.	opb.	tot	tot/ax.	ax.	ipb.	opb.	tot	tot/ax.	ax.	ipb.	opb.	tot	tot/ax.
CA-a	-27	-12	27	-57	2.1	-27	-11	29	-58	2.1	-27	-10	28	-57	2.1
c	"	10	-5	-38	1.4	"	5	-6	-35	1.3	"	0	0	-27	1.0
CA-e	-78	2	-6	-84	1.1	-78	5	-6	-86	1.1	-82	0	0	-82	1.0
g	"	97	59	-191	2.4	"	96	60	-191	2.5	"	0	0	-82	1.0
CA-i	-76	98	59	-191	2.5	-76	96	60	-189	2.5	-77	0	0	-77	1.0
k	"	-42	-4	-118	1.6	"	-42	-3	-118	1.6	"	0	0	-77	1.0
CA-m	-31	65	-3	-96	3.1	-31	69	-3	-100	3.2	-30	115	0	-145	4.8
o	"	-9	34	-66	2.2	"	10	33	-66	2.1	"	-6	34	-65	2.1
CC-c	108	-8	-4	140	1.3	108	0	0	108	1.0	101	0	0	101	1.0
e	"	55	31	171	1.6	"	54	31	170	1.6	"	0	0	101	1.0
CC-g	205	58	33	271	1.3	206	54	31	268	1.3	219	0	0	219	1.0
i	"	9	5	215	1.1	"	9	5	216	1.1	"	8	4	228	1.1
CC-k	109	177	102	313	2.9	110	189	109	328	3.0	104	222	128	360	3.5
m	"	-180	-103	316	2.9	"	-199	-115	340	3.1	"	-188	-109	321	3.1
A-ca	199	21	1	220	1.1	200					200				
cc	"	-22	7	222	1.2	"					"				
C-ca	-193	-39	-5	-231	1.2	-194					-200				
cc	"	38	2	-232	1.2	"					"				
E-ca	172	54	1	226	1.3	172					199				
cc	"	-22	8	195	1.1	"	no bending on brace members → tot/ax. = 1.0				"	no bending on brace members → tot/ax. = 1.0			
G-ca	-181	60	36	-250	1.4	-183					-198				
cc	"	-26	-28	-219	1.2	"					"				
I-ca	-196	51	39	-260	1.3	-199					-238				
cc	"	-43	-38	-253	1.3	"					"				
K-ca	155	-1	3	158	1.0	151					182				
cc	"	26	17	186	1.2	"					"				
M-ca	-175	54	12	-231	1.3	-173					-161				
cc	"	80	-34	-262	1.5	"					"				
O-ca	225	5	-13	238	1.1	226					216				
cc	"	51	41	290	1.3	"					"				

Table 15b: Analysed nominal strains $\epsilon \cdot 10^{-6}$ for numerical idealizations S_2 - M_{4-5} and measured strains of girder 5.

S_2	M_4					M_5					tested girder 5				
member	ax.	ipb.	opb.	tot	tot/ax.	ax.	ipb.	opb.	tot	tot/ax.	ax.	ipb.	opb.	tot	tot/ax.
CA-a	-27	-13	27	-57	2.1	-27	-11	27	-56	2.1	-27	-14	27	-57	2.1
c	"	6	-6	-35	1.3	"	5	-5	-34	1.3	"	2	-29	-56	2.1
CA-e	-77	6	-3	-84	1.1	-77	0	-6	-83	1.1	-75	14	-32	-110	1.5
g	"	117	64	-210	2.7	"	108	61	-201	2.6	"	99	113	-225	3.0
CA-i	-75	117	67	-210	2.8	-75	108	61	-199	2.7	-68	134	111	-242	3.6
k	"	-47	-4	-122	1.6	"	-33	-3	-108	1.5	"	-52	-25	-125	1.8
CA-m	-31	58	-5	-89	2.9	-31	55	-1	-86	2.8	-33	49	-20	-85	2.6
o	"	33	14	-65	2.1	"	-6	32	-63	2.0	"	-10	32	-66	2.0
CC-c	108	-13	-7	123	1.1	108	-13	-7	122	1.1	104	-14	-8	120	1.2
e	"	64	37	182	1.7	"	63	36	181	1.7	"	55	32	168	1.6
CC-g	202	67	38	279	1.4	204	60	34	273	1.3	190	58	34	257	1.4
i	"	14	8	218	1.1	"	10	6	216	1.1	"	28	16	222	1.2
CC-k	110	171	99	308	2.8	109	166	96	300	2.8	105	153	88	282	2.7
m	"	-176	-100	312	2.8	"	-171	-99	307	2.8	"	-170	-98	301	2.9
A-ca	200	38	0	238	1.2	199	56	-28	262	1.3	196	49	-54	269	1.4
cc	"	-42	8	242	1.2	"	-49	28	255	1.3	"	-42	39	253	1.3
C-ca	-192	-29	-6	-222	1.2	-191	-65	-11	-256	1.3	-191	-61	-27	-258	1.4
cc	"	44	2	-236	1.2	"	54	11	-246	1.3	"	49	-7	-240	1.3
E-ca	165	70	2	235	1.4	169	80	9	250	1.5	155	99	0	254	1.6
cc	"	-33	11	200	1.2	"	-50	16	222	1.3	"	-62	-28	223	1.4
G-ca	-176	71	41	-258	1.5	-180	61	35	-250	1.4	-162	93	148	-337	2.1
cc	"	-31	-33	-221	1.3	"	-28	-26	-219	1.2	"	-36	-80	-250	1.5
I-ca	-188	66	48	-270	1.4	-195	85	-40	-289	1.5	-173	90	107	-315	1.8
cc	"	-54	-41	-256	1.4	"	-67	31	-269	1.4	"	-90	-68	-285	1.6
K-ca	149	13	2	162	1.1	155	23	22	187	1.2	140	-33	-2	173	1.2
cc	"	15	13	169	1.1	"	48	7	204	1.3	"	39	31	190	1.4
M-ca	-176	68	-12	-245	1.4	-176	132	-7	-308	1.8	-179	119	-43	-306	1.7
cc	"	-89	38	-273	1.6	"	-145	-20	-322	1.8	"	-146	-12	-325	1.8
O-ca	226	6	-22	249	1.1	225	36	-23	267	1.2	223	33	-80	310	1.4
cc	"	51	52	299	1.3	"	46	52	295	1.3	"	50	93	329	1.5

Table 16a. Analysed nominal strains $\epsilon \cdot 10^{-6}$ for numerical idealizations M_{1-3} of girder 6 (S_5 - M_{1-3}).

S_5	M_1					M_2					M_3				
member	ax.	ipb.	opb.	tot	tot/ax.	ax.	ipb.	opb.	tot	tot/ax.	ax.	ipb.	opb.	tot	tot/ax.
CA-a	-14	-6	15	-30	2.1	-14	-6	16	-31	2.2	-14	-6	16	-31	2.2
c	"	5	-3	-20	1.4	"	2	-4	-18	1.3	"	0	0	-14	1.0
CA-e	-41	1	-3	-44	1.1	-41	2	-4	-45	1.1	-43	0	0	-43	1.0
g	"	51	31	-100	2.4	"	51	31	-101	2.5	"	0	0	-43	1.0
CA-i	-40	52	30	-100	2.4	-40	51	31	-100	2.5	-41	0	0	-41	1.0
k	"	-24	-2	-64	1.6	"	-24	-2	-64	1.6	"	-18	2	-59	1.4
CA-m	-16	36	2	-52	3.3	-16	38	-2	-54	3.4	-16	46	2	-62	3.8
o	"	-5	-19	-36	2.2	"	-5	19	-36	2.3	"	-4	19	-35	2.2
CC-c	57	-4	-2	61	1.1	57	0	0	57	1.0	57	0	0	57	1.0
e	"	29	17	87	1.5	"	29	17	91	1.6	"	0	0	57	1.0
CC-g	108	31	18	144	1.3	108	29	17	142	1.3	114	0	0	114	1.0
i	"	3	2	112	1.0	"	3	2	112	1.0	"	4	2	118	1.0
CC-k	57	97	56	169	3.0	58	104	60	178	3.1	56	120	70	195	3.5
m	"	-100	-57	172	3.0	"	-111	-64	186	3.2	"	-108	-62	180	3.2
A-ca	106	11	1	117	1.1	106					106				
cc	"	-12	3	119	1.1	"					"				
C-ca	-102	-21	-2	-124	1.2	-103					-106				
cc	"	21	1	-123	1.2	"					"				
E-ca	92	28	0	120	1.3	92					106				
cc	"	-11	5	104	1.1	"	no bending on brace members ⇒ tot/ax. = 1.0				"	no bending on brace members ⇒ tot/ax. = 1.0			
G-ca	-97	35	20	-137	1.4	-98					-105				
cc	"	-17	-15	-120	1.2	"					"				
I-ca	-104	28	21	-139	1.3	-106					-123				
cc	"	-24	21	-136	1.3	"					"				
K-ca	83	-3	-2	87	1.1	81					93				
cc	"	16	10	102	1.2	"					"				
M-ca	-93	32	7	-126	1.4	-92					-88				
cc	"	-46	-19	-142	1.5	"					"				
O-ca	119	2	-7	126	1.1	120					118				
cc	"	29	23	156	1.3	"					"				

Table 16b: Analysed nominal strains $\epsilon \cdot 10^{-6}$ for numerical idealizations S_2 - M_{4-5} and measured strains of girder 6.

S_5	M_4					M_5					tested girder 6				
member	ax.	ipb.	opb.	tot	tot/ax.	ax.	ipb.	opb.	tot	tot/ax.	ax.	ipb.	opb.	tot	tot/ax.
CA-a	-14	-7	15	-31	2.2	-14	-7	16	-31	2.2	-13	-7	15	-30	2.3
c	"	5	-5	-21	1.5	"	3	-5	-29	2.1	"	2	-8	-21	1.6
CA-e	-41	1	-6	-47	1.1	-41	-3	-5	-47	1.2	-38	4	-8	-47	1.2
g	"	58	38	-110	2.7	"	60	34	-110	2.7	"	54	44	-107	2.8
CA-i	-40	58	38	-109	2.7	-40	59	34	-108	2.7	-37	60	45	-112	3.0
k	"	-23	-4	-63	1.6	"	-21	-3	-61	1.5	"	-23	-10	-62	1.7
CA-m	-16	36	-4	-52	3.3	-16	28	1	-44	2.8	-15	29	-4	-44	2.9
o	"	-5	19	-35	2.2	"	-3	17	-33	2.1	"	-11	15	-34	2.3
CC-c	57	-6	-3	64	1.1	57	-4	-3	-62	1.1	54	-6	-4	61	1.1
e	"	32	18	94	1.7	"	29	17	-91	1.6	"	30	17	88	1.6
CC-g	107	33	19	145	1.4	107	31	18	143	1.4	99	29	17	133	1.3
i	"	7	4	115	1.1	"	5	3	113	1.1	"	7	4	107	1.1
CC-k	58	100	-57	173	3.0	58	92	53	164	2.8	54	90	52	158	2.9
m	"	-101	-58	174	3.0	"	-97	-55	170	2.9	"	-95	-55	164	3.0
A-ca	106	-17	-2	123	1.2	106	19	-7	126	1.2	104	7	-16	121	1.2
cc	"	18	6	125	1.2	"	17	14	128	1.2	"	-9	16	122	1.2
C-ca	-102	-28	-5	-130	1.3	-102	-32	3	-134	1.3	-103	-16	13	-123	1.2
cc	"	27	2	-129	1.3	"	24	-6	-127	1.2	"	18	-9	-123	1.2
E-ca	90	35	2	125	1.4	90	38	-3	128	1.4	87	29	-2	115	1.3
cc	"	-16	4	106	1.2	"	-20	12	113	1.3	"	-17	8	106	1.2
G-ca	-94	36	27	-139	1.5	-94	36	36	-145	1.5	-91	51	49	-162	1.8
cc	"	-16	-23	-122	1.3	"	-21	-27	-121	1.3	"	-29	-38	-139	1.5
I-ca	-102	31	28	-144	1.4	-102	38	36	-154	1.5	-99	44	37	-156	1.6
cc	"	-25	-28	-140	1.4	"	-45	-25	-153	1.5	"	-49	-34	-158	1.6
K-ca	81	-13	1	94	1.2	82	-40	-2	122	1.5	80	-16	-3	96	1.2
cc	"	16	8	99	1.2	"	44	10	127	1.5	"	25	11	107	1.3
M-ca	-93	27	6	-120	1.3	-94	77	6	-171	1.8	-92	52	-4	-144	1.6
cc	"	-43	-20	-140	1.5	"	-78	-15	-173	1.8	"	67	-7	-159	1.7
O-ca	119	7	11	132	1.1	120	-9	-12	135	1.1	118	2	-23	141	1.2
cc	"	25	27	156	1.3	"	31	27	161	1.3	"	37	33	168	1.4

63

For the ϵ_{ax} and ϵ_{tot} results obtained from the tested girders 5, 6, 7 and 8, the figures 35 and 36 show the relation between ϵ_{ax} (horizontal axis) and the ratio ϵ_{tot} / ϵ_{ax} (vertical axis). This relation forms a first indication on the importance of secondary bending moments regarding the fatigue design of joints. For the minimum, maximum and average strain ratio ϵ_{tot} / ϵ_{ax}, the test results from figures 35 and 36 are summarized in table 17.
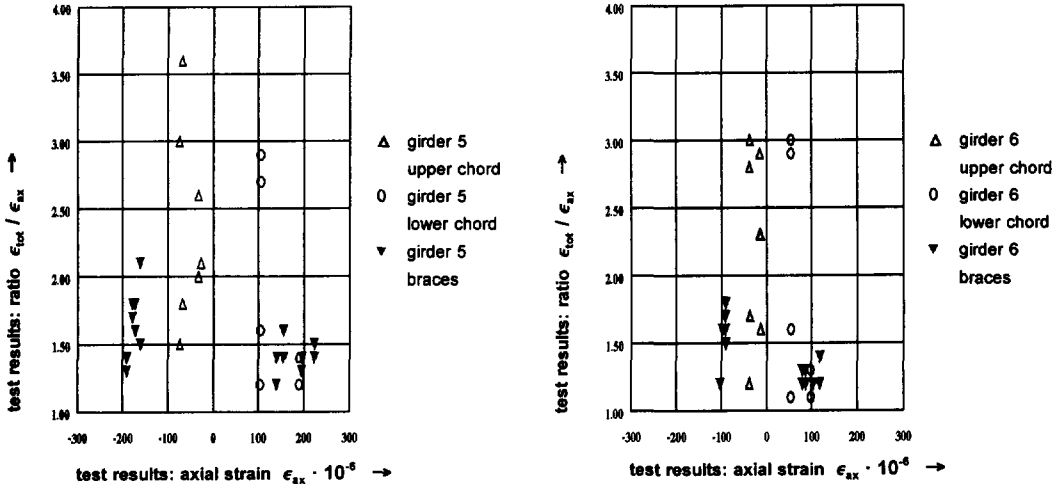
Figure 35. Relation between ϵ_{ax} and the ratio ε_{tot} / ε_{ax} for tested girder 5 (left figure) and tested girder 6 (right figure).
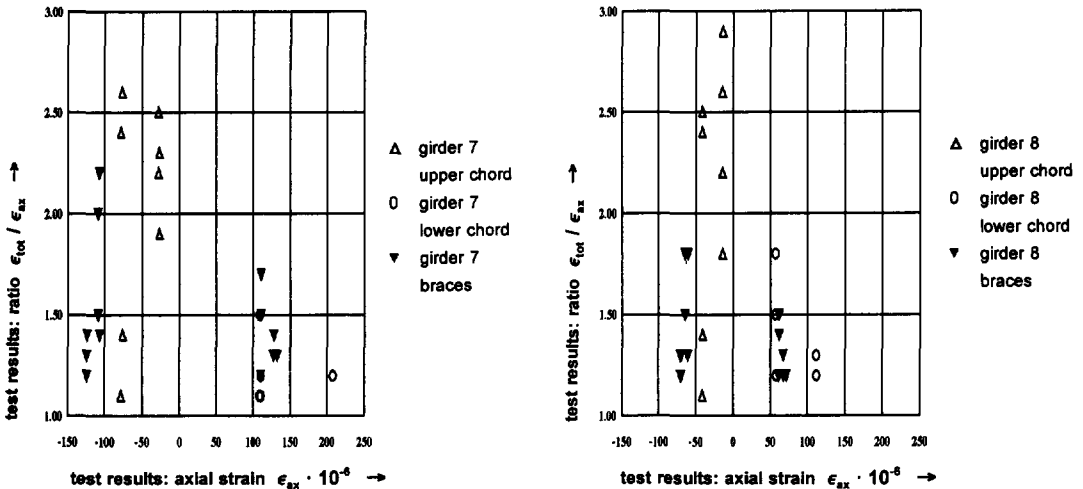
Figure 36. Relation between ϵ_{ax} and the ratio ϵ_{tot} / ϵ_{ax} for tested girder 7 (left figure) and tested girder 8 (right figure).

Table 17.   Measured ratio on ϵ_{tot} / ϵ_{ax} for the tested girders 5, 6, 7 and 8.

Ratio ϵ_{tot} / ϵ_{ax}	Upper chord	Lower chord	Braces	Upper chord	Lower chord	Braces
	girder 5 (S_2)			girder 6 (S_6)		
minimum ratio	1.5	1.2	1.2	1.2	1.1	1.2
maximum ratio	3.6	2.9	2.1	3.0	3.0	1.8
average ratio	2.4	1.8	· 1.5	2.3	1.8	1.4
	girder 7 (S_7)			girder 8 (S_8)		
minimum ratio	1.1	1.1	1.2	1.1	1.2	1.2
maximum ratio	2.6	1.5	2.2	2.9	1.8	1.8
average ratio	2.1	1.2	1.5	2.1	1.4	1.3

In an identical way as described for the figures 35 and 36 and table 17, the numerical results from the analysed girders S_{1-6} using idealization M_5 (beam elements with FE modelled joints) are given in figures 37 and 38 and table 18.
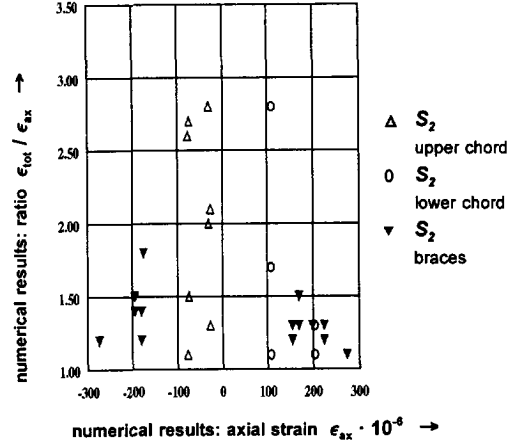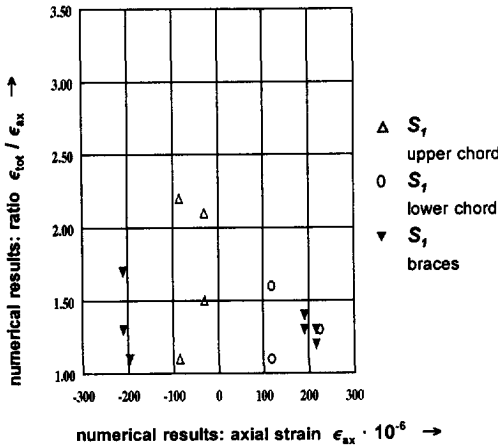
Figure 37.
Relation between ϵ_{ax} and the ratio ϵ_{tot} / ε_{ax} for the analysed girders S_{1-3} using girder idealization M_5 (beam elements with FE modelled joints).
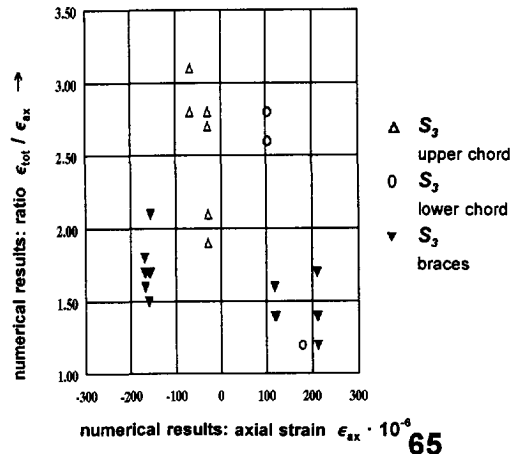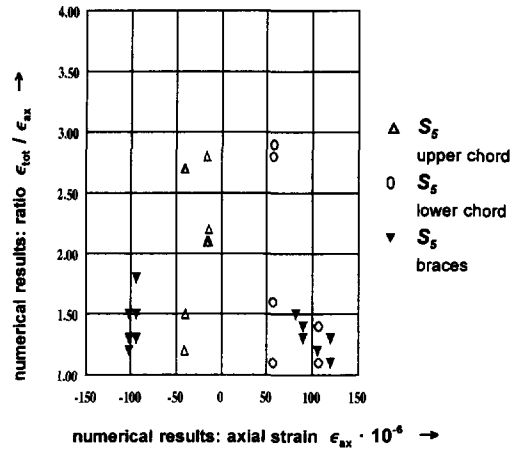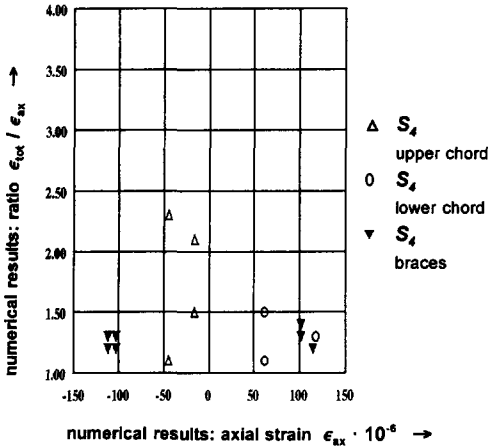
Figure 38.
Relation between ϵ_{ax} and the ratio ϵ_{tot} / ϵ_{ax} for the analysed girders S_{4-6} using girder idealization M_5 (beam elements with FE modelled joints).
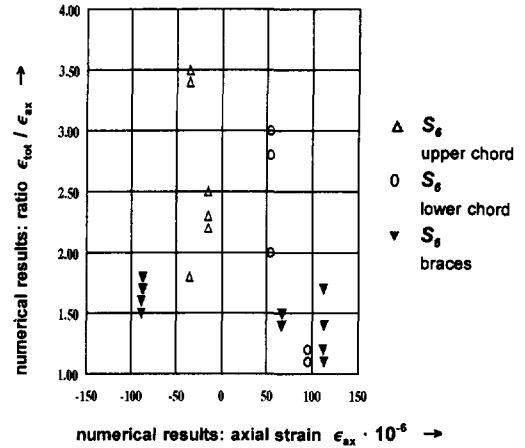
Table 18. Analysed ratio on ϵ_{tot} / ϵ_{ax} for the girders S_{1-6} using girder idealization M_5. (Explanation on the configuration of the girders S_{1-6} is given in table 11).

Ratio ϵ_{tot} / ϵ_{ax}	Upper chord	Lower chord	Braces	Upper chord	Lower chord	Braces	Upper chord	Lower chord	Braces
	S_1			S_2			S_3		
minimum ratio	1.1	1.1	1.1	1.1	1.1	1.1	1.9	1.2	1.2
maximum ratio	2.2	1.6	1.7	2.8	2.8	1.8	3.1	2.8	2.1
average ratio	1.8	1.3	1.3	2.1	1.8	1.4	2.7	2.2	1.6
	S_4			S_5			S_6		
minimum ratio	1.1	1.1	1.2	1.2	1.1	1.1	1.8	1.1	1.1
maximum ratio	2.3	1.5	1.4	2.8	2.9	1.8	3.5	3.0	1.8
average ratio	1.8	1.3	1.3	2.2	1.8	1.4	2.5	2.2	1.6

The influence of the joint parameters β and γ on the measured strain ratio $\epsilon_{tot} / \epsilon_{ax}$ for the tension loaded brace members of the lower chord joints is shown in figure 39.
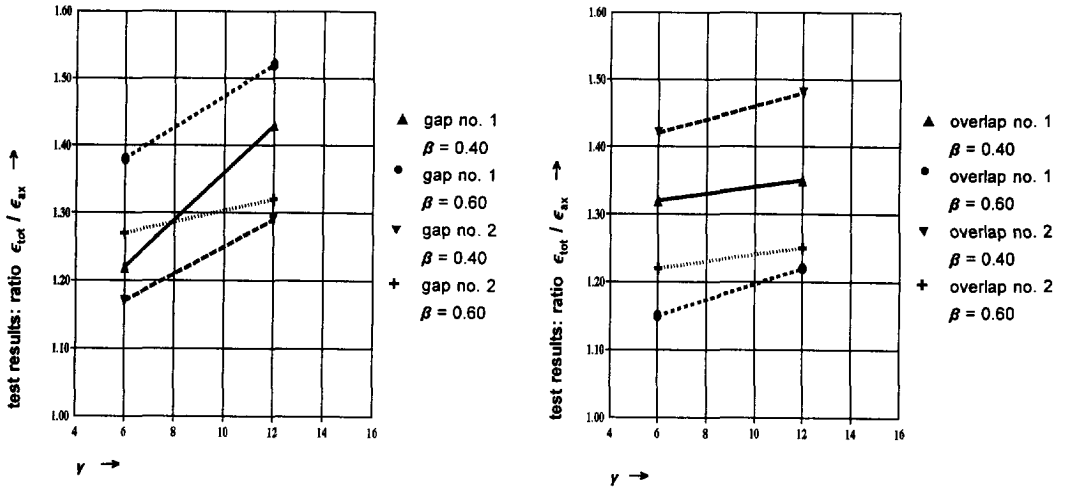
Figure 39. Relationship between joint parameters β and γ and strain ratio $\epsilon_{tot} / \epsilon_{ax}$. Gap joints left figure and overlap joints right figure).

From the experimental results (tested girders 5, 6, 7 and 8) and the numerical results (analysed combinations S_i - M_j) on the load distribution of multiplanar tubular lattice girders, the following conclusions are made.

- Axial strain distribution ϵ_{ax}
Comparison between numerical and experimental results.
<u>Chord member:</u>
$M_{1,2,3,4,5}$:   All numerical idealizations considered give nearly similar values on ϵ_{ax} (differences within 10%) and a good agreement with experimental results.
<u>Brace member:</u>
$M_{1,2,4,5}$:   Numerical idealizations $M_{1,2,4,5}$ give nearly similar values on ϵ_{ax} (differences within 10%), and a good agreement with experimental results.
M_3 :   Numerical idealization M_3 (all member ends pin ended) generally overestimates ϵ_{ax} (differences up to 20% are found).
Considering the results on comparison and the (dis)advantages as summarized in table 10, the use of numerical idealization M_1 (beam elements with rigid joints) or M_2 (continuous chord members and pin ended brace members) is recommended when analysing the axial load distribution ϵ_{ax}. However, as mentioned in chapter 4.2, depending on the type of structure and the type of joint, the axial joint flexibility $K_{ij;ax}$ can significantly affect the axial load distribution, which puts restrictions on the use of M_1 and M_2.

67

- Total strain ϵ_{tot}

Comparison between numerical and experimental results.

<u>Chord member:</u>

$M_{1,4,5}$:   A good agreement on ϵ_{tot} (differences within 15%) between the numerical and experimental results exists only, when using numerical idealizations $M_{1,4,5}$.

$M_{2,3}$:   Numerical idealizations $M_{2,3}$ (member ends pin ended) largely underestimates ϵ_{tot} (differences above 100% exist).

<u>Brace member:</u>

$M_{1,4,5}$:   For the numerical idealizations $M_{1,4,5}$, when comparing the numerical results with the experimental results, differences up to 40% on ϵ_{tot} exist, and as a rule, all numerical idealizations underestimates ϵ_{tot}.

The best agreement with the test results is found using method M_5, for which all joints are FE modelled.

M_1 : alter.   Use of an alternative numerical idealization on M_1, where the fictitious brace member parts inside the chord member are given brace properties instead of taking these infinitely stiff, gives inaccurate ϵ_{tot} for the brace members. This is especially true for girders containing overlap joints, where differences above 100% exist.

Results on the use of the alternative method M_1 are shown in figure 40.

$M_{2,3}$:   Numerical idealizations $M_{2,3}$ largely underestimates ϵ_{tot} (differences above 100% exist).
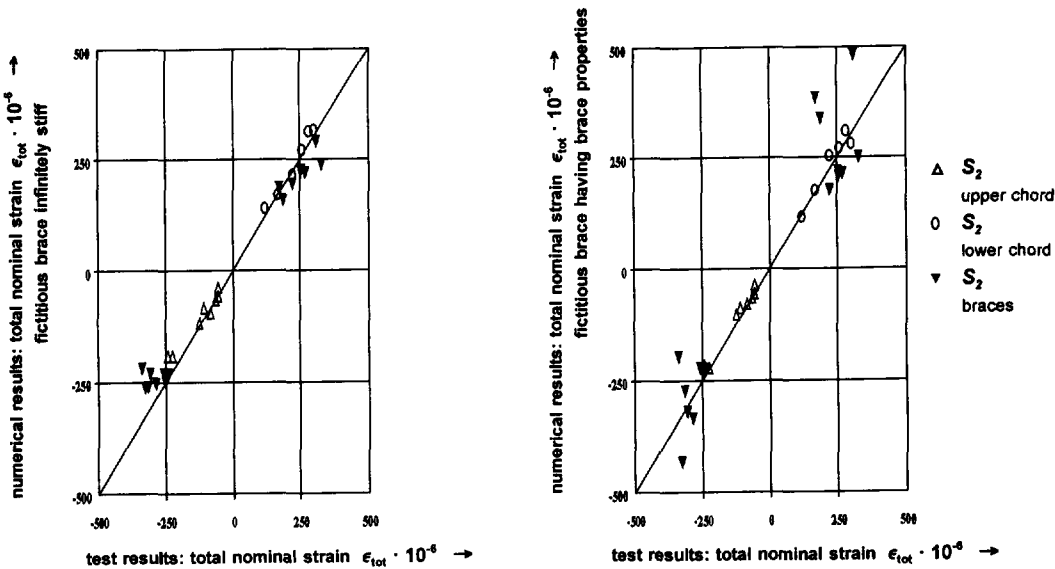
Figure 40. Influence of different geometrical properties for the fictitious brace member parts inside the chord member on the load distribution ϵ_{tot} for analysed girder S_2 (tested girder 5).

68

Considering the results on comparison and the (dis)advantages as summarized in table 10, when analysing the total strains ϵ_{tot} of structures subjected to fatigue loading, the use of numerical idealizations $M_{1,5}$ is recommended above the other numerical idealizations $M_{2,3,4}$.

However, for the brace members the recommended idealization M_1 still underestimates the real ϵ_{tot} up to 40%, which is due to the difference on bending strains.

A (large) disadvantage of the recommended idealization M_5 is the complexity in use.

- Contribution of bending strains on the total strain

For the experimental as well as numerical results, the contribution of bending strains on the total strain by means of the magnitude of the ratio $\epsilon_{tot} / \epsilon_{ax}$ mainly depends on the type of member (upper chord, lower chord, braces) and on the type of joint (gap, overlap).

A relatively small influence of the joint parameters β and γ on the ratio $\epsilon_{tot} / \epsilon_{ax}$ exists. From figure 39 it is found that:

- Increase of γ results in an increase of the ratio $\epsilon_{tot} / \epsilon_{ax}$.
  This is especially the case for gap joints.
- For the gap joints, increase of β results in an increase of the ratio $\epsilon_{tot} / \epsilon_{ax}$.
- For the overlap joints, increase of β results in a decrease of the ratio $\epsilon_{tot} / \epsilon_{ax}$.

For the experimental and numerical results, the obtained average magnitude of the ratio $\epsilon_{tot} / \epsilon_{ax}$ is for the upper chord, lower chord and braces summarized in table 19, in which also the existing multiplication factors on ϵ_{ax} to account for secondary bending moments in the fatigue design procedure for uniplanar tubular lattice structures according to [F12] are given.

Table 19. Average ratio $\epsilon_{tot} / \epsilon_{ax}$ for multiplanar tubular lattice girders obtained from this study and recommended multiplication factors [F12] on ϵ_{ax} to account for bending moments in the fatigue design procedure for uniplanar tubular lattice structures.

Type of K, KK joint	Multiplanar tubular lattice girder (triangular cross section)			Uniplanar tubular lattice girder	
	ratio $\epsilon_{tot} / \epsilon_{ax}$ (obtained from this study)			recommended multiplication factors on ϵ_{ax} [F12]	
	Chord		Brace	Chord	Brace
	Upper (CA)	Lower (CC)			
gap	1.8	1.3	1.5	1.5	1.3
50% overlap	2.2	1.8	1.5		
100% overlap	2.6	2.2	1.5		
overlap				1.5	1.2

As shown in table 19, when comparing the results on ϵ_{tot} / ϵ_{ax} for the multiplanar girders with the multiplication factors on ϵ_{ax} for the uniplanar structures, the contribution of bending strains on the total strain is for multiplanar lattice structures for both chord and brace members significantly larger.

Chapter 6.2.4, gives for the girders tested the contribution of hot spot bending strains on the total hot spot strains which affects the fatigue behaviour (instead of the contribution of nominal bending strains on the total nominal strains as discussed in this chapter). The use of multiplication factors is further discussed in more detail.

5. EXPERIMENTAL INVESTIGATION ON THE FATIGUE BEHAVIOUR OF MULTIPLANAR TUBULAR JOINTS IN LATTICE GIRDERS

Nearly all published experimental work on the fatigue behaviour of welded tubular joints carried out so far has been on uniplanar joints.

On the fatigue behaviour of multiplanar KK joints, which are one of the most common types of joints e.g. in offshore structures, limited experimental work on SCFs using acrylic test specimen without including the weld have been carried out by Lloyd's Register of Shipping.

The lack of sufficient information on SCFs is because of the complexity of such joints and the high costs of adequately strain gauging experimental steel models.

5.1 *Experimental investigation*

To investigate the fatigue behaviour of tubular multiplanar joints in lattice girders, experiments have been carried out on four different multiplanar triangular lattice girders. The configuration and joint parameters of girder 5 (S_2), girder 6 (S_5), girder 7 (S_7) and girder 8 (S_8) are given in figures 41 and 42 and table 11.

For the joints of the lower chord of girders 5 to 8, measurements to determine the hot spot strains $\epsilon_{h.s.}$ have been carried out. The girders have been subjected to fatigue loading until each joint of the lower chord has failed in succession.

Based on this investigation, a $S_{r_{h.s.}}$ - N_f design curve is determined for multiplanar KK joints.

Details of Test Specimens

The circular hollow sections used for the girders are hot finished, with a steel grade S235 in accordance with EN 10210-1.

The dimensions of the members as well as the welds at the crown and saddle positions for the main joints have been measured. The material properties f_y (minimum yield strength), f_u (tensile strength) and ϵ_u (elongation) of the hollow sections have been determined with tensile tests (dp5).

The overlap joints in girders 5 and 6 have a 100% overlap and in the girders 7 and 8 a 50% overlap. The angle in transverse direction to the chord axis between the braces φ_{op} is 60°. The eccentricity (e) between the chord axis and the intersection of the brace axis is zero for the gap joints in girders 5 and 6. For the joints in girders 7 and 8, the eccentricity is 48 mm, which avoids an out-of-plane overlap.

Figure 42 gives the relevant details.

The girders are welded with rutile electrodes in accordance with the standards ASME SFA-5.1 and ISO 2560. Figure 43 shows the weld preparation, the welding details and the welding sequences.

Figure 41. Configuration of tested girders 5, 6, 7 and 8.
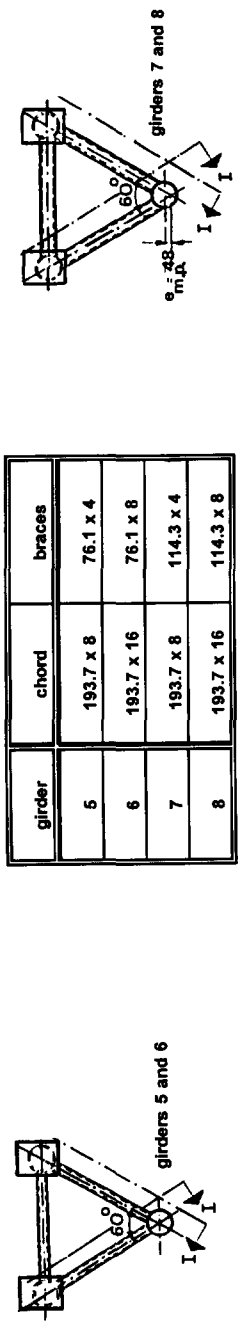
girder	chord	braces
5	193.7 x 8	76.1 x 4
6	193.7 x 16	76.1 x 8
7	193.7 x 8	114.3 x 4
8	193.7 x 16	114.3 x 8

girders 7 and 8
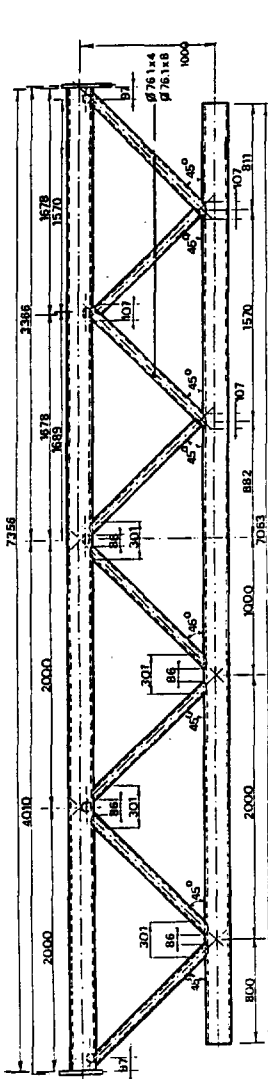
girders 5 and 6

view I-I: girders 5 and 6

view I-I: girders 7 and 8
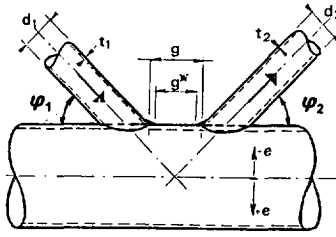
gap joint

50% overlap joint
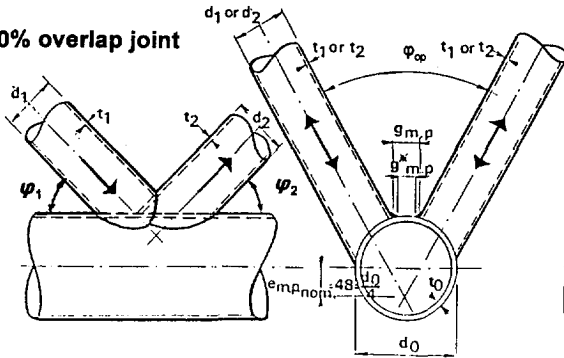
100% overlap joint
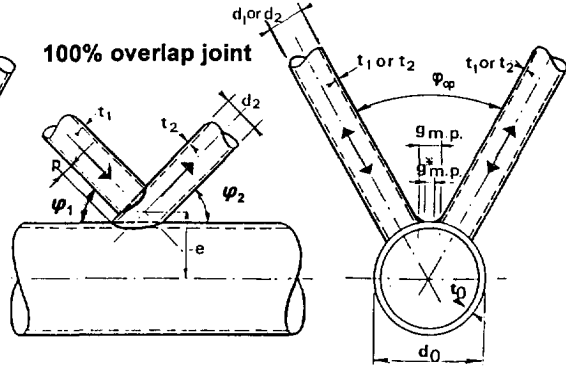
Figure 42.   Configuration of basic types of joints
of tested girders 5, 6, 7 and 8.

girders 5 and 6

girders 7 and 8

welding sequences

along these length
not welded to the chord
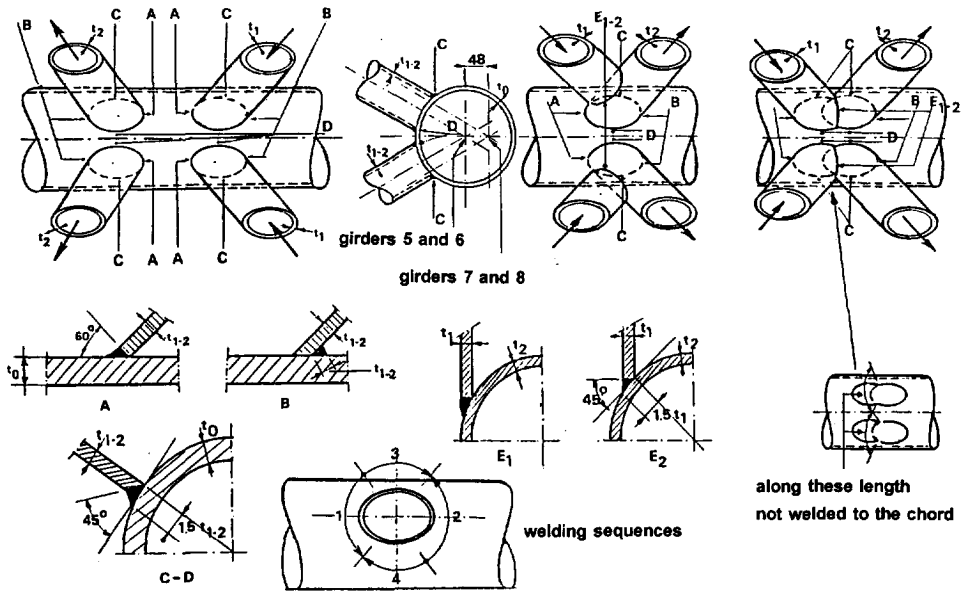
Figure 43.   Welding details and welding sequences for the tested girders 5, 6, 7 and 8.

73

The test rig together with a schematic view of the girders is shown in figure 44. A load F on the girder is applied by means of a jack. The jack load is measured with a dynamometer fitted on the jack. All the girders are tested first under a static loading, followed by a sinusoidal constant amplitude fatigue loading with a load ratio $R = F_{min} / F_{max} = 0.1$ and a frequency of 1 Hz.

Failure of the joint is assumed to have occurred when a through wall crack is observed.

strain gauges for
measuring reaction forces

lateral supports

jack +
dynamometer

F

• hinges
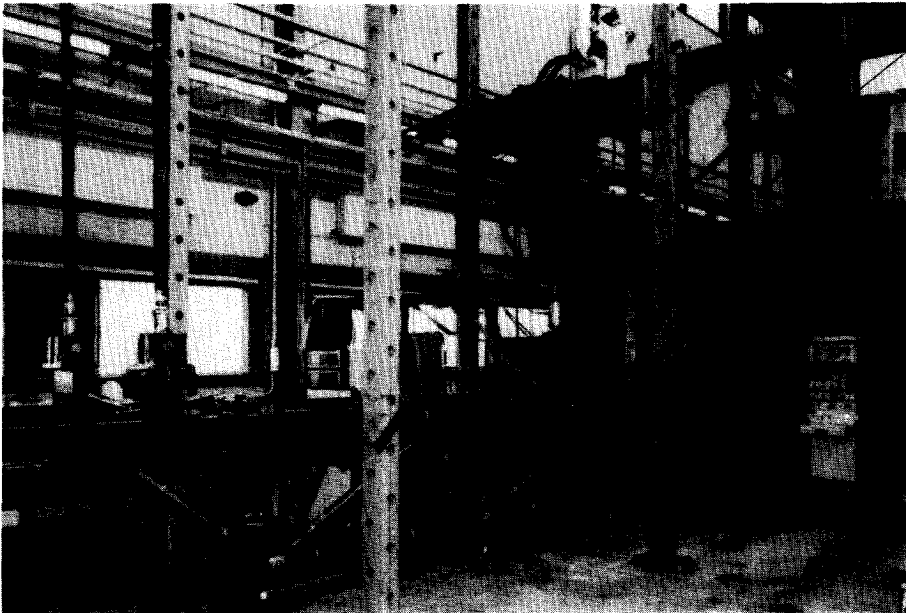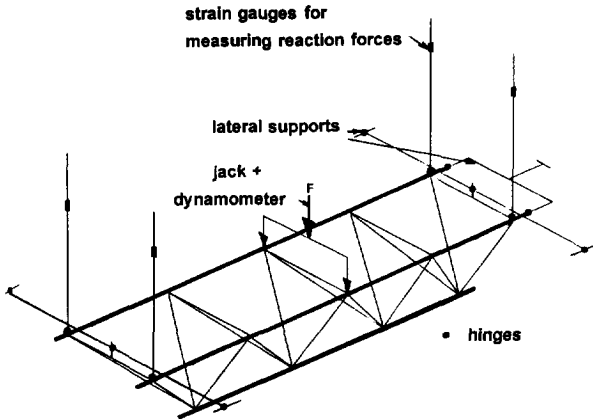
Figure 44.   Fully instrumented girder in test rig.

5.2 *Experimental measurements*

Hot spot strains (and SNCFs).

For the determination of the hot spot strain $\epsilon_{h.s.}$ at the weld toes, all four joints of the lower chord of the girders have been provided with strip gauges in a number of crown, saddle and inbetween locations. As an example, figure 45 shows some strip gauges around a multiplanar gap joint in girder 5. An illustration of the locations of the strip gauges around the main joints in girder 7 is given in figure 46.
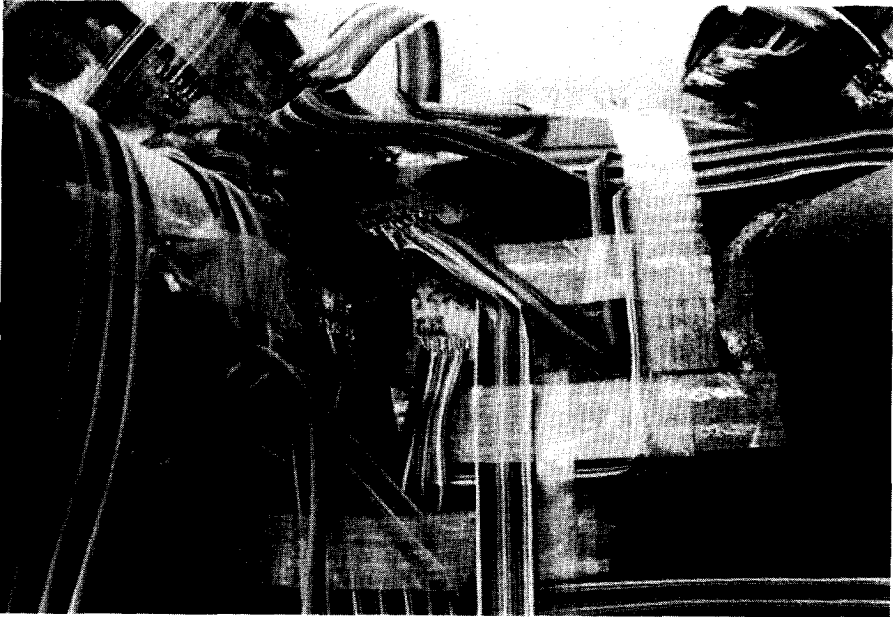
Figure 45.   Strip gauges around a multiplanar joint.
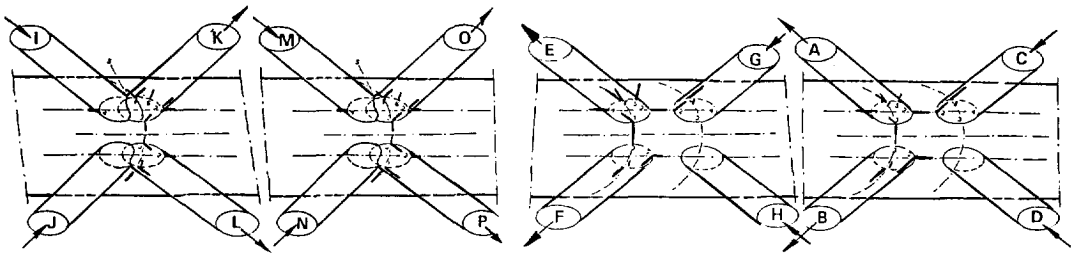
Figure 46.   Illustration of the strip gauges for the main joints of girder 7.

75

The hot spot strain $\epsilon_{h.s.}$ at the weld toes in chord and braces is determined from a linear extrapolation method according to table 1 and figure 5. From the strain measurements, SNCFs have been determined as described in chapter 1.3.
Table 20 gives a summary of the hot spot strains $\epsilon_{h.s.}$ and SNCFs at the weld toes of chord and braces for the main joints in girder 7. For complete details of $\epsilon_{h.s.}$ and SNCF results for all the tested girders 5 to 8, reference is made to [F23].

For the value of $\epsilon_{h.s.}$ around the brace to chord intersection, the following conclusions can be drawn:

- *For the gap and 100% overlap joints.*
  The highest (positive) $\epsilon_{h.s.}$ around the intersection of the tensile loaded brace to the chord occurs in the gap region at the toe and the inbetween locations of both the chord and brace member. The $\epsilon_{h.s.}$ around the entire intersection of the compression loaded brace to the chord (gap joints) are negative.

- *For the 50% overlap joints.*
  The highest (positive) $\epsilon_{h.s.}$ around the intersection of the tensile and compression loaded brace to the chord occurs at the brace heel location of the tensile loaded brace and at the chord heel location of the compression loaded brace.

- Generally, for all three main types of multiplanar KK joints investigated, the $\epsilon_{h.s.}$ for both the chord saddle and brace saddle locations are when compared to the $\epsilon_{h.s.}$ for the chord and brace crown and inbetween locations small. This is caused by the combination of chord and brace member loads, namely:

  - *Chord member loads $F_{ch;ax}$, $M_{ch;ip}$ and $M_{ch;op}$ result in largest $\epsilon_{h.s.}$ at the crown locations of the chord member.*
  - *Combined brace member loads $F_{br;ax;a-d}$, $M_{br;ip;a-d}$ and $M_{br;op;a-d}$ result in largest $\epsilon_{h.s.}$ at some of the saddle, crown and inbetween locations of the chord and brace members.*

- The highest SNCF in the gap joints due to the combined loading varies from 1.3 to 2.3 and for the overlap joints from 0.9 to 2.5.

76

Table 20. Measured hot spot strains $\epsilon_{h.s.}$ and SNCFs in girder 7 at F = 100kN.

Gap joint 1

line*	$\epsilon_{h.s.}$	$\epsilon_{h.s.}$ aver.	ϵ_{nom}	SNCF aver.
E.1-B	142	132	168	0.78
F.1-B	121		170	
G.1-B	-42		168	-0.25
E.1-C	41	41	168	0.24
E.2-B	253	264	168	1.56
F.2-B	275		170	
G.2-B	-187		168	-1.11
E.2-C	300	296	168	1.75
F.2-C	291		170	
E.3-B	122	122	168	0.73
E.3-C	96	96	168	0.57
E.4-C	100	100	168	0.60
E.5-C	380	380	168	2.26**

Gap joint 2

line	$\epsilon_{h.s.}$	$\epsilon_{h.s.}$ aver.	ϵ_{nom}	SNCF aver.
A.1-B	88	103	169	0.61
B.1-B	117		169	
C.1-B	-30		169	-0.18
A.1-C	85	85	169	0.50
A.2-B	308	284	169	1.68
B.2-B	260		169	
C.2-B	-283		169	-1.68
A.2-C	180	175	169	1.04
B.2-C	170		169	
A.3-B	113	113	169	0.67
A.3-C	108	108	169	0.64
A.4-C	-26	-26	169	-0.15
A.5-C	283	283	169	1.68**

Overlap joint 1

line	$\epsilon_{h.s.}$	$\epsilon_{h.s.}$ aver.	ϵ_{nom}***	SNCF aver.
K.1-B	188	138	137	1.00
L.1-B	87		138	
K.1-C	-98	-98	137	-0.78
K.2-B	95	95	137	0.69
K.2-C	60	60	137	0.44
L.2-C	60		138	
K.3-B	53	81	137	0.59
L.3-B	108		138	
K.3-C	13	13	137	0.10
I.4-C	230	230	137	1.68**
K.5-B	56	56	137	0.41
K.6-C	-62	-62	137	-0.45

Overlap joint 2

line	$\epsilon_{h.s.}$	$\epsilon_{h.s.}$ aver.	ϵ_{nom}	SNCF aver.
O.1-B	130	134	159	0.80
P.1-B	138		175	
O.1-C	-50	-50	159	-0.31
O.2-B	205	205	159	1.29**
O.2-C	-7	-6	159	-0.04
P.2-C	-4		175	
O.3-B	120	125	159	0.75
P.3-B	130		175	
O.3-C	-15	-15	159	-0.09
M.4-C	180	180	159	1.13
O.5-B	39	39	159	0.25
O.6-C	-2	-2	159	-0.01

* The location of the lines is shown in figure 46.

** Maximum SNCF.

*** $\epsilon_{nom} = \epsilon_{ax} + \sqrt{\epsilon_{ipb}^2 + \epsilon_{opb}^2}$.

Fatigue life.

The fatigue tests have been carried out for determination of the number of cycles to initiation of cracks and failure of the joints. During the fatigue tests, the strain distribution in the members and around the main joints have been measured at regular intervals, so that changes in hot spot strains and nominal strains due to initiation of cracks and crack growth could be determined. For all joints, with the exception of the overlap joints in girder 7, the cracks start at the location where the highest hot spot strains (and SNCFs) occurs and extends along the weld toe of chord or brace over a certain length until a through crack occurs.

All of the 16 main joints, with the exception of gap joint 2 of girder 6, and gap joint 2 as well as overlap joint 2 of girder 7, failed in the chord. In the gap joint 2 of girders 6 and 7 failure occurred in the brace, whereas in overlap joint 2 of girder 7 a combined failure occurred in the chord and brace.

Table 21 summarizes the test results from the static load tests and the fatigue tests. As an example, figure 47 shows a joint failure.
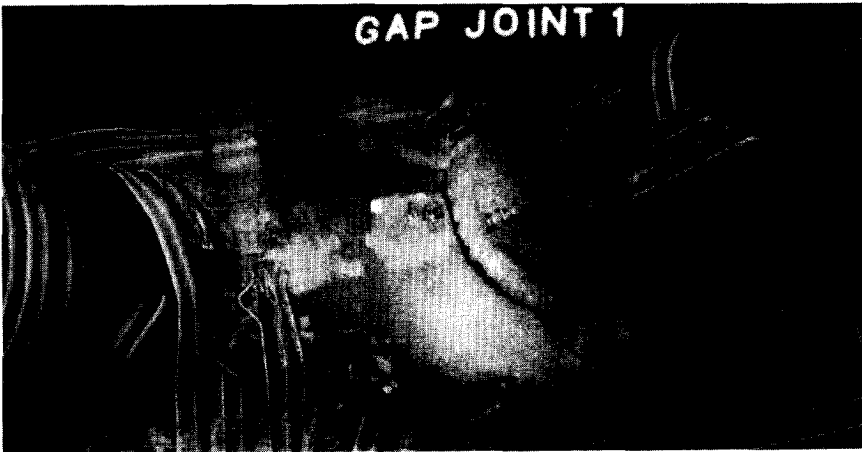
Figure 47.   Failure in a gap joint.

From the fatigue test results, $S_{r_{h.s.}}$ - N_f curves have been derived.

Since these curves are based on stresses and the measurements on strains, a conversion is carried out from the measured strains into stresses by using an average factor as given below, which is on the basis of existing information [F3] and the results of the numerical calibration given in chapter 6.

$SCF = 1.2 \cdot SNCF.$

Figure 48 shows the mean $S_{r_{h.s.}}$ - N_f line for all the multiplanar KK joints tested together with the DEn S_r - N curve (see also figure 8), which is also used for uniplanar joints with t = 16 mm.

From figure 48 it is found that the scatter of the fatigue data is small, and the

slope of the mean line is m = -3.7. Also, it can be seen that the mean line and slope through the data points is in good agreement with those of the DEn mean line.
As shown in figure 49, a thickness correction for the fatigue data results in an increase of scatter.

t [mm]	joints in CHS
4	o
8	o
16	O

Figure 48.   Main fatigue data derived from multiplanar KK joints without thickness correction.
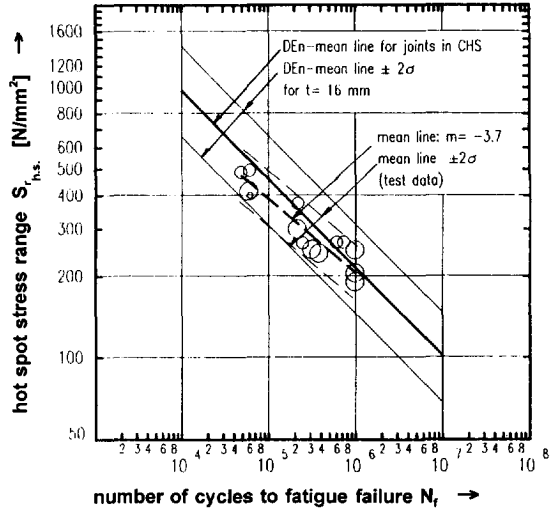
t [mm]	joints in CHS
4	o
8	o
16	O

Figure 49.   Main fatigue data derived from multiplanar KK joints with thickness correction.
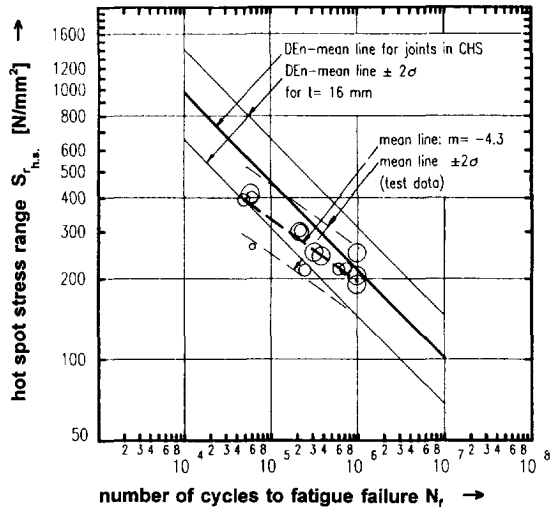
From the results given in figures 48 and 49, it is proposed that the DEn design curve for uniplanar joints in CHS should also be applied for the multiplanar KK joints for thicknesses of 4 to 16 mm. No thickness correction is therefore needed. The equation of this design curve is :

$$log\ (\ N_f) = 12.4756\ -3\ log\ (\ S_{r h.s.})\quad with\quad (10^3 < N_f < 5 \cdot 10^6).$$

79

Table 21. Test results from the static load tests and fatigue tests.

Joint	Dimensions chord	Dimensions brace	R	Load range F_r [kN]	ε_{nom} (*10^-6)	S_{nom} [N/mm²]	$\varepsilon_{h.s.}$ (*10^-6) Chord	$\varepsilon_{h.s.}$ (*10^-6) Brace	$S_{h.s.}$ [N/mm²] Chord	$S_{h.s.}$ [N/mm²] Brace	SNCF Chord	SNCF Brace	SCF Chord	SCF Brace	Location Chord	Location Brace	N_i (*10^6)	N_f (*10^6)	Mode of failure	N_f / N_i	$S_{h.s.}$ corrected to thickness [N/mm²] (DEn)
GIRDER 5																					
Gap 1	φ193.7x8	φ76.1x4	0.1	321	703	148	1059	-	267	-	1.51	-	1.81	-	E.2-C	-	0.200	0.723	chord	3.62	217
Gap 2					812	171	1059	-	267	-	1.30	-	1.56	-	B.2-C	-	0.130	0.598	chord	4.60	217
Overlap 1					600	126	1477	-	372	-	2.46	-	2.95	-	K.4-C	-	0.030	0.214	chord	7.13	302
Overlap 2					1053	221	1920	-	484	-	1.82	-	2.18	-	O.4-C P.4-C	-	0.010	0.048	chord	4.80	393
GIRDER 6																					
Gap 1	φ193.7x16	φ76.1x8	0.1	585	632	133	965	-	243	-	1.53	-	1.83	-	F.2-C	-	0.100	0.375	chord	3.75	243
Gap 2					725	152	-	1053	-	265	-	1.45	-	1.74	-	B.2-B	0.010	0.244	brace	24.40	215
Overlap 1					632	133	1188	-	299	-	1.88	-	2.25	-	K.4-C	-	0.020	0.210	chord	10.50	299
Overlap 2					1000	210	1638	-	413	-	1.64	-	1.97	-	O.4-C	-	0.006	0.058	chord	9.67	413
GIRDER 7																					
Gap 1	φ193.7x8	φ114.3x4	0.1	513	862	181	1949	-	491	-	2.26	-	2.71	-	E.5-C	-	0.030	0.060	chord	2.0	399
Gap 2					867	182	-	1580	-	398	-	1.82	-	2.19	-	A.2-B A.5-B	0.010	0.060	brace	6.0	263
Overlap 1					708	149	-	-	-	-	-	-	-	-	-	-	-	>0.220+	not failed	-	-
Overlap 2					856	180	-	-	-	-	-	-	-	-	O.3-C	-	0.025	0.093	chord brace	3.72	-
GIRDER 8																					
Gap 1	φ193.7x16	φ114.3x8	0.1	603	512	108	995	-	251	-	1.94	-	2.32	-	F.5-C	-	0.065	0.310	chord	4.77	251
Gap 2					494	104	814	-	205	-	1.65	-	1.97	-	A.5-C	-	0.310	0.978	chord	3.15	205
Overlap 1					458	96	994	-	250	-	2.17	-	2.60	-	K.4-C	-	0.310	>0.978+	not failed	>3.15	250
Overlap 2					500	105	754	-	190	-	1.51	-	1.81	-	O.4-C	-	0.320	>0.978+	failed	>3.06	190

6. CALIBRATION OF NUMERICAL WORK WITH EXPERIMENTAL RESULTS

6.1 *Introduction*

For the calibration of the numerical work on stress and strain concentration factors described in chapter 7, sixteen experimentally investigated joints of girders 5 to 8, as described in chapter 5, have been used.

The numerical modelling of tubular joint flexibility and tubular joint stress concentration factors has been defined in chapter 3, and the numerical modelling of lattice structures with flexible joints has been defined in chapter 4. Based on the results given in chapters 3 and 4, it is decided for the numerical hot spot strain (and SNCF) calibration, to model the weld of the joint by 20-n solid elements and the joint member parts by 20-n solid or 8-n shell elements and placing this joint in a beam modelled girder according to the numerical idealization M_1. This means that all other joints are modelled with rigid ended beam elements only, without taking the effect of joint flexibility into account.
An example is given in figure 50.
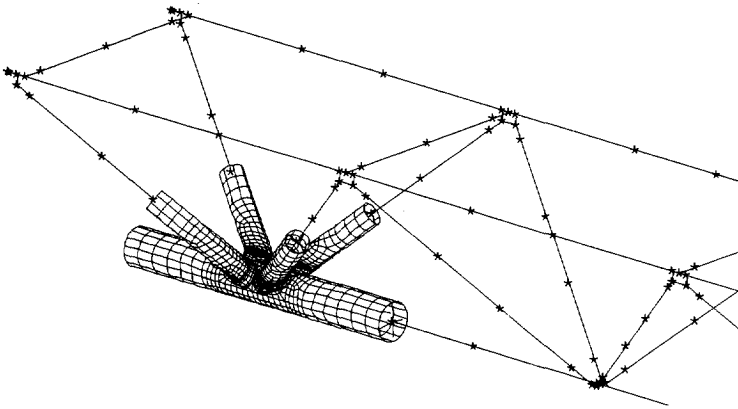
Figure 50. Numerical model for the hot spot strain calibration of KK gap joint 2 in girder 5.

Since the measured dimensions of the hollow sections were nearly the same as the nominal dimensions, the last mentioned are used for both the joint and girder members.

Numerical calibration of experimental results are carried out for:

- Extrapolated nominal strains ϵ_{nom} for the brace members under tension of the joints tested.
- Strain concentration factors (SNCFs).
- Ratio SCF/SNCF.
- Hot spot strains $\epsilon_{h.s.}$ using the individual measured chord and brace member strains and multiplication of these strains by SNCFs obtained from a parameter study of welded multiplanar KK joints as described in chapter 7.

6.2   Numerical calibration

6.2.1   Calibration of extrapolated nominal strains

Because the experimentally defined SNCFs are determined by $SNCF_{m.n.o} = \frac{\epsilon_{h.s.;m.n.o}}{\epsilon_{extrap.;nom}}$, a calibration of $\epsilon_{extrap.;nom}$ has been carried out firstly.
The results of this calibration (using a FE model as shown in figure 50) are summarized in table 22.

Table 22. Comparison between numerically and experimentally determined extrapolated nominal strains (10^{-6}) in the tension braces for the joints tested by fatigue of girders 5, 6, 7 and 8.

Girder	Joint no.	Extrapolated nominal strains ($\cdot 10^{-6}$)						Ratio	Ratio	Ratio
		Numerical			Experimental			$\dfrac{\epsilon_{nom;num}}{\epsilon_{nom;exp}}$	$\dfrac{\epsilon_{nom;num}}{\epsilon_{ax;num}}$	$\dfrac{\epsilon_{nom;exp}}{\epsilon_{ax;exp}}$
		ϵ_{ax}	ϵ_{ip}	ϵ_{op}	ϵ_{ax}	ϵ_{ip}	ϵ_{op}			
5	gap 1	170	38	18	151	62	28	0.97	1.24	1.43
	gap 2	199	30	19	193	44	39	0.93	1.17	1.29
	overlap 1	154	52	16	136	40	31	1.12	1.35	1.35
	overlap 2	225	62	44	220	54	93	0.92	1.34	1.47
6	gap 1	91	16	10	89	14	5	1.06	1.39	1.29
	gap 2	105	11	10	104	9	15	0.99	1.14	1.17
	overlap 1	82	25	8	80	26	12	1.01	1.32	1.33
	overlap 2	120	36	23	119	38	36	0.95	1.36	1.42
7	gap 1	122	38	15	111	49	29	0.97	1.33	1.35
	gap 2	133	33	20	128	38	15	1.01	1.29	1.32
	overlap 1	120	4	18	111	5	25	1.01	1.15	1.24
	overlap 2	142	2	28	132	10	25	1.06	1.20	1.25
8	gap 1	64	20	6	62	21	5	1.01	1.33	1.47
	gap 2	69	13	6	67	14	5	1.02	1.21	1.23
	overlap 1	63	9	2	62	10	10	0.94	1.15	1.15
	overlap 2	74	5	16	70	6	11	1.09	1.23	1.23

From the results given in table 22, it is concluded that:

- A good agreement between numerical and experimental extrapolated nominal strains ϵ_{nom} exist. The maximum differences in ϵ_{nom} varies from

$0.92 < \dfrac{\epsilon_{nom;num}}{\epsilon_{nom;exp}} < 1.12$.

- The ratios $\dfrac{\epsilon_{nom\,;num}}{\epsilon_{ax\,;num}}$ and $\dfrac{\epsilon_{nom\,;exp}}{\epsilon_{ax\,;exp}}$ show a large influence of axial strains compared to bending strains on the total strains.

6.2.2 Calibration of SNCFs

Results of the numerically determined strain concentration factors SNCFs (and SCFs) for the sixteen tested multiplanar joints are given in tables 23 and 24, in which the comparison with experimental results is also given.
Figures 51 and 52 illustrate the results on calibration of SNCFs, showing a reasonable agreement, considering the small SNCF values.

Figure 51.   Comparison between experimentally and numerically determined SNCF values.
(Girder 5 left figure and girder 6 right figure).

Figure 52.   Comparison between experimentally and numerically determined SNCF values.
(Girder 7 left figure and girder 8 right figure).

83

Table 23. SNCF and SCF values at various locations of the joints in girders 5 and 6.
note: ** = very small SNCF values.
For joint locations in the girders see figure 32 and measurement lines see figure 46.

girder 5

gap joint 1

line	numerical results SNCF	numerical results SCF	SCF/SNCF	exp. results SNCF	num./exp. ratio SNCF
E.1-B	1.04	1.13	1.08	1.18	0.88
G.1-B	-1.00	-1.10	1.10	-1.28	0.78
E.1-C	0.54	0.76	1.41	0.53	1.02
E.2-B	0.71	0.81	1.14	0.67	1.06
G.2-B	-0.54	-0.59	1.10	-0.73	0.74
E.2-C	1.74	2.08	1.20	1.51	1.15
E.3-B	0.81	0.85	1.05	0.86	0.94
E.3-C	0.58	0.85	1.46	1.26	0.46
E.4-B	0.81	0.86	1.06	0.27	**
G.4-B	-1.51	-1.68	1.11	-1.28	1.18
E.4-C	0.31	0.41	1.33	0.32	**
E.5-B	0.97	1.06	1.09	1.21	0.80
E.5-C	1.23	1.47	1.20	1.32	0.93

gap joint 2

line	numerical results SNCF	numerical results SCF	SCF/SNCF	exp. results SNCF	num./exp. ratio SNCF
A.1-B	1.06	1.16	1.10	1.23	0.86
A.2-B	0.71	0.76	1.08	1.19	0.60
A.2-C	1.44	1.72	1.20	1.37	1.06
A.3-C	0.69	0.78	1.13	0.48	**
A.5-B	0.96	1.06	1.10	1.02	0.94
A.5-C	1.11	1.37	1.23	1.07	1.04

overlap joint 1

line	numerical results SNCF	numerical results SCF	SCF/SNCF	exp. results SNCF	num./exp. ratio SNCF
K.1-B	0.71	0.84	1.18	0.62	1.15
K.1-C	-1.28	-1.34	1.04	-1.44	0.88
K.2-B	0.43	0.42	0.97	0.32	**
K.2-C	0.49	0.51	1.04	0.34	**
K.3-B	0.80	0.72	0.91	0.54	1.48
K.3-C	-0.13	-0.13	1.00	-0.48	**
K.4-C	2.15	2.73	1.27	2.46	0.88
K.5-B	0.02	0.11		0.19	**
1.5-B	-0.12	-0.04		-0.31	**

overlap joint 2

line	numerical results SNCF	numerical results SCF	SCF/SNCF	exp. results SNCF	num./exp. ratio SNCF
O.1-B	1.22	1.36	1.12	1.13	1.08
O.1-C	-0.33	-0.28	0.85	0.07	**
O.3-B	0.80	0.78	0.98	0.55	1.46
O.4-C	-2.17	2.44	1.13	1.86	1.17

girder 6

gap joint 1

line	numerical results SNCF	numerical results SCF	SCF/SNCF	exp. results SNCF	num./exp. ratio SNCF
E.1-B	0.99	1.11	1.12	1.15	0.86
G.1-B	-0.96	-1.03	1.08	-1.52	0.63
E.1-C	0.43	0.63	1.46	0.44	**
E.2-B	1.34	1.57	1.17	1.51	0.89
G.2-B	-0.93	-0.85	0.92	-0.91	1.02
E.2-C	1.45	1.69	1.17	1.38	1.05
E.3-B	1.01	1.10	1.09	0.97	1.04
E.3-C	0.75	1.02	1.36	0.89	0.85
E.4-C	0.24	0.31	1.29	0.19	**

gap joint 2

line	numerical results SNCF	numerical results SCF	SCF/SNCF	exp. results SNCF	num./exp. ratio SNCF
A.1-B	0.86	0.95	1.11	1.16	0.75
C.1-B	-0.91	-1.04	1.14	-0.95	0.96
A.1-C	0.57	0.68	1.19	0.61	0.93
A.2-B	1.37	1.49	1.09	1.49	0.93
C.2-B	-1.16	1.39	1.20	-1.09	1.06
A.2-C	1.30	1.52	1.18	1.16	1.12
C.2-C	-0.23	-0.40	1.74	-0.48	**
A.3-B	1.04	1.11	1.07	0.84	1.23
A.3-C	0.94	1.17	1.24	0.74	1.27
A.4-C	-0.11	-0.05	0.45	0.19	**

overlap joint 1

line	numerical results SNCF	numerical results SCF	SCF/SNCF	exp. results SNCF	num./exp. ratio SNCF
K.1-B	0.53	0.02	0.04	0.75	0.71
K.1-C	-0.96	-0.95	0.99	0.76	1.26
K.3-B	0.48	0.10	0.21	0.50	0.97
K.3-C	-0.73	-0.83	1.14	-0.32	**
K.4-C	2.38	2.72	1.14	1.88	1.27
K.4-B	0.36	0.23	0.64	0.26	**

overlap joint 2

line	numerical results SNCF	numerical results SCF	SCF/SNCF	exp. results SNCF	num./exp. ratio SNCF
O.1-B	0.83	0.60	0.73	0.96	0.87
O.1-C	-0.33	-0.28	0.85	-0.09	**
O.3-B	-0.71	0.49	0.69	0.58	1.22
O.3-C	-0.48	0.42	0.88	-0.35	**
O.4-C	2.11	2.38	1.13	1.64	1.29
O.5-B	0.49	0.41	0.83	0.49	1.00

Table 24. SNCF and SCF values at various locations of the joints in girders 7 and 8.
note: ** = very small SNCF values.
For joints locations in the girders see figure 32 and measurement lines see figure 46.

girder 7

Gap joint 1

line	numerical results SNCF	numerical results SCF	SCF/SNCF	exp. results SNCF	num./exp. ratio SNCF
E.1-B	0.88	0.93	1.06	0.84	1.05
G.1-B	-0.27	-0.21	0.78	-0.25	**
E.1-C	0.87	0.91	1.06	0.24	**
E.2-B	1.08	1.16	1.08	1.51	0.71
G.2-B	-0.74	-0.75	1.02	-1.11	0.67
E.2-C	1.72	1.93	1.12	1.79	0.97
E.3-B	0.57	0.67	1.18	0.73	0.78
E.3-C	0.33	0.61	1.84	0.57	0.56
E.4-C	0.59	0.66	1.12	0.60	0.99
E.5-C	1.82	2.05	1.13	2.26	0.81

gap joint 2

line	numerical results SNCF	numerical results SCF	SCF/SNCF	exp. results SNCF	num./exp. ratio SNCF
A.1-B	0.63	0.62	0.98	0.52	1.21
C.1-B	-0.41	-0.43	1.05	-0.80	**
A.1-C	0.59	0.67	1.13	0.50	1.19
A.2-B	1.10	1.19	1.08	1.53	0.72
C.2-B	-1.10	-1.17	1.06	-1.68	0.65
A.2-C	0.87	0.97	1.12	1.07	0.81
A.3-B	0.52	0.54	1.04	0.67	0.78
A.3-C	0.48	0.65	1.35	0.64	0.75
A.4-C	-0.02	0.03	1.50	-0.15	**
A.5-C	1.34	1.55	**	1.68	0.80

overlap joint 1

line	numerical results SNCF	numerical results SCF	SCF/SNCF	exp. results SNCF	num./exp. ratio SNCF
K.1-B	1.23	1.18	0.96	1.37	0.89
K.1-C	-0.97	-0.75	1.24	-0.78	1.24
K.2-B	-0.62	0.67	0.90	0.69	0.90
K.2-C	0.40	0.57	0.93	0.44	**
L.3-B	0.87	0.78	1.12	0.78	1.11
K.3-C	-0.04	0.12		0.10	**
I.4-C	1.58	1.73	1.10	1.68	0.95
K.5-B	0.51	0.39	1.25	0.41	**
K.6-C	-0.13	0.00		-0.45	**

overlap joint 2

line	numerical results SNCF	numerical results SCF	SCF/SNCF	exp. results SNCF	num./exp. ratio SNCF
O.1-B	1.05	0.74	0.71	0.80	1.31
O.1-C	-0.44	-0.39	0.88	-0.31	**
O.2-B	0.96	0.83	0.87	1.29	0.75
O.2-C	-0.04	-0.11		-0.04	**
O.3-B	0.75	0.64	0.85	0.75	1.00
O.3-C	-0.08	0.01		-0.09	**
M.4-C	1.03	0.96	0.93	1.13	0.92
O.5-B	0.33	0.25		0.25	
O.6-C	-0.37	-0.32		-0.01	**

girder 8

gap joint 1

line	numerical results SNCF	numerical results SCF	SCF/SNCF	exp. results SNCF	num./exp. ratio SNCF
E.1-B	0.62	0.69	1.11	0.69	0.90
G.1-B	-0.59	-0.41	0.69	-0.12	**
E.1-C	0.03	0.15		0.35	**
E.2-B	1.07	1.13	1.06	1.21	0.88
G.2-B	-0.67	-0.66	0.99	-0.75	0.89
F.2-C	1.95	2.16	1.11	1.94	1.01
E.3-B	0.69	0.75	1.09	0.95	0.73
E.5-B	0.76	0.76	1.00	0.82	0.93
E.5-C	1.47	1.64	1.12	2.21	0.67

gap joint 2

line	numerical results SNCF	numerical results SCF	SCF/SNCF	exp. results SNCF	num./exp. ratio SNCF
A.1-B	0.63	0.62	0.99	0.49	1.28
C.1-B	-0.51	-0.36	0.71	-0.25	**
A.1-C	0.23	0.27	1.05	0.55	0.42
A.2-B	1.07	1.12	1.05	1.71	0.63
C.2-B	-1.05	-1.06	1.01	-1.34	0.78
A.3-B	0.66	0.66	1.00	0.61	1.09
A.5-B	0.6	0.65	1.02	0.73	0.90
A.5-C	1.15	1.26	1.10	1.85	0.70

overlap joint 1

line	numerical results SNCF	numerical results SCF	SCF/SNCF	exp. results SNCF	num./exp. ratio SNCF
K.1-B	1.10	1.06	0.96	1.05	1.05
K.1-C	-0.68	-0.47	0.69	-0.32	**
K.2-B	1.00	1.08	1.08	0.99	1.01
K.3-B	0.98	0.96	0.98	0.95	1.03
K.3-C	0.08	0.25		0.10	**
K.4-C	2.08	2.21	1.06	2.17	0.96
K.5-B	1.13	1.12	0.99	1.21	0.94
K.5-C	-0.19	0.00		0.03	**
K.6-C	-0.67	-0.45	0.68	-0.29	**
K.7-C	-0.50	-0.35	0.70	0.01	**

overlap joint 2

line	numerical results SNCF	numerical results SCF	SCF/SNCF	exp. results SNCF	num./exp. ratio SNCF
O.1-B	0.81	0.81	1.00	0.94	0.86
O.1-C	-0.25	-0.19		-0.08	**
O.2-B	1.28	1.38	1.08	1.21	1.05
O.3-B	0.81	0.78	0.96	0.91	0.89
O.3-C	0.02	0.09		0.02	**
O.4-C	1.31	1.34	1.02	1.51	0.87
O.5-B	0.93	0.93	1.00	1.05	0.89
O.5-C	0.21	0.10		-0.12	**
O.6-C	-0.29	-0.17		-0.16	**
O.7-C	-0.40	-0.33		-0.21	**

6.2.3 Calibration of the ratio SCF/SNCF

As mentioned in chapter 5, a ratio for SCF/SNCF has to be established for converting measured hot spot strains $\epsilon_{h.s.}$ into hot spot stresses $\sigma_{h.s.}$ for use in the fatigue design curves. The results of the numerically determined ratio for
SCF/SNCF for the sixteen tested multiplanar joints, considering all locations around the perimeter, are given in tables 23 and 24 and figures 53 and 54. An average ratio of SCF/SNCF = 1.2 is obtained, which supports previous work on uniplanar joints. It is mentioned, however, that for SCFs and SNCFs with absolute values smaller than 0.5, a large scatter on this ratio exist, namely:
0.80 < SCF/SNCF < 1.40. For the locations along the weld toe where fatigue failure occurs, the average ratio SCF/SNCF is 1.14 and the ratio SCF/SNCF varies from 1.02 < SCF/SNCF < 1.27 (see table 25). The existence of the scatter in SCF/SNCF is specifically for tubular joints by means of constitutive equations and parameter study results explained and discussed in chapter 7.
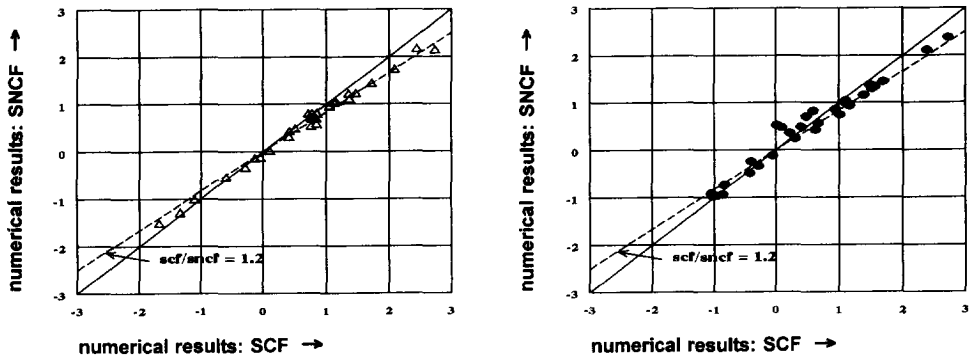
Figure 53.   Comparison between numerically determined SNCF and SCF values.
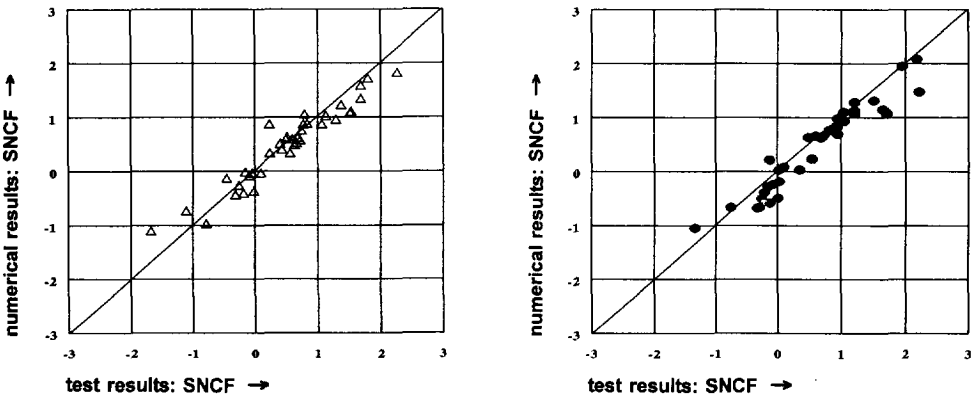(Girder 5 left figure and girder 6 right figure).
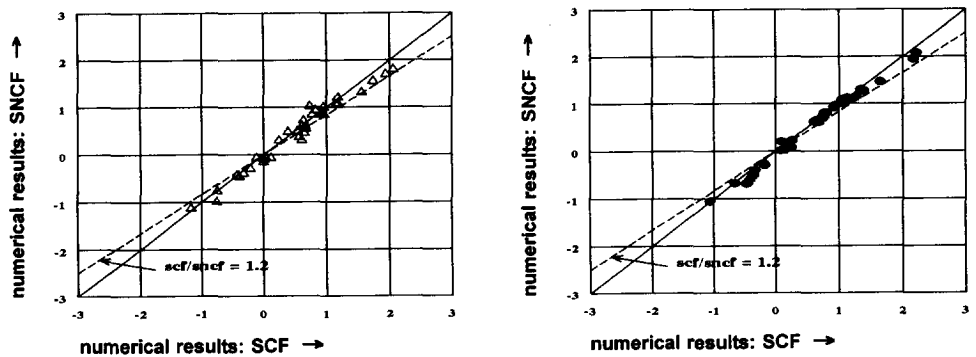
Figure 54.   Comparison between numerically determined SNCF and SCF values.
(Girder 7 left figure and girder 8 right figure).

Table 25.   Numerically determined ratio SCF/SNCF for the locations of fatigue failure.

Girder	Joint							
	Gap 1		Gap 2		Overlap 1		Overlap 2	
	Location	$\frac{SCF}{SNCF}$	Location	$\frac{SCF}{SNCF}$	Location	$\frac{SCF}{SNCF}$	Location	$\frac{SCF}{SNCF}$
5	E.2-C	1.20	A.2-C	1.20	K.4-C	1.27	O.4-C	1.17
6	E.2-C	1.17	A.2-B	1.09	K.4-C	1.14	O.4-C	1.13
7	E.5-C	1.13	A.2-B	1.08	-	-	-	-
8	E.5-C	1.12	A.5-C	1.10	K.4-C	1.06	O.4-C	1.02

6.2.4 *Calibration of hot spot strains based on individual loads*

Due to the non-uniform stiffness along the intersection of a brace to chord member connection, the magnitude of hot spot strain $\epsilon_{h.s.}$ entirely depends on the location (crown, saddle and inbetween) considered.
As an example, for the reference effects of brace member loads, as explained in chapter 7, axial forces and out-of plane bending moments generally give the highest $\epsilon_{h.s.}$ at the chord saddle and brace saddle locations, whereas in-plane bending moments give the highest $\epsilon_{h.s.}$ at the chord and brace crown and inbetween locations. For the axial chord member loads, the highest $\epsilon_{h.s.}$ always occurs at the chord crown locations.
Besides reference effects, depending on the type of joint, joint parameters β, γ, τ, φ_{ip} and φ_{op} and type of loading, large carry-over effects at crown, saddle and inbetween locations occur. Therefore, no fixed locations of $\epsilon_{h.s.}$ can be given, as in the case of reference effects.
A calibration on $\epsilon_{h.s.}$ using the individual measured brace and chord member strains (extrapolated) from the tested girders 5 to 8 and SNCFs obtained from a parameter study as described in chapter 7 has been carried out for the gap joints.
The $\epsilon_{h.s.}$ is determined according to the definition on total hot spot stress based on stress concentration factors given in chapter 1.3.

Results of the $\epsilon_{h.s.}$ determined in this way are given in figures 55 and 56 and table 26, together with experimental results of $\epsilon_{h.s.}$.
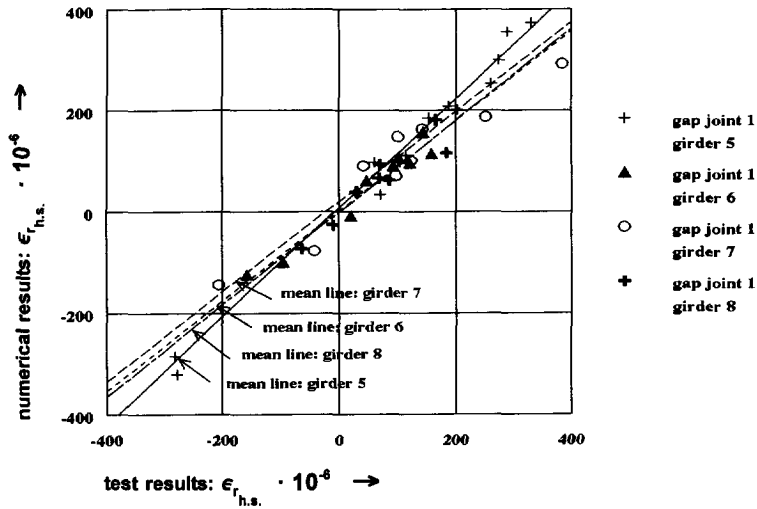
Figure 55. Comparison between numerically and experimentally determined hot spot strains $\epsilon_{h.s.}$ for gap joint 1 of girders 5 to 8.
Numerical determined hot spot strains based on measured chord and brace member strains (axial + bending) and multiplied by the corresponding SNCFs obtained from the parameter study results (see chapter 7).
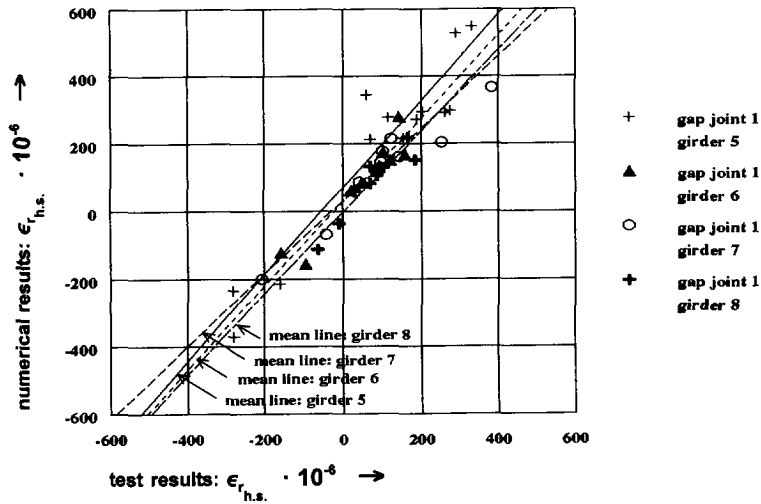
Figure 56. Comparison between numerically and experimentally determined hot spot strains $\epsilon_{h.s.}$ for gap joint 1 of girders 5 to 8.
Numerical determined hot spot strains based on measured chord member strains (axial + bending) and 1.5 times measured axial brace member strains, and both multiplied by the corresponding SNCFs obtained from the parameter study results (see chapter 7).
(The factor 1.5 for the brace members is obtained from the results given in table 19).

Table 26. Contribution of individual measured axial and bending strains ($\cdot\ 10^{-6}$) of the chord and brace members on the total hot spot strains for gap joint 1 of girders 5 to 8.

| Line	Girder	Brace loads: $\epsilon_{h.s.;br}$ ***				Chord loads: $\epsilon_{h.s.;ch}$ ***			Brace + chord loads: $\epsilon_{h.s.}$ = $\epsilon_{h.s.;br} + \epsilon_{h.s.;ch}$	Ratio $\epsilon_{h.s.}$ **** numerical experimental
		$\epsilon_{h.s.;ax}$ [3]	$\epsilon_{h.s.;ip}$ [4]	$\epsilon_{h.s.;op}$ [5]	α_{br} ** [6]	$\epsilon_{h.s.;ax}$ [7]	$\epsilon_{h.s.;ip}$ [8]	α_{ch} ** [9]		
E.1-B	5	170	13	54	1.39	38	-22	0.42	253	0.97
	6	92	1	-4	0.96	12	-5	0.58	96	0.80
	7	78	9	32	1.52	44	0	1.00	163	1.15
	8	40	0	6	1.15	21	-1	0.95	66	1.14
G.1-B	5	-181	5	-125	1.66	38	-22	0.42	-285	1.01
	6	-90	-1	-40	1.46	12	-5	0.58	-124	0.79
	7	-75	1	-47	1.61	44	0	1.00	-77	1.83
	8	-38	0	-6	1.16	21	-3	0.86	-26	
E.1-C	5	206	8	-94	0.58	-31	23	0.25	112	0.98
	6	66	2	-3	0.99	-17	13	0.24	61	1.32
	7	82	10	35	1.55	-37	0	1.00	90	2.19
	8	25	3	3	1.24	20	0	1.00	39	
E.2-B	5	141	38	0	1.27	3	-9	-2.00	185	1.25
	6	105	7	0	1.07	9	-7	0.22	114	0.72
	7	136	37	9	1.33	0	5	--	187	0.74
	8	82	14	1	1.17	6	-4	0.33	99	0.97
G.2-B	5	-145	20	0	0.86	3	-9	-2.00	-131	0.82
	6	-110	14	0	0.88	9	-12	-0.33	-99	1.04
	7	-133	26	-26	1.00	0	-11	--	-144	0.77
	8	-79	11	0	0.87	6	-11	-0.83	-73	1.16
E.2-C	5	270	68	13	1.30	143	-120	0.16	374*	1.13
	6	134	10	0	1.07	79	-67	0.15	156*	1.09
	7	238	67	-5	1.26	125	-3	0.98	422	1.41
	8	94	28	0	1.30	77	-18	0.77	181	1.10
E.3-B	5	155	-3	50	1.30	40	-34	0.15	208	1.11
	6	107	0	-4	0.96	13	-10	0.23	106	1.05
	7	110	0	-59	0.46	50	0	1.00	101	0.83
	8	58	0	-10	0.83	19	-5	0.73	62	0.73
E.3-C	5	201	17	118	1.67	-3	-33	12.0	300	1.09
	6	102	3	17	1.20	-20	-12	1.60	90	0.98
	7	113	15	-32	0.85	-25	0	1.00	71	0.74
E.4-B	5	236	-126	0	0.47	-9	-4	1.44	97	1.62
G.4-B	5	-241	-67	0	1.28	-9	-4	1.44	-321	1.15
E.4-C	5	42	-33	0	0.21	150	-125	0.17	34	
	6	-18	-2	0	1.11	87	-75	0.14	-8	
	7	17	-19	-3	-0.29	153	0	1.00	148	1.48
E.5-B	5	186	34	-15	1.10	17	-21	-0.23	201	0.99
	8	76	11	-4	1.09	18	-8	0.56	93	1.34
E.5-C	5	304	72	-22	1.16	73	-71	0.02	356	1.23
	7	206	62	-33	1.14	57	0	1.00	292*	0.76
	8	81	19	-6	1.16	30	-8	0.73	116*	0.63

*   Indicates positions of joint failure

**   Using the column numbering: α_{br} =   [6] =   ([3] + [4] + [5]) / [3]

        α_{ch} =   [9] =   ([7] + [8]) / [7]

***   Using the column numbering: $\epsilon_{h.s.;br}$ =   [3] + [4] + [5]

        $\epsilon_{h.s.;ch}$ =   [7] + [8]

****   Ratio given for $|\ \epsilon_{h.s.;br} + \epsilon_{h.s.;ch}\ | > 50 \cdot 10^{-6}$

89

From the results of the calibration of hot spot strains $\epsilon_{h.s.}$ based on individual loads (measured chord and brace member strains) and numerically determined SNCFs (reference and carry-over effects), the following conclusions are given:

- The numerical and experimental results on $\epsilon_{h.s.}$ as illustrated in figure 55 for gap joints 1 show an acceptable agreement.
- Generally, the largest determined $\epsilon_{h.s.}$ ($= \epsilon_{h.s.;br} + \epsilon_{h.s.;ch}$) for the gap joints 1 and 2 investigated occurs at the chord crown location in the gap region for the brace member under tension, which is the same location where fatigue cracking starts. At some chord and brace saddle and inbetween locations of the gap region for the brace member under tension, values of $\epsilon_{h.s.}$ are found which are only slightly smaller than the largest one.
- As shown in table 26, for the relevant total $\epsilon_{h.s.}$ of gap joints 1, the contribution of chord member loads (axial and in-plane bending) cannot be neglected. Therefore, chord member loads should always be considered when analysing $S_{r_{h.s.}}$.
- Comparison of $\epsilon_{h.s.}$ for the brace and chord member locations shows that the contribution of bending strains $\epsilon_{h.s.;ip}$ and $\epsilon_{h.s.;op}$ on the total strains $\epsilon_{h.s.}$ varies around the brace to chord intersection line. But for the brace member loads with large values of $\epsilon_{h.s.}$, the ratio α_{br} (see column 6 of table 26) varies approximately within the range of $1.0 < \alpha_{br} < 1.6$, so that the highest values of 1.6 are close to the average ratio of 1.5 as given in table 19.
  For the chord member loads with large values of $\epsilon_{h.s.}$ however, the ratio α_{ch} (see column 9 of table 26) varies largely and differs considerably from the average ratio of 1.3 as given in table 19.

7. PARAMETER STUDY ON SCFs AND SNCFs OF WELDED UNIPLANAR AND MULTIPLANAR TUBULAR JOINTS

7.1 *Introduction*

For uniplanar joints considerable research on stress concentration factors has been carried out, but there is still a lack of information. It is found that large differences in SCFs exist between those published in various publications. This is due to the difference in numerical modelling of tubular joints (see chapter 3.4) and the method of determining SCFs (see chapter 7.2).
Furthermore, only a few load cases (brace member loads) have been considered in the past. From the calibration results given in chapter 6.2.4 however, it is shown that chord member loads can in a large number of instances be as important as brace member loads. Also, the SCFs have been determined in the past, for a limited number of locations around the perimeter of the brace to chord intersection (mainly the saddle locations).

The results of the numerical calibration on the ratio *SCF/SNCF* given in chapter 6.2.3 have shown the existence of a large scatter. No thorough investigation, particularly numerical, is carried out on this ratio for tubular joints.
For multiplanar joints, which are frequently used, only limited information on SCFs is available.

For the reasons given above, a parameter study on the determination of SCFs as well as SNCFs for several types of uniplanar and multiplanar joints has been carried out. The SCFs are required for practical use so that the hot spot stress range $S_{r_{h.s.}}$ can be determined.
The SNCFs are required to determine the SCF/SNCF ratios for each type of joint as well as for direct comparison of SNCF values with experiments to establish accuracy of the numerical work.

7.2 *Method of SCF and SNCF determination*

Before commencing a parameter study on SCFs (and SNCFs), the following points have to be established:

1   *The finite element (FE) model and weld shape to be used.*
2   *Method of extrapolation and extrapolation region.*
3   *Limits of the extrapolation region with reference to size effect.*
4   *Type of stress to be considered.*
5   *The locations around the reference brace for SCF and SNCF determination.*
6   *Load cases to be analysed.*
7   *Boundary conditions to be used in the FE model.*

Other points, such as the influence of element type, mesh refinement, integration scheme, weld shape and boundary conditions on SCFs have already been discussed in chapter 3.4.

7.2.1   FE model and weld shape to be used

From the conclusions given in chapter 3.4, the joints are modelled with 20-n parabolic solid elements, with the weld shape included. For practical reasons, a butt weld shape that complies with the AWS-code [F2], as frequently used in the offshore industry, is used in the FE model.

Note: Although the existence of an influence of change of weld toe position on SCF is mentioned by [F4, F65], no reliable information is found, which takes this effect into account when determining SCFs. It is proposed, that correction factors related to the leg lengths of the weld should be used when considering other types of weld shape. Further research on this aspect is recommended.

7.2.2   Extrapolation method

For exclusion of effects caused by the global geometry of the weld (flat, concave, convex) and the condition at the weld toe (angle, undercut), an extrapolation of stresses (and strains) to the weld toe location from a defined extrapolation region is carried out for the hot spot stress approach. The extrapolation region, as shown in figure 5, is defined by a specified minimum distance $l_{r,min}$ and a maximum distance $l_{r,max}$ measured from the weld toe location.
Because of the existence of various extrapolation methods (see table 2), a study has been carried out on the influence of extrapolation methods on SCFs.
The three main methods of extrapolation (*a, b* and *c*) considered are:

a. Linear curve fitting (by means of the least squares method) through all the data points in and around the region considered, and extrapolating the obtained curve to the weld toe location.
b. Parabolic (quadratic) curve fitting through all the data points in and around the region considered, and extrapolating the obtained curve to the weld toe location.
c. Parabolic (quadratic) curve fitting through all the data points in and around the region considered, and determining stresses at the two specified positions of the extrapolation region using the obtained curve. A linear extrapolation to the weld toe location is carried out from the stresses of these specified locations.

Figure 57 illustrates the use of the three extrapolation methods *a, b* and *c*.
In this figure the stress distribution is shown for the chord saddle location of an axially loaded reference brace member ($F_{br;ax;a}$) of a KK joint with joint parameters $\beta = 0.40$, $\gamma = 12$, $\tau = 1.00$, $\varphi_{ip} = 60°$ and $\varphi_{op} = 180°$.

The study on the extrapolation region is directly related to the study on the extrapolation method, namely the possibility on accuracy of linear or parabolic

92

curve fitting through the data points in and around the extrapolation region nearby the weld toe.
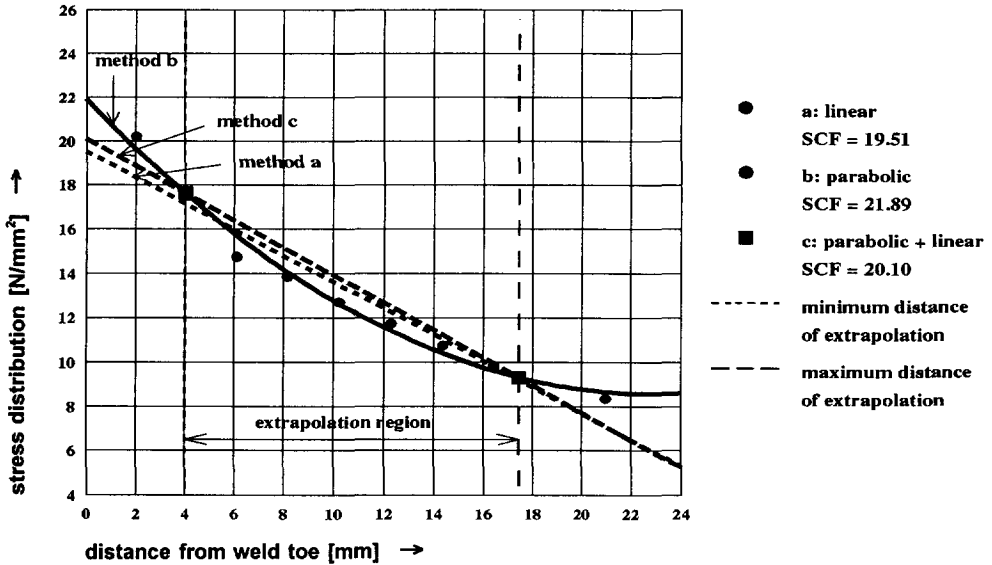
Figure 57. Influence of extrapolation method on the determination of SCFs.

From the study on the influence of extrapolation methods (and region of extrapolation) on SCFs for crown - saddle - inbetween locations, carried out using different types of joints and load cases, it is found that:

- When no extrapolation method is used at all, i.e. where the SCFs are numerically determined on the basis of nodal stresses at the weld toe only, smaller SCFs (especially for the chord member locations) are to be expected, as compared to SCFs obtained by using an extrapolation method.
   The reason for the different results is that at the weld toe node, an average stress of the elements of different thicknesses common to this node is determined. Figure 58 illustrates the differences in SCFs for a KK joint with joint parameters $\beta = 0.40$, $\gamma = 12$, $\tau = 1.00$, $\varphi_{ipl} = 60°$ and $\varphi_{opl} = 180°$. In this figure, SCFs (15 load cases analysed: see chapter 7.2.6) are given for the 8 locations on the chord member and the 8 locations on the brace member.
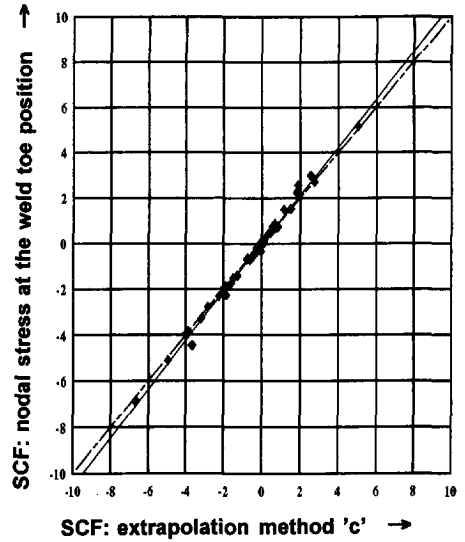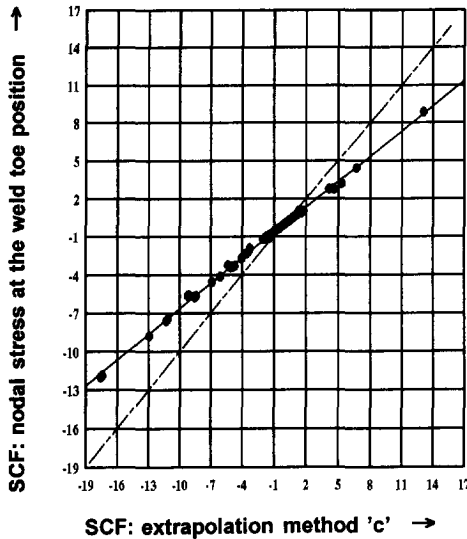
Figure 58.   Influence on SCFs when nodal stresses at the weld toe location are used only.
(Chord saddle location left figure and brace saddle location right figure).

- Inside the extrapolation region proposed by the Working Group III, Tubular joints, of the ECCS (see table 1 and figure 5) the stress gradient can be properly described <u>only</u> as a parabolic function. This because, in general, a parabolic stress gradient exist, which continuous beyond the proposed region. However, a parabolic extrapolation of stresses to the weld toe location is very sensitive to small changes in the data points. For that reason, the extrapolation method c (parabolic curve fitting through the data points and linear extrapolation to the weld toe) will be used for the subsequent work.

7.2.3   Limits of the extrapolation region with reference to scale effect

For one type of a TT joint (180°) so-called an X joint with joint parameters
β = 0.70, γ = 18.0, τ = 1.00 and various chord dimensions (d_0 = 100; 200; 400 and 800 mm), a study has been carried out on the differences in SCF. For all four chord dimensions, a weld shape that complies to the AWS-code has been modelled.
The influence of changes in chord diameter on the stress distribution near the weld toe, when using the extrapolation method c and extrapolation region as described in table 1, is shown in figure 59. SCFs for the chord saddle location are shown in figure 60.

94

The distances for the extrapolation region of the four chord dimensions used are summarized in table 27.
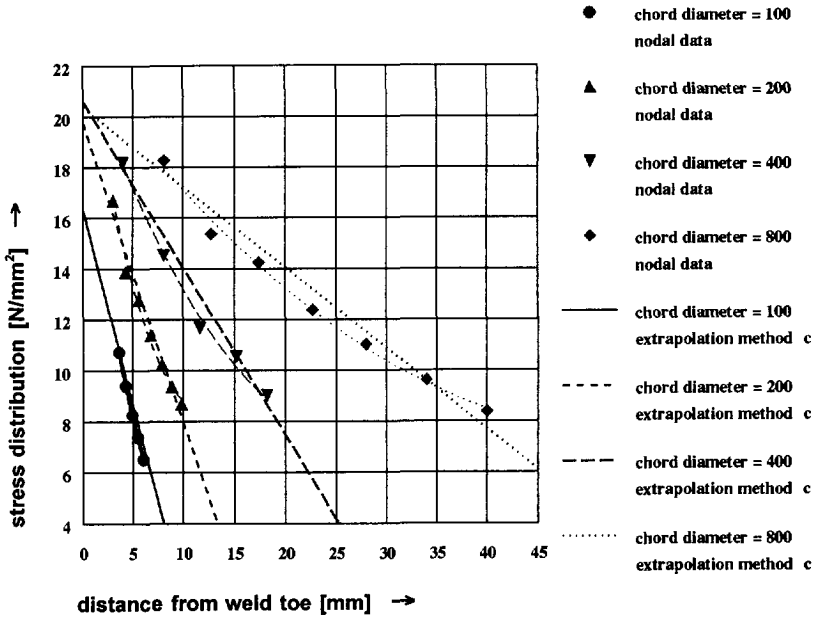
Figure 59. The influence of changes in chord diameter on numerically determined gradient of the stress distribution nearby the weld toe location.
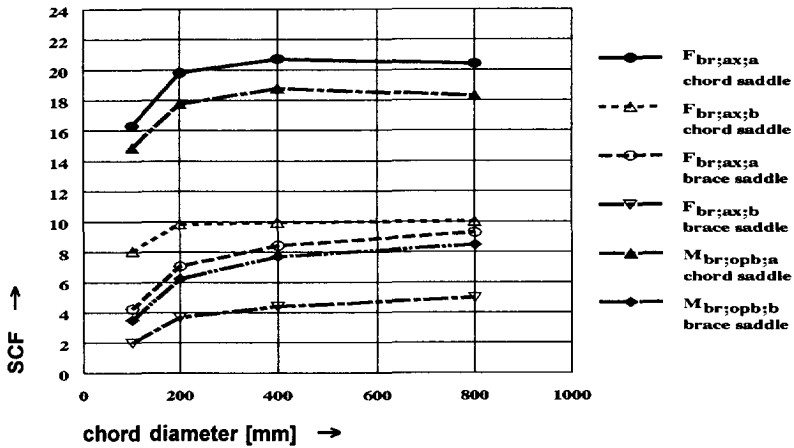
Figure 60. The influence of changes in chord diameter on the determined SCFs for the chord saddle and brace saddle location of an X joint.

Table 27.   Distances of the extrapolation region for the chord saddle
location according to the formulae given in table 1.

TTjoint (180°) with: $\beta = 0.70$; $\gamma = 18$; $\tau = 1.00$							
Chord [mm]		Minimum distance [mm]		Maximum distance [mm]		Extrapolation region [mm]	
d_o	t_o	$l_{r,min}$	$l_{r,min} / t_o$	$l_{r,max}$	$l_{r,max} / t_o$	$\Delta l_r = l_{r,max} - l_{r,min}$	$\Delta l_r / t_o$
100	2.78	4.00	1.44	4.36	1.57	0.36	0.13
200	5.56	4.00	0.72	8.73	1.57	4.73	0.85
400	11.11	4.44	0.40	17.45	1.57	13.01	1.17
800	22.22	8.89	0.40	34.91	1.57	26.02	1.17

When using the extrapolation region according to table 1, limits with reference to joint size (chord diameter d_o and joint parameter γ) are found.
As shown in table 27, decrease of d_o might result in a large reduction of $\Delta l_r / t_o$.
As illustrated in figures 59 and 60, it is found that the combination of the defined extrapolation region Δl_r and the location of the start of the extrapolation region given by $l_{r,min}$ causes an increase of differences in SCFs when decreasing the chord diameter d_o.
This is especially the case when using small values of γ ($\gamma < 10$). Beside this, an increase of d_o results in a decrease of the gradient of the stress distribution to the weld toe (see also figure 59) and so a decrease of sensitivity on extrapolation.
For the parameter study, in order to avoid the possible large sensitivity of extrapolation region on SCFs when using the equations given in table 1, a chord diameter $d_o > 400$ mm with $\gamma > 12$ is advised.

Note: To the authors opinion;
        compared to the extrapolation region defined in table 1, a more simplified and less sensitive extrapolation region can be used for both the chord and brace member locations, namely:
        chord member: $l_{r,min} = 0.4 \cdot t_o$ and $l_{r,max} = 1.4 \cdot t_o$
        brace member: $l_{r,min} = 0.4 \cdot t_1$ and $l_{r,max} = 1.4 \cdot t_1$
        This region is similar to the region used for rectangular hollow section joints [F61].

7.2.4   Type of stress to be considered

In most studies up till now, the SCFs determined numerically are based on the use of principal stresses only [F13, et al].
A limited investigation has been carried out for some types of multiplanar joints on the influence of type of stress used on SCFs. Two types of stresses are considered, namely:

96

- *Principal stresses.*
- *Primary stresses in a direction perpendicular to the chord weld toe for the chord member locations and in a direction parallel to the axis of the brace member for the brace member locations (this direction mostly differs from the direction perpendicular to the brace weld toe).*

Figure 61 shows an example of the difference obtained on SCF by using the principal and primary stresses.
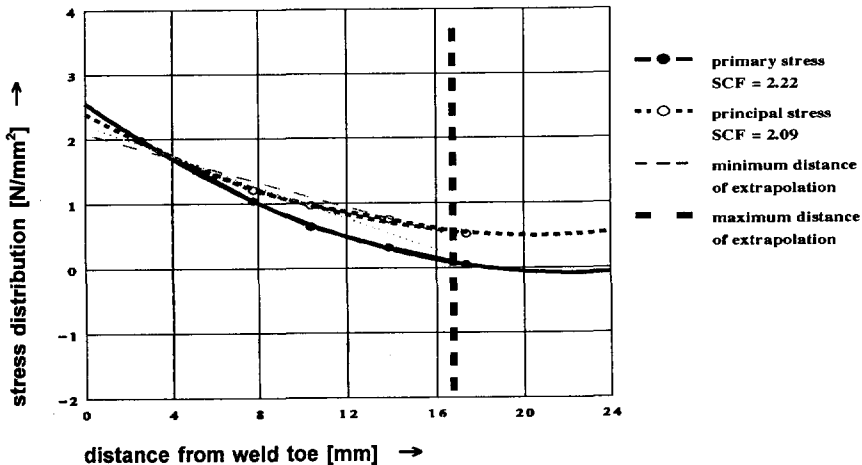
Figure 61. Difference in SCF by using primary and principal stresses.

From the investigation on the influence of type of stress used for SCFs, it is found that:

- *The direction of principal stresses inside the extrapolation region changes, which causes problems when extrapolating stresses to the weld toe location.*
- *For the extrapolation method and extrapolation region used, use of principal stresses (and strains) can result in lower SCFs compared to SCFs due to primary stresses [F46]. For instance, the orientation of the principal stress near the weld toe is perpendicular to the toe. Further away, inside the extrapolation region, the orientation may change, and therefore the extrapolated principal stress drops in comparison to the extrapolated primary stress. Figure 61 illustrates this phenomenon.*

Although, generally small differences (<10%) in SCFs are found in the limited investigation carried out for some types of joints, it has been decided to use primary stresses only. The use of primary stresses is also supported by the direction of crack growth, which is usually along the toe of the weld.

97

7.2.5 Locations around the reference brace for SCF (SNCF) determination

From the investigation on modelling for tubular joint SCFs and results on calibration of numerical work based on individual loads as described in chapter 6.2.4, the locations of interest for both chord and brace member are the crown, saddle and inbetween.
Figure 62 (see also figure 2) shows the 8 locations of the chord and 8 locations of the brace member, where SCF and SNCF values are determined.
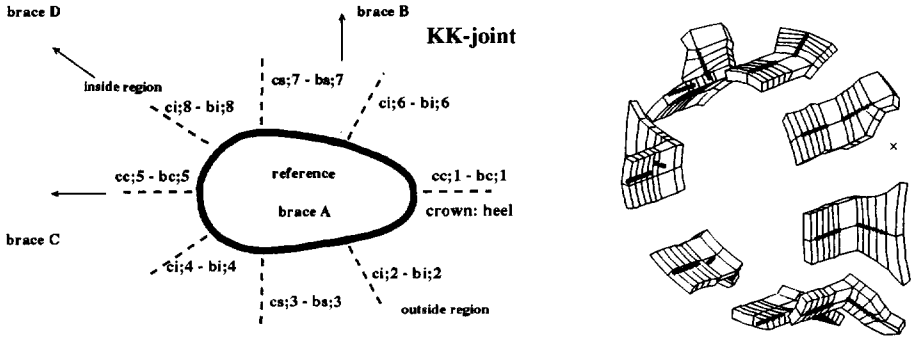
Figure 62. Selected elements and nodes for the SCF and SNCF determination.

7.2.6 Load cases to be analysed

The following load cases are analysed:

Brace member(s): $F_{br;ax}$; $M_{br;ip}$; $M_{br;op}$.
Chord member: $F_{ch;ax}$; $M_{ch;ip}$; $M_{ch;op}$.

As an example, analysing a KK joint results in $2_{(a)} \cdot 8_{(b)} \cdot 15_{(c)} = 240$ SCF and 240 SNCF values, where:

(a) = Chord + reference brace member (totally 2 member parts).

(b) = Number of locations of interest on a member, see figure 62 (totally 8 on each member part).

(c) = Number of load cases, three load cases for the chord member and three load cases for each brace member: KK joint ⇒ four brace members.

Because of the large resistance of tubular members against torsion, torsional brace moments $M_{br;t}$ might occur which causes non-negligible hot spot stresses.
No information on this exist and therefore, a study on the influence of torsional

98

brace moments $M_{br;t}$ on SCFs has been carried out [F46].
It appears that as an acceptable approximation, SCFs due to $M_{br;t}$ can be determined by resolving $M_{br;t}$ into an out-of-plane bending component $M_{br;op}$ as shown in figure 63, and considering the SCFs due to this component only (the SCFs caused by $M_{br;w}$ are found to be small compared to SCFs caused by $M_{br;op}$).
To avoid unnecessary SCF data, this load case is therefore not analysed separately.
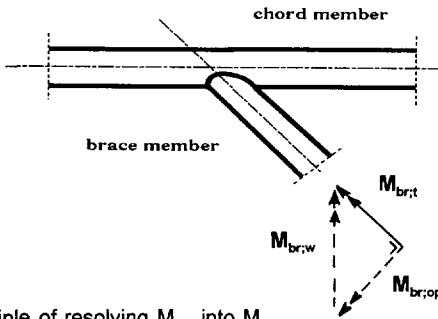
Figure 63. Principle of resolving $M_{br;t}$ into $M_{br;op}$.

As an illustration, figure 64 shows for a KK joint with joint parameters β = 0.60, γ = 24, τ = 1.00, φ_{ip} = 30° and φ_{op} = 90° results of SCFs for the 8 locations on the chord member and 8 locations of the brace member. On the horizontal axis the SCFs are given for the load cases $M_{br;op;a}$, $M_{br;op;b}$, $M_{br;op;c}$ and $M_{br;op;d}$. On the vertical axis the SCFs are given for the load cases $M_{br;t;a}$, $M_{br;t;b}$, $M_{br;t;c}$ and $M_{br;t;d}$, which causes when resolving $M_{br;t}$ into a component $M_{br;op}$ (and $M_{br;w}$) the same value of $M_{br;op}$ as used for the horizontal axis.
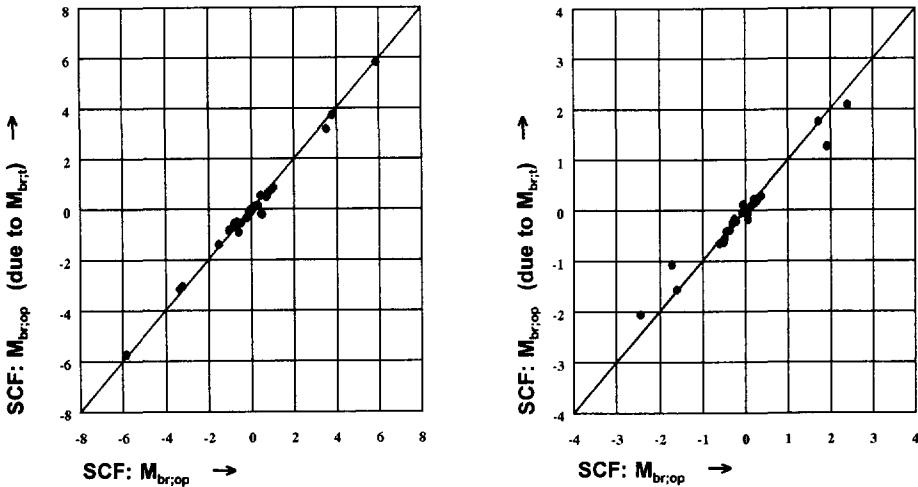
Figure 64. Relation between SCFs for a KK joint with brace members loaded by $M_{br;op}$ and $M_{br;t}$.
(Chord member locations left figure and brace member locations right figure).

99

7.2.7 Boundary conditions to be used in the FE model

The decision is made to use a boundary system with a pin ended chord member and a free ended brace member. In addition to this, for equilibrium purpose, one side of the chord member is also fixed against rotation around the chord axis. For the boundary conditions used, in case of brace member loads, moments in the chord member are introduced which affect the SCFs (see chapter 3.4.2). To obtain data on SCFs and SNCFs which are independent of the boundary condition used, compensating moments are applied to obtain the effect of the brace member loading only. An example is given in figure 65, in which the compensating moments for an axially loaded brace member of a T joint are given for the locations of interest (crown, saddle and inbetween), namely:

locations 1, 5 (crown) $M_{compensating} = 0.50 \cdot F_{br;ax} \cdot x1$
locations 2, 4, 6, 8 (inbetween) $M_{compensating} = 0.50 \cdot F_{br;ax} \cdot x2$
locations 3, 7 (saddle) $M_{compensating} = 0.25 \cdot F_{br;ax} \cdot L$

In all previous studies, the obtained SCFs incorporate the effect of the bending moment in the chord for e.g. by inclusion of an α parameter with $\alpha = 2L / d_o$. Therefore, the results on SCFs, especially those for carry-over effects (see chapter 3.4.2), are largely boundary depending. The method used is found to be more realistic, since the results are independent of the boundary condition used.
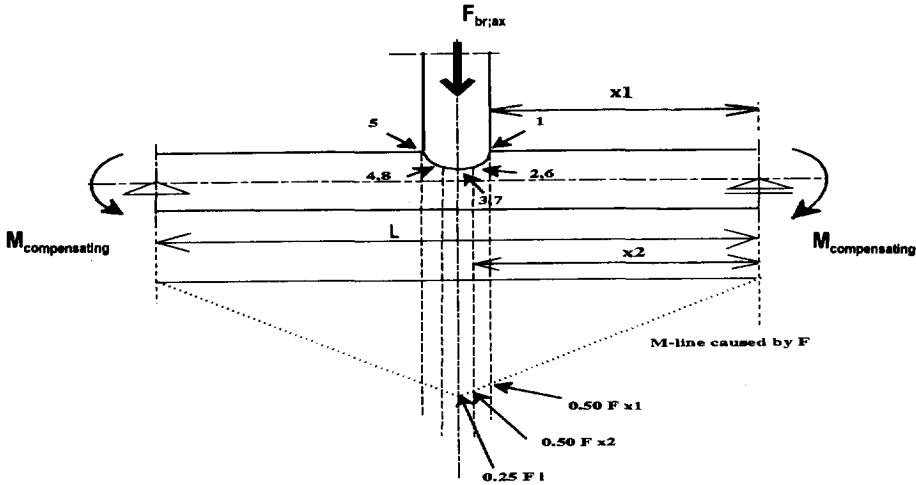
Figure 65. An example on compensating moments applied to obtain SCFs independent of boundary conditions used.

7.3 Relationship between SCF and SNCF

Because of the almost isotropic behaviour of steel and assuming that $\sigma_z = 0$ (plane-stress condition), the relationship between σ_x and ϵ_x can be written as:

100

$$\frac{\sigma_x}{E \cdot \epsilon_x} = (\frac{1 + v \cdot \frac{\epsilon_y}{\epsilon_x}}{1 - v^2})$$ in which:

x = The direction perpendicular to the weld toe (chord member locations), or parallel to the axis of the brace member (brace member locations).

y = The direction parallel to the weld toe (chord member locations), or along the brace member surface perpendicular to the axis of the brace member (brace member locations).

z = The direction perpendicular to the member surface.

v = 0.30 (Poissons ratio for steel).

With v = 0.30, this equation when expressed in hot spot terms results in the simplified form of:

$$\frac{\sigma_{x,h.s.}}{E \cdot \epsilon_{x,h.s.}} = (1.10 + 0.33 \cdot \frac{\epsilon_y}{\epsilon_{x,h.s.}})$$ so that: $$\frac{SCF}{SNCF} = (1.10 + 0.33 \cdot \frac{\epsilon_y}{\epsilon_{x,h.s.}}).$$

It follows that the ratio SCF/SNCF entirely depends on the ratio $\frac{\epsilon_y}{\epsilon_{x,h.s.}}$.

The assumption that $|\frac{\epsilon_y}{\epsilon_{x;h.s.}}| < 1.0$, which is expected to be correct for large values for SCF, results into the relationship: $0.8 < \frac{SCF}{SNCF} < 1.4$.

7.4 Joint types and geometries analysed

The type of (gap) joints and geometries analysed and discussed are summarized in tables 28 and 29.

Table 28. Geometries used for the parameter study (braces perpendicular to the chord axis).

Type of joint. (FE models are shown in figure 6)	Number of joints analysed	Joint parameters			Number of SCFs and SNCFs analysed
		β	γ	τ	
T joint	48	$0.30 \leq \beta \leq 0.90$	$12 \leq \gamma \leq 30$	$0.25 \leq \tau \leq 1.00$	9216
TT joint φ_{op} = 45° φ_{op} = 70° φ_{op} = 90° φ_{op} = 135° φ_{op} = 180° (X joint)	12 12 36 36 48	$\beta = 0.30$ $\beta = 0.30$ $0.30 \leq \beta \leq 0.65$ $0.30 \leq \beta \leq 0.70$ $0.30 \leq \beta \leq 0.90$	$12 \leq \gamma \leq 30$	$0.25 \leq \tau \leq 1.00$	3456 3456 10368 10368 13824
XX joint (φ_{op} = 90°-180°-270°)	60	$0.30 \leq \beta \leq 0.60$	$8 \leq \gamma \leq 32$	$0.25 \leq \tau \leq 1.00$	17280

Table 29. Geometries used for the parameter study (braces inclined to the chord axis).

Type of joint. (FE models are shown in figure 7)	Number of joints analysed	Joint parameters			Number of SCFs and SNCFs analysed
		β	γ	τ	
Y joint					
$\varphi_{ip} = 30°$	48	$0.25 \leq \beta \leq 0.75$			23040
$\varphi_{ip} = 45°$	48	$0.25 \leq \beta \leq 0.90$	$12 \leq \gamma \leq 30$	$0.25 \leq \tau \leq 1.00$	23040
$\varphi_{ip} = 60°$	48	$0.25 \leq \beta \leq 0.90$			23040
K joint					
$\varphi_{ip} = 30°$	48	$0.25 \leq \beta \leq 0.75$			23040
$\varphi_{ip} = 45°$	36	$0.25 \leq \beta \leq 0.60^{*}$	$12 \leq \gamma \leq 30$	$0.25 \leq \tau \leq 1.00$	17280
$\varphi_{ip} = 60°$	24	$0.25 \leq \beta \leq 0.40$			11520
KK joint					
$\varphi_{ip} = 30°: \varphi_{op} = 45°$	36	$0.25 \leq \beta \leq 0.40$			17280
$: \varphi_{op} = 90°$	36	$0.25 \leq \beta \leq 0.60$			17280
$: \varphi_{op} = 180°$	48	$0.25 \leq \beta \leq 0.75$			23040
$\varphi_{ip} = 45°: \varphi_{op} = 45°$	36	$0.25 \leq \beta \leq 0.50$			17280
$: \varphi_{op} = 90°$	36	$0.25 \leq \beta \leq 0.60$	$12 \leq \gamma \leq 30$	$0.25 \leq \tau \leq 1.00$	17280
$: \varphi_{op} = 180°$	36	$0.25 \leq \beta \leq 0.60$			17280
$\varphi_{ip} = 60°: \varphi_{op} = 45°$	24	$0.25 \leq \beta \leq 0.40$			11520
$: \varphi_{op} = 90°$	24	$0.25 \leq \beta \leq 0.40$			11520
$: \varphi_{op} = 180°$	24	$0.25 \leq \beta \leq 0.40$			11520

*   general: size of β limited to avoid overlaps.

For the joints analysed, the chord length is taken $L_{ch} \geq 6d_{o}$, and the brace length $L_{br} \geq 3d_{1}$.

The joint parameters (β, γ, τ and φ_{ip}) of the carry-over brace member(s) are taken equal to those of the reference brace member.

Because of the enormous amount of data obtained when analysing a joint (see column 6 of tables 28 and 29), the results of SCFs and SNCFs are stored in data files.

Besides the data files, graphs for SCFs are made for convenience in use and understanding of the behaviour. The results given as data files, graphs and evaluation of the SCF and SNCF results are presented in separate reports for each type of joint investigated.

The reports also contain results (and evaluation) of the comparison with other available experimental and numerical work.

Experimentally obtained SCFs for $\beta > 0.95$ are excluded for comparison because of the large sensitivity of the weld shape on SCFs. Also, SCFs for $\alpha < 8.0$ are excluded because of the influence of boundary condition on SCFs.

7.5 Results of the investigation for joints with braces perpendicular to the chord axis

The results of the investigation on joints with braces perpendicular to the chord axis are reported in detail in [F41-F45, F47] and therefore, only the main results and conclusions will be summarized in this thesis.

This chapter summarizes results and conclusions on T joints, TT joints and XX joints independently.

Results on SCFs due to chord member loads and results on the ratio SCF/SNCF, which are found to be common to all types of T, TT and XX joints investigated, are given separately in chapter 7.5.6.

7.5.1 Results and conclusions of the investigation on T joints [F41]

Comparison with experimental data.

From literature study it is found that most experimental work on T joints have been carried out using acrylic models without fillets [F62], and only limited experimentally determined SCF values based on steel models with $\beta \leq 0.95$ and $\alpha \geq 8$ are available.

Table 30 summarizes the results of the comparison between numerical data from this parameter study and experimental data from tested steel models. In the comparison, all brace and chord loads are considered.

Table 30.   Comparison between numerical and experimental data on SCFs for T joints.

Test results Steel models	Load case	Chord			Joint parameters			SCFs experimental		Ratio parameter study experimental		Ratio wordsworth experimental	Ratio efthymiou experimental
		support	d_o [mm]	α	β	γ	τ	cs	bs	cs	bs	bs	bs
[F3]	$F_{br,ax}$ $F_{br,ax}$ $F_{br,ax}$	pin ended	457 457 914	10 10 10	0.50 0.25 0.50	14.3 14.3 14.3	0.50 0.39 0.50	6.7 4.7 7.7		1.16 1.00 1.02			
[F56]	$M_{br,op}$ $M_{br,op}$	fixed ended	457 457	14 14	0.25 0.25	14.3 14.3	0.39 0.28	2.6 1.8	2.0 1.7	1.00 0.95	1.00 1.00	1.20 1.18	1.50 1.53
[F29]	$F_{br,ax}$ $M_{br,op}$ $M_{br,op}$	pin ended	508 508 508	8 8 8	0.80 0.80 0.80	20.0 20.0 31.8	1.00 1.00 1.00		8.2 7.3 10.6		1.01 1.12 1.02	1.40 1.82 1.94	1.11 1.22 1.15

From table 30 it is concluded that the results of this parameter study are in good agreement with the experimental results.

103

Comparison with numerical work from Wordsworth and Smedley [F62].

For the brace member loads $F_{br;ax}$, $M_{br;ip}$ and $M_{br;op}$, a set of T joint formulae are given by Wordsworth and Smedley (Lloyd's Register of Shipping Research Laboratory, UK.). These formulae are based on an extensive study of experimentally tested small acrylic models where welds are not modelled.

Chord member locations:
It is found that the relevant SCFs for the chord crown and chord saddle locations show an acceptable agreement (differences within ±15%) between these parameter study results and the results given by formulae from Wordsworth and Smedley. Figure 66 shows the differences in SCF results for a T joint with $\tau = 0.50$.
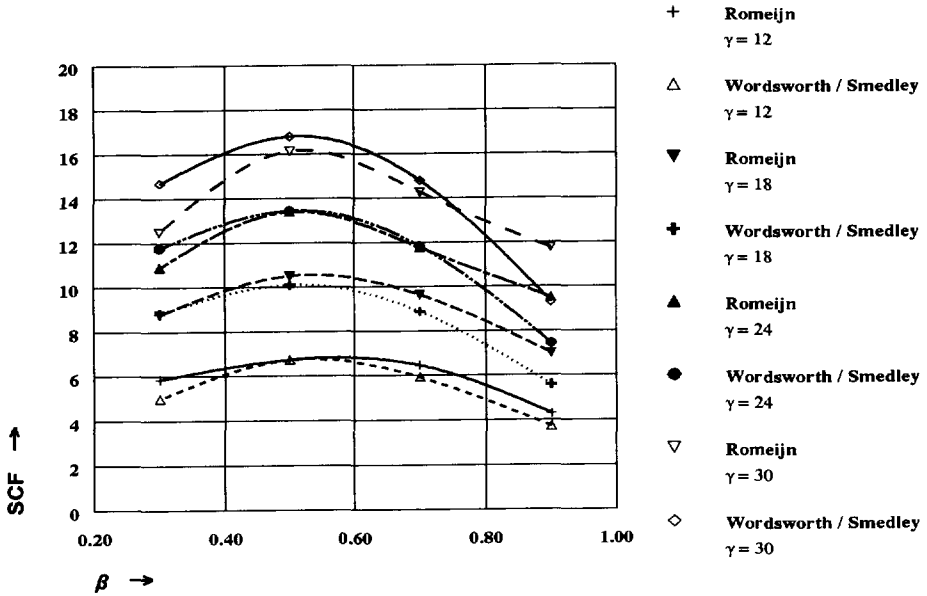
Figure 66.   T joint with $\tau = 0.50$: comparison of SCFs from the parameter study with SCFs from Wordsworth and Smedley.

Brace member locations:
The relevant SCFs for the brace crown and saddle locations show large differences (within ±100% ; see column 13 of table 30). The SCF formulae given by Wordsworth and Smedley give conservative values for the brace crown and brace saddle locations, because they are based upon measurements at the outer surface of the chord to brace connection, instead of the weld toe location, resulting in higher SCFs (see also results on modelling for tubular joint SCFs given in chapter 3.4).

104

Comparison with numerical work from Efthymiou [F13].

For the brace member loads $F_{br;ax}$, $M_{br;ip}$ and $M_{br;op}$, T joint formulae have been developed by Efthymiou at Shell International Petroleum Maatschappij B.V.), the Netherlands. These formulae are based on FE analyses only. The joints have been modelled with shell elements and for the weld area solid elements. The SCFs given by Efthymiou are based on the maximum principal stress linearly extrapolated to the weld toe.
For T joints, the primary stress perpendicular to the weld toe (crown and saddle locations) coincide with the maximum principal stress.

Chord member locations:
    Comparison of the relevant SCFs from this parameter study and the SCF formulae given by Efthymiou, shows that for $a > 12$ an acceptable agreement for the chord crown and chord saddle locations exist (differences within $\pm 15\%$). For $a < 12$, the formulae given by Efthymiou show for the saddle locations a large influence of a on the SCFs for the brace member loads $F_{br;ax}$ and $M_{br;op}$. This causes large differences between the SCFs from the Efthymiou formulae and those from the parameter study as well as from the experiments. As an example, figures 67 and 68 in which the SCF results are shown for a T joint with joint parameters $\beta = 0.50$, $\gamma = 30$ and $\tau = 1.00$ illustrate the differences.
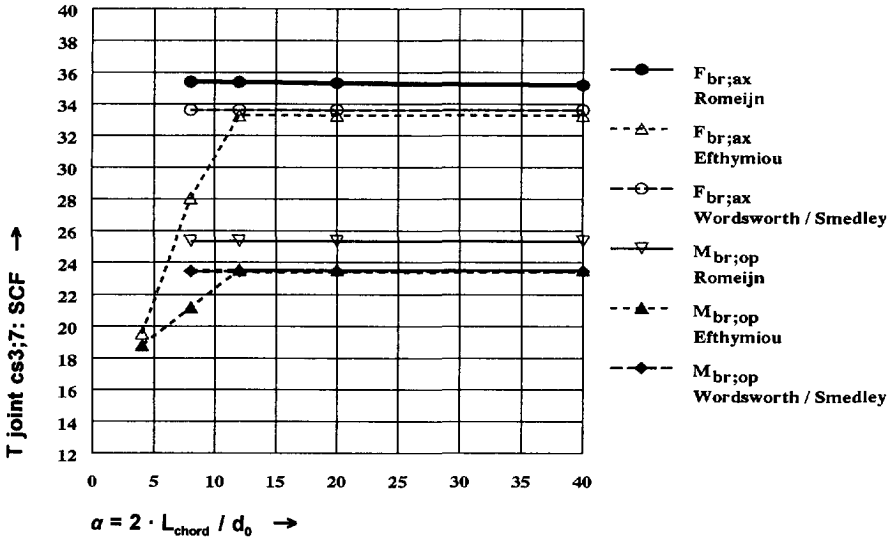
Figure 67.   Influence of short chord correction factors (for $a < 12$) given by Efthymiou on the SCFs for the cs;3,7 location and comparison with parameter study results and results given by Wordsworth and Smedley.
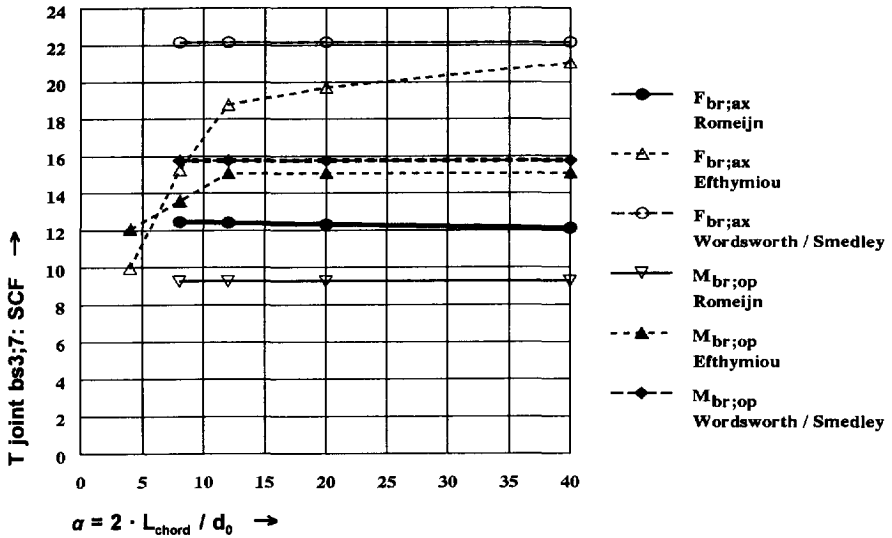
Figure 68.   Influence of short chord correction factors (for $\alpha < 12$) given by Efthymiou on the SCFs for the bs;3,7 location and comparison with parameter study results and results given by Wordsworth and Smedley.

Brace member locations:

Comparison of the relevant SCFs from the parameter study and the SCF formulae given by Efthymiou, with $\alpha > 12$ to avoid the sensitivity of the short chord correction factors on SCFs, shows large differences (within ±200%) for the brace crown and brace saddle locations. The parameter study as well as the analyses carried out by Efthymiou include the weld shape, so that the method of modelling is not the reason for the differences. An explanation on the differences cannot directly be given. As shown in column 14 of table 30 large differences also exist between experimental data and SCFs from formulae given by Efthymiou. This is especially the case for $\alpha > 12$ (no short chord correction factor applied by Efthymiou).

When comparing the SCF formulae given by Wordsworth/Smedley and Efthymiou, large differences also exist for the brace member locations, which is expected because of the different locations where SCFs are determined (outer surface of the intersection between the brace and chord members versus the weld toe location). However, for $\alpha > 12$ in many cases the SCFs given by Efthymiou are larger than the SCFs given by Wordsworth and Smedley, which from modelling aspects, see also chapter 3.4, cannot be explained.

Figure 69 shows the differences in SCF results for the brace saddle location of an axially loaded T joint brace member ($F_{br;ax;a}$) with joint parameter $\alpha = 8\text{-}40$ and $\tau = 0.25$, which are the limits of validity range for the SCFs formulae given by Wordsworth and Smedley.

106

Figure 69 chart

Legend:

- ▲ Efthymiou $\gamma = 12$; $\alpha = 8$
- ● Efthymiou $\gamma = 18$; $\alpha = 8$
- ◆ Efthymiou $\gamma = 24$; $\alpha = 8$
- ■ Efthymiou $\gamma = 30$; $\alpha = 8$
- △ Efthymiou $\gamma = 12$; $\alpha = 40$
- ○ Efthymiou $\gamma = 18$; $\alpha = 40$
- ◇ Efthymiou $\gamma = 24$; $\alpha = 40$
- □ Efthymiou $\gamma = 30$; $\alpha = 40$
- ✦ Wordsworth / Smedley $\gamma = 12$; $\alpha = 8-40$
- ▽ Wordsworth / Smedley $\gamma = 18$; $\alpha = 8-40$
- + Wordsworth / Smedley $\gamma = 24$; $\alpha = 8-40$
- ▼ Wordsworth / Smedley $\gamma = 30$; $\alpha = 8-40$

Y-axis: SCF (0 to 12)
X-axis: β → (0.00, 0.20, 0.40, 0.60, 0.80, 1.00)
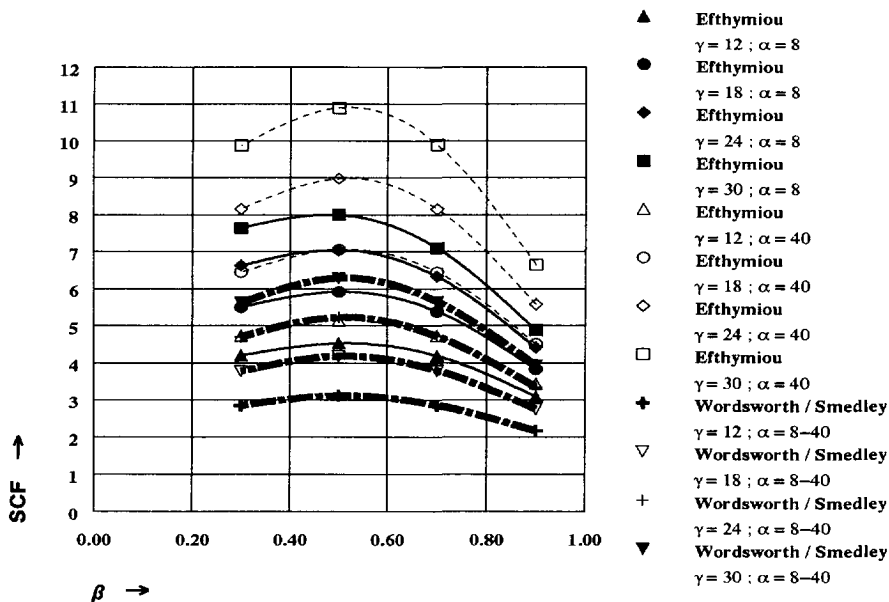
Figure 69. SCFs for the brace saddle location of a T joint with r = 0.25. SCFs obtained from formulae given by Wordsworth/Smedley and Efthymiou.

7.5.2 Results and conclusions of the investigation on TT joints [F42-F45]

Comparison with experimental data.

Limited experimentally obtained SCFs for TT joints with ψ_{op} = 180° [F3, F28, F47] and TT joints with ψ_{op} = 90° [F3, F30] based on steel models with β < 0.95 and $\alpha \geq 8.0$ exist.
For the TT joint with ψ_{op} = 90°, SCF results also exist from acrylic models where the SCFs are determined on the outer surface of the intersection between the brace and chord member [F62]. For the TT joints with ψ_{op} = 45°, 70° and 135° no experimental data exist. From the comparison of T joint results between SCFs obtained on acrylic models without the weld shape included and SCFs obtained from steel models it is found that for the chord member locations an acceptable agreement in SCFs exist (differences within ±15%). Therefore, because of the very limited experimental results from steel models on SCFs for TT joints with ψ_{op} = 90°, the SCF results on the chord member locations from acrylic models are also used for comparison purposes. The results of the comparison between the numerical data of this parameter study and experimental data are given in table 31 for the TT joints with ψ_{op} = 90° and in table 32 for the TT joints with ψ_{op} = 180°.

107

Table 31.   Comparison between numerical and experimental data on SCFs for TT joints with φ_{op} = 90°.

Test results	Load case	Chord			Joint parameters			SCFs experimental			Ratio parameter study / experimental			Ratio efthymiou / experimental		
		support	d_o [mm]	α	β	γ	τ	cs;3	cs;7	cc	cs;3	cs;7	cc	cs;3	cs;7	cc
[F3] (steel models)	$F_{br;ax;a}$	pin	914.4	10	0.50	14.3	0.50		8.1			1.00			0.91	
	$F_{br;ax;b}$	ended						-2.8	-5.5		0.82	0.91		1.36	0.69	
[F62] (acrylic models)	$F_{br;ax;a}$	pin	152.4	13.5	0.50	12.0	0.50	6.8	6.6	3.7	1.05	1.03	1.00	0.94	0.94	0.81
	$F_{br;ax;b}$	ended						-2.3	-4.0		0.87	1.05		1.39	0.80	
	$M_{br;op;a}$							-5.1	5.1		1.06	1.06		0.92	0.92	
	$M_{br;op;b}$							-1.4	-0.7		0.80	1.00				
	$M_{br;ip;a}$									2.3			0.87			0.91
[F30] (steel models)	$F_{br;ax;a}$	pin	--	12	0.50	12.0	0.50	7.0			1.02			0.91		
	$F_{br;ax;b}$	ended						-2.3			0.87			1.39		

Table 32.   Comparison between numerical and experimental data on SCFs for TT joints with φ_{op}=180°.

Test results (steel models)	Load case	Chord			Joint parameters			SCFs experimental			Ratio par. study / experimental			Ratio efthymiou / experimental			Ratio smedley / experimental		
		support	d_o [mm]	α	β	γ	τ	cs	cc	bs	cs	cc	bs	cs	cc	bs	cs	cc	bs
[F47] (balanced loaded)	$F_{br;ax}$	pin	406	12	0.60	20.0	1.00	41.2	2.6	14.8	0.86	1.00	0.93	0.79	1.19	1.16	0.83		1.53
	$M_{br;ip}$	ended	406	12	0.60	20.0	1.00		4.2			1.21			0.73			1.23	
	$F_{br;op}$		406	12	0.60	20.0	1.00	18.5		6.8	0.99		1.03	0.90		2.01	0.96		1.74
[F3] (balanced loaded)	$F_{br;ax}$	pin ended	914	10	0.50	14.4	0.50	10.9		7.3	1.00		0.98	1.02		2.18	1.07		1.15
[F28] (unbalanced loaded)	$F_{br;ax;a}$	fixed ended	473	8.46	0.72	10.4	0.94	13.1		8.8	0.92		0.92	0.65		0.69		no formulae	

From tables 31 and 32, it is concluded that the results of this parameter study are in reasonable agreement with the experimental results.

Comparison with numerical work from Wordsworth and Smedley [F65].
Wordsworth and Smedley give some SCF formulae for a TT joint (180°) with balanced axially loaded brace members $F_{br;ax;a}$ + $F_{br;ax;b}$ and for balanced out-of-plane bending moment loaded brace members $M_{br;op;a}$ + $M_{br;op;b}$. They also propose the use of the T joint formulae for (unbalanced) in-plane moment $M_{br;ip;a}$ loaded brace member 'a' of the TT joint (180°). The comparison of SCF data from the parameter study with SCF formulae given by Wordsworth and Smedley results in

108

similar conclusions as mentioned for the T joint, namely that acceptable agreement is obtained for the SCFs on the chord member, and large differences for the SCFs on the brace member. Those large differences also exist when comparing with experimental data (see column 20 of table 32). The reasons for the differences observed are the same as those given in chapter 7.5.1. which discusses the SCF comparisons for T joints.

Comparison with numerical work from Efthymiou [F13].
SCF formulae on TT joints (180°) are given by Efthymiou for a loaded reference brace member 'a' ($F_{br;ax;a}$, $M_{br;ip;a}$ and $M_{br;op;a}$) and/or a loaded carry-over brace member b ($F_{br;ax;b}$, $M_{br;ip;b}$ and $M_{br;op;b}$).
Efthymiou also published SCF influence functions on carry-over effects (due to $F_{br;ax;b}$ only) when varying the out-of-plane angle φ_{op} between the two braces 'a' and b. A comparison of SCF data from this parameter study with the SCF formulae by means of influence functions given by Efthymiou shows large differences in SCF results for the saddle and crown locations of the chord and brace member. As an example, figures 70 and 71 illustrate the differences in SCFs due to $F_{br;ax;b}$ for the chord and brace saddle locations of a TT joint with various values of φ_{op}. From the parameter study results, and the test results given in table 31, it is shown that large differences in SCFs due to $F_{br;ax;b}$ exist for the two saddle locations cs;3 and cs;7. The influence functions on SCFs given by Efthymiou, however, assume the same SCF value for both saddle locations. For the chord crown and brace crown locations, the influence functions given by Efthymiou represent nominal chord bending stresses caused by axially loaded brace member b. These stresses do not include the hot spot stresses due to the non uniform stiffness of the joint, which makes a realistic comparison impossible.
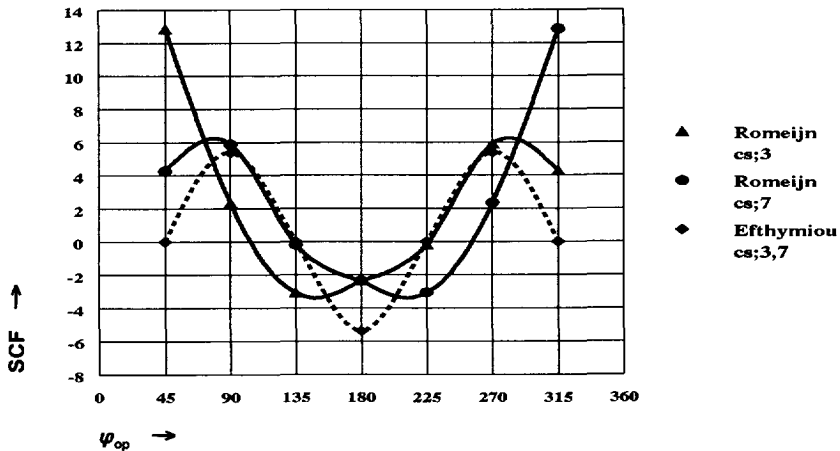
Figure 70. SCFs due to $F_{br;ax;b}$ for the chord saddle locations of brace 'a' of a TT joint with different φ_{op}. Results shown for $\beta = 0.30$, $\gamma = 30$ and $\tau = 1.00$.
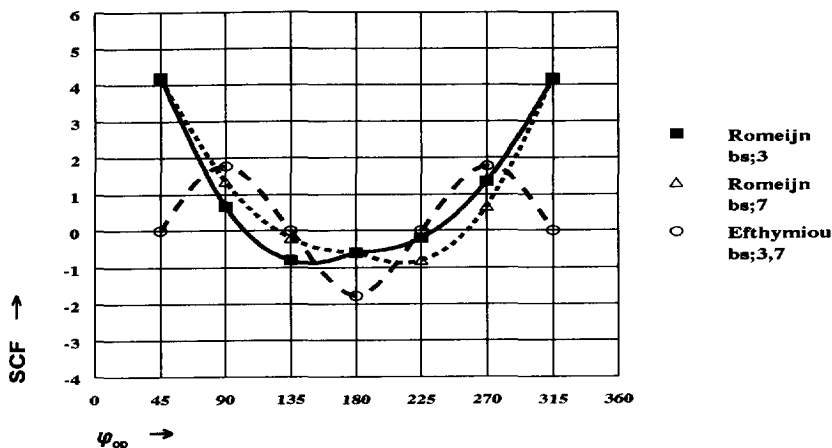
Figure 71. SCFs due to $F_{br;ax;b}$ for the brace saddle locations at brace 'a' of a TT joint with different φ_{op}. Results shown for $\beta = 0.30$, $\gamma = 30$ and $\tau = 1.00$.

7.5.3 *Importance of out-of-plane carry-over effects on SCFs*

From an investigation on SCFs caused by out-of-plane carry-over effects (SCFs due to load cases $F_{br;ax;b}$, $M_{br;ip;b}$ and $M_{br;op;b}$), with varying joint parameters β, γ, τ and φ_{op}, it is found that these SCFs in many cases cannot be neglected. This is dependent on a combination of the following aspects.

-       *The type of carry-over loading considered.*
-       *The location of interest.*
-       *The joint parameters considered.*

Some results showing the importance of SCFs caused by out-of-plane carry-over effects are summarized in table 33.
About the importance of SCFs caused by out-of-plane carry-over effects it is concluded that:

-    The influence of changes in γ and τ on out-of-plane carry-over effects, although considerable for γ, is generally small compared to the influence of changes in β and φ_{op}.
-    For the chord saddle and brace saddle locations, the load cases $F_{br;ax;b}$ and $M_{br;op;b}$ cause large carry-over effects. This is especially the case with increasing β. Figures 72 and 73 show for a TT joint with $\varphi_{op} = 180°$ and $\tau = 1.00$ the influence of β on SCFs caused by reference effects ($F_{br;ax;a}$) and carry-over effects ($F_{br;ax;b}$).
-    As illustrated in figures 70 and 71, depending on φ_{op}, the SCF results for the two saddle locations (chord and brace member) might differ entirely. Comparison of the test results given in columns 9 and 10 of table 31 results in the

110

same conclusions on the existence of a large difference in SCFs between the two saddle locations.

- The carry-over effects caused by $M_{br;ip;b}$ are negligible for all locations considered.
- The carry-over effects caused by $M_{br;op;b}$ are negligible for the chord crown and brace crown locations.
- When varying φ_{op}, a harmonic function for SCFs due to carry-over effects exists, and the largest absolute SCFs caused by the carry-over effects are found in the region forming the shortest gap. (See also figures 70 and 71).
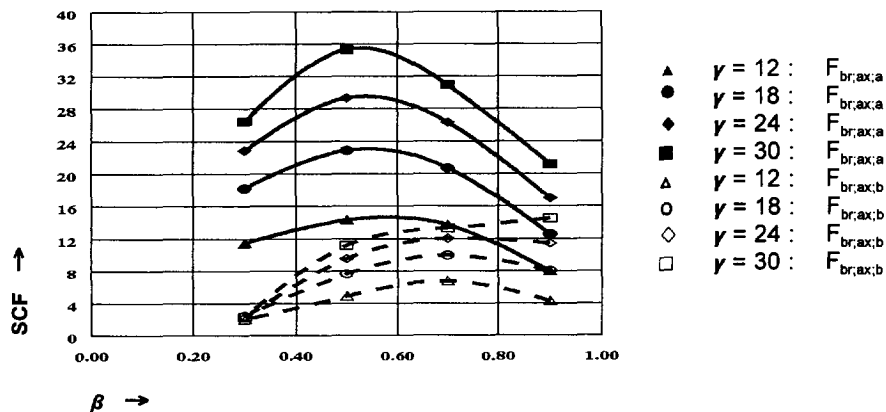
Figure 72.   Influence of β on SCFs caused by reference effects $F_{br;ax;a}$ and carry-over effects $F_{br;ax;b}$. TT joint with φ_{op} = 180° and τ = 1.00. SCFs given for the cs;3,7 locations of the reference brace.
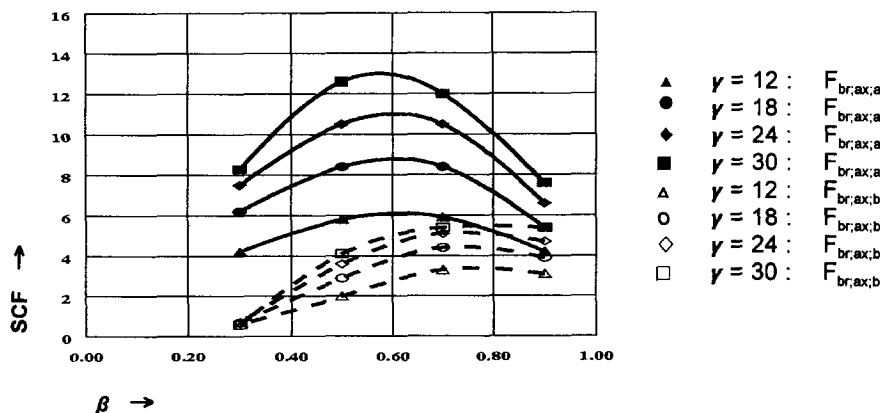
Figure 73.   Influence of β on SCFs caused by reference effects $F_{br;ax;b}$ and carry-over effects $F_{br;ax;b}$. TT joint with φ_{op} = 180° and τ = 1.00. SCFs given for the bs;3,7 locations of the reference brace.

111

Table 33. Importance of out-of-plane carry-over effects for TT joints.
(0.25 ≤ τ ≤ 1.00 and 12 ≤ γ ≤ 30).

φ_{op}	β	Load case			Location of interest					
		$F_{br;ax;b}$	$M_{br;ip;b}$	$M_{br;op;b}$	cc	bc	cs;3	cs;7	bs;3	bs;7
45°	0.30	*			-	-	++	+	++	++
			*		-	--	--	--	--	--
				*	-	--	+	+	-	-
70°	0.50	*			++	--	+++	++	+++	+
			*		-	--	--	--	--	--
				*	-	-	+	+	+	+
90°	0.30	*			-	-	+	+	+	+
			*		--	--	--	--	--	--
				*	--	--	+	+	-	-
	0.50	*			-	-	+	+++	+	+++
			*		--	--	--	--	--	--
				*	--	--	+	+	+	+
	0.65	*			++	--	++	+++	++	+++
			*		-	-	--	--	--	--
				*	+	-	++	+	++	++
135°	0.30	*			--	--	+	--	+	-
			*		--	--	--	--	--	--
				*	--	--	-	-	--	--
	0.50	*			-	-	+	-	+	-
			*		--	--	--	--	--	--
				*	--	--	+	+	-	+
	0.70	*			-	--	++	++	++	++
			*		--	--	--	--	--	--
				*	--	--	+	+	+	++
180°	0.30	*			-	-	+		+	
			*		--	--	--		--	
				*	--	--	--		--	
	0.50	*			-	-	++		++	
			*		--	--	--		--	
				*	--	--	-		-	
	0.70	*			-	-	+++		+++	
			*		-	--	--		--	
				*	--	--	+		+	
	0.90	*			+++	-	+++		+++	
			*		-	--	--		--	
				*	--	--	++		++	

SCF$_{ce}$ are scfs caused by carry-over effects (brace member loads $F_{br;ax;b}$, $M_{br;ip;b}$ and $M_{br;op;b}$).
SCF$_{re}$ are scfs caused by reference effects (brace member loads $F_{br;ax;a}$, $M_{br;ip;a}$ and $M_{br;op;a}$).

+++	=	SCFs$_{ce}$ > 50% · SCFs$_{re}$ and SCFs$_{ce}$ > 0.50.
++	=	SCFs$_{ce}$ > 30% · SCFs$_{re}$ and SCFs$_{ce}$ > 0.50.
+	=	SCFs$_{ce}$ > 10% · SCFs$_{re}$ and SCFs$_{ce}$ > 0.50.
-	=	SCFs$_{ce}$ < 0.50.
--	=	SCFs$_{ce}$ < 0.10.

7.5.4 Influence of the presence of an out-of-plane member on SCFs due to reference loading

The influence of the presence of the carry-over brace member b on SCFs due to reference loading which was ignored up to now, is found to be dependent on a combination of the following aspects:

- The reference loading considered.
- The location of interest.
- The joint parameters considered.

From comparison of SCFs of T joints and TT joints it is found that the influence of the presence of the out-of-plane carry-over brace member b on SCFs due to reference loadings $M_{br;ip;a}$ and $M_{br;op;a}$ can be neglected. This because, for the T and TT joints analysed, the maximum differences in SCFs for all locations considered (crown, saddle and inbetween) are found to be smaller than $\pm 10\%$.

For the reference loading $F_{br;ax;a}$, however, the influence of the presence of the out-of-plane carry-over brace member b on SCFs due to reference loading cannot always be neglected.

As an example for $F_{br;ax;a}$, due to the existence of the out-of-plane carry-over brace member b, a large influence on SCFs (differences with relation to T joints within 40%) is found for the two saddle locations. Figure 74 illustrates the difference in SCFs between a T joint and a TT joint with $\varphi_{op} = 90°$.

Figure 74 shows that for $\beta > 0.50$ and axial loading on the reference brace, the SCFs for the chord saddle location at the gap location between the two braces 'a' and b are much smaller then those for the other chord saddle location.
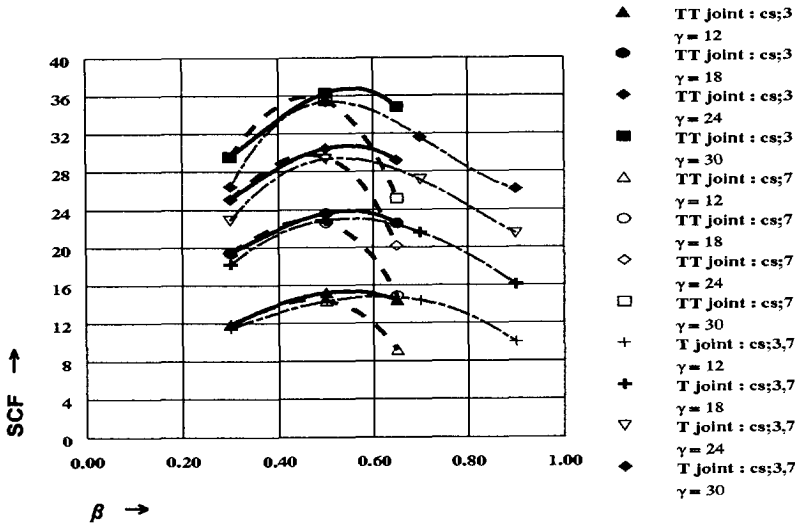
Figure 74. Differences in SCFs caused by $F_{br;ax;a}$ for the saddle locations of a T joint and a TT joint with $\varphi_{op} = 90°$. $\tau = 1.00$.

113

Results showing the influence of the presence of the out-of-plane carry-over brace member b on SCFs caused by the reference loading $F_{br;ax;a}$ are summarized in table 34. This table shows the maximum range of the ratio *SCF T joint / SCF TT joint*, which exists for the combination $\gamma_{min};\tau_{min}$ (lower bound) and $\gamma_{max};\tau_{max}$ (upper bound). The results given in table 34 leads to the additional conclusion that the influence of the presence of the out-of-plane carry-over brace member b on SCFs due to reference loading $F_{br;ax;a}$ mainly depends on the size of the smallest gap region (combination of β and φ_{op}).

In general, for all locations considered, decrease of the size of the gap region results in a decrease of SCFs caused by the reference loading $F_{br;ax;a}$.

Table 34.   Influence of the presence of carry-over brace member b on SCFs caused by the reference loading $F_{br;ax;a}$. Maximum range of the ratio *SCF T joint / SCF TT joint* shown.

φ_{op}	β	Lower bound	Upper bound	Location of interest					
		$\gamma=12;\tau=0.25$	$\gamma=30;\tau=1.00$	cc	bc	cs;3	cs;7	bs;3	bs;7
45°	0.30	*		0.96	0.97	1.00	1.05	1.01	1.01
			*	1.38	1.05	0.89	0.96	0.87	0.87
70°	0.50	*		1.05	1.00	1.10	1.13	1.01	1.05
			*	1.31	1.03	1.21	1.21	1.03	1.07
90°	0.30	*		0.98	0.98	0.98	0.99	1.00	1.00
			*	1.13	1.04	0.89	0.89	0.90	0.90
	0.50	*		1.06	1.01	0.96	0.99	1.00	1.00
			*	1.21	1.03	0.98	1.00	1.00	1.00
135°	0.30	*		1.00	0.98	1.00	1.00	1.00	1.00
			*	1.00	1.01	0.88	0.89	0.87	0.87
	0.50	*		1.00	1.01	0.99	0.98	1.04	1.03
			*	0.98	1.01	1.10	1.10	1.12	1.11
	0.70	*		1.00	1.01	0.99	1.02	1.04	1.04
			*	1.00	1.02	1.13	1.13	1.15	1.15
180°	0.30 and 0.50	*	*	all ≈ 1.00					
	0.70	*		1.00	1.00	1.02	1.02		
			*	1.01	1.01	1.03		1.03	
	0.90	*		1.00	1.00	1.16		1.13	
			*	1.02	1.03	1.23		1.21	

7.5.5   Results and conclusions of the investigation on XX joints   [F47]

Comparison with experimental data.

As part of a Joint Industry Programme for research on the ultimate static strength

of multiplanar XX joints, measurements have also been carried out for the determination of SNCFs [*F47*]. Nine multiplanar XX joints have been investigated. As an illustration figure 75 shows the strip gauges for measuring the strains at the saddle and crown locations for one of the tested XX joints. All tested XX joints have the same joint parameters, namely, α = 12, β = 0.60, γ = 20, τ = 1.00 and a chord dimension of $\varnothing$ 406.4 x 10.
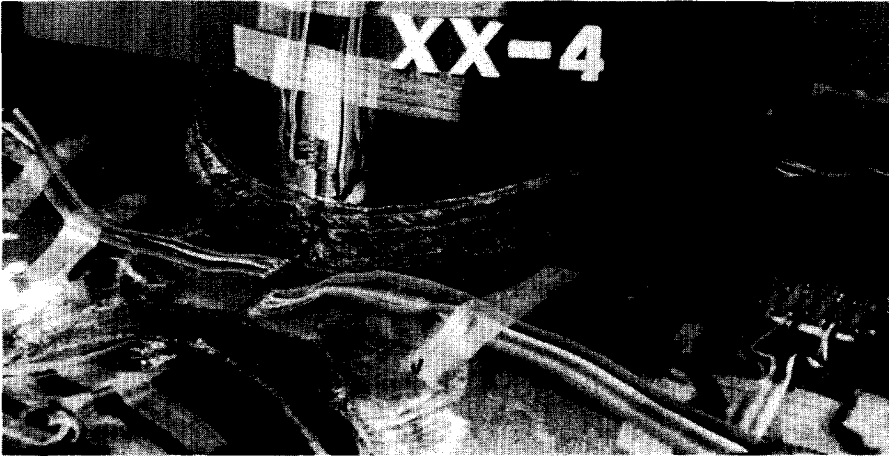
Figure 75. Strip gauges for measuring the strains at the saddle and crown locations of an XX joint.

The results of the comparison between numerical and experimental data are given in table 35 and figure 76.
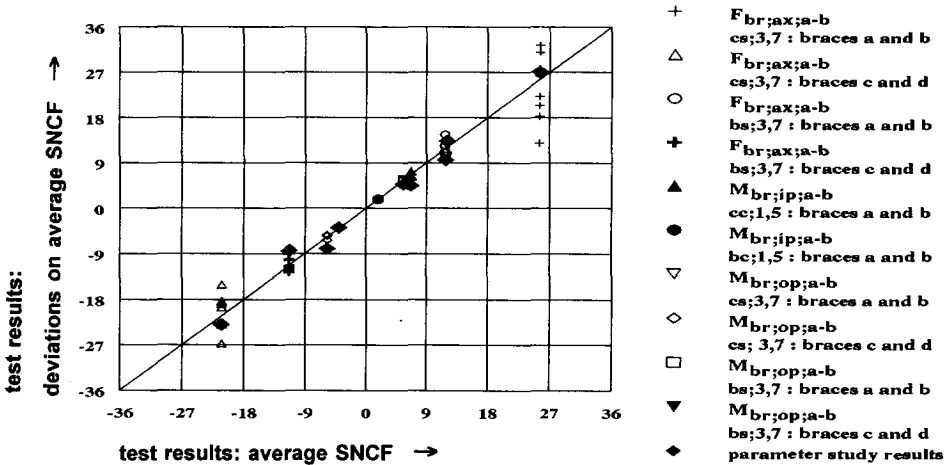
Figure 76. XX joints: comparison of experimental data on SNCFs with results from the parameter study. (Relevant SNCFs > 2.0 shown only).

115

Table 35.   Comparison between numerical and experimental data on SNCFs for XX joints.

Tested joint	Load case (balanced)	Experimental data on SNCFs							
		loaded brace members				unloaded brace members			
		cs	cc	bs	bc	cs	cc	bs	bc
XX2	$F_{br;ax;a-b}$	26.4	1.5	12.3	0.3	-23.1	0.5	-11.4	0.2
XX3	$F_{br;ax;a-b}$	31.0	1.7			-26.7	0.4	-8.3	
XX3	$F_{br;ax;c-d}$		1.5	10.0			0.7	-9.0	
XX4	$F_{br;ax;a-b}$	26.3	2.0	14.7		-22.6	0.3	-12.2	
XX4	$F_{br;ax;c-d}$	27.8	2.6	12.5		-19.6	0.4	-12.5	
XX6	$M_{br;ip;a-b}$		7.3		2.1				
XX7	$F_{br;ax;c-d}$	22.2		11.2		-18.6	1.3	-13.1	-0.10
XX7	$M_{br;ip;a-b}$	0.0	6.4	-0.1	1.7	0.2		0.1	
XX8	$F_{br;ax;c-d}$	32.4		12.5		-22.6	1.1	-11.9	0.0
XX8	$M_{br;ip;a-b}$	0.1	6.3	-0.1	1.6	-0.1		-0.1	
XX10	$M_{br;op;a-b}$	13.4		5.9		-5.3		-3.9	
XX11	$F_{br;ax;c-d}$	20.4		10.5		-18.3		-12.7	
XX11	$M_{br;op;a-b}$	10.5		5.1		-6.3		-3.9	
XX12	$F_{br;ax;c-d}$	18.3		11.0		-19.0		-10.2	
XX12	$M_{br;op;a-b}$	12.4		5.4		-5.5		-4.3	
average test results	$F_{br;ax;a-b}$	25.6	1.8	11.8	0.3	-21.3	0.7	-11.3	0.1
	$M_{br;ip;a-b}$	0.0	6.7	-0.1	1.8	0.0		0.0	
	$M_{br;op;a-b}$	12.1		5.5		-5.7		-4.0	
ratio SNCF* parameter study experimental	$F_{br;ax;a-b}$	1.06		0.81		1.08		0.74	
	$M_{br;ip;a-b}$		0.66						
	$M_{br;op;a-b}$	1.11		0.87		1.42		0.95	

*   Ratio given for experimental SNCF > 2.0

Taking into account the large scatter on SNCFs from the tested XX joints, which is mainly caused by deviations in size of weld shape, as shown in figure 76 a reasonable agreement with the results from this parameter study exists.

Proposed SCF and SNCF formulae for balanced loaded XX joints.

By use of a multivariable least squares curve fitting package, the SCF and SNCF data obtained from the parameter study on XX joints is converted into SCF and SNCF formulae. Formulae are developed for the relevant combinations as summarized in table 36. For further information on the developed formulae reference is made to [F47].
In comparison to T joints and TT joints no other numerical work on SCFs for reference as well as carry-over effects exists, specifically for XX joints.

116

Table 36. Proposed SCF and SNCF formulae for balanced loaded XX joints.

Load case (balanced only)	Formulae numbering with relation to location of interest						
	cs;3,7 braces 'a', b	cs;3,7 braces c, d	bs;3,7 braces 'a', b	bs;3,7 braces c, d	cc;1,5 braces 'a', b	cc;1,5 braces c, d	bc;1,5 braces 'a', b
	reference effect	carry-over effect	reference effect	carry-over effect	reference effect	carry-over effect	reference effect
$F_{br;ax;a}$ + $F_{br;ax;b}$	SCF1 SNCF1	SCF2 SNCF2	SCF3 SNCF3	SCF4 SNCF4			
$F_{ch;ax}$					SCF5 SNCF5		SCF6 SNCF6
$M_{br;ip;a}$ + $M_{br;ip;b}$					SCF7 SNCF7	SCF8 SNCF8	SCF9 SNCF9
$M_{br;op;a}$ + $M_{br;op;b}$	SCF10 SNCF10	SCF11 SNCF11	SCF12 SNCF12	SCF13 SNCF13			

7.5.6 SCFs caused by chord member loads

From the parameter study it is found that the influence of the presence of an out-of-plane carry-over brace member *b* on SCFs caused by chord member loads can be neglected. Figure 77 shows the negligible differences on SCFs caused by $F_{ch;ax}$ for the chord crown location of a T joint and a TT joint. Therefore, only the results of SCFs for the chord member loads on a T joint are discussed.
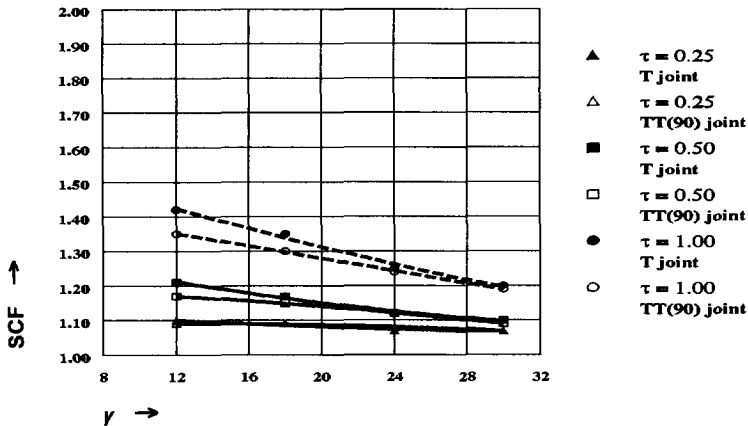
Figure 77. Influence of the presence of an out-of-plane brace member on SCFs caused by $F_{ch;ax}$ for the chord crown location. Comparison T joint - TT (90°) joint; β = 0.50.

A small variation in SCFs exists for the whole range of joint parameters considered. The range of SCFs obtained are given in table 37, whereas the values for the

chord crown and brace saddle locations for $F_{ch;ax}$ are shown in figures 78 and 79.

Table 37.   Range of SCFs caused by chord member loads (brace members: φ_{ip} = 90°).

Location	Range of SCFs	
	load case	
	$F_{ch;ax}$	$M_{ch;ip}$ [·]
chord crown	1.00 < SCF < 1.60	1.10 < SCF < 1.70
brace crown	-0.15 < SCF < 0.10	-0.10 < SCF < 0.30
chord saddle	-0.20 < SCF < 0.10	-0.40 < SCF < 0.00
brace saddle	-0.30 < SCF < 0.70	-0.30 < SCF < 0.50

*   Causing a nominal bending stress of 1 N/mm² at the chord outer surface along the plane of the crown.
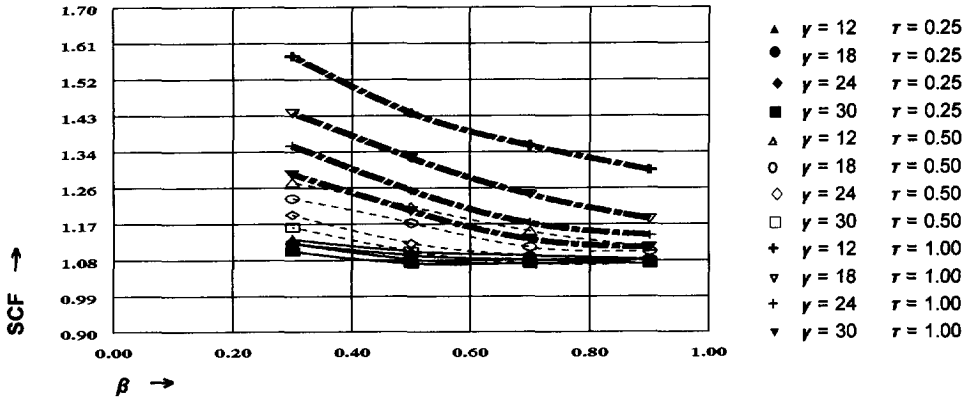
Figure 78.   SCFs for the chord crown location caused by $F_{ch;ax}$.
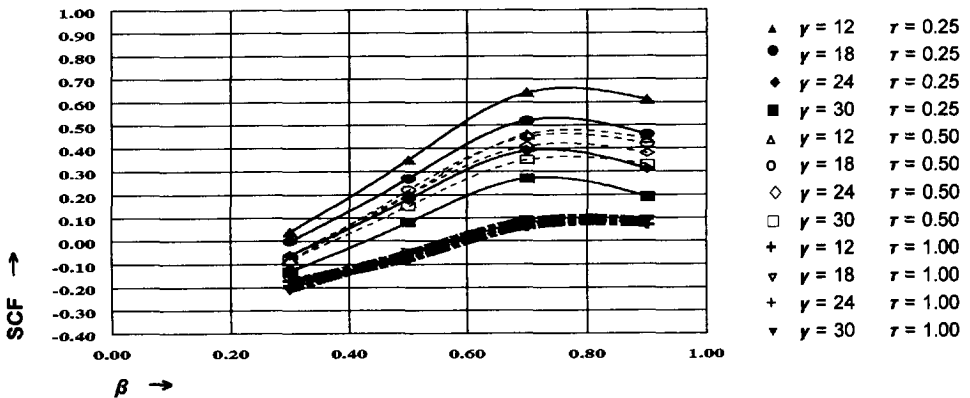
Figure 79.   SCFs for the brace saddle location caused by $F_{ch;ax}$.

118

From the SCF results due to chord member loads (axial + bending), the following conclusions are made:

Chord crown location.
- As expected, the highest SCFs are found for this location.
- SCFs due to chord bending $M_{ch;ip}$ are found to be slightly larger (10%) compared to SCFs due to $F_{ch;ax}$.
- The value of SCF increases with decreasing β, γ and increasing τ.

Brace saddle location.
- SCFs due to chord bending $M_{ch;ip}$ are found to be smaller than SCFs due to $F_{ch;ax}$ (up to a maximum of 25%).
- The value of SCF increases with decreasing γ and τ, while for the β influence the maximum SCF occurs for about $\beta = 0.70$.

7.5.7 Results on the relationship between SCF and SNCF

The relationship between SCF and SNCF, identified as snf (=SCF/SNCF) is found to be dependent on the combination of load cases, locations of interest and joint parameters considered. The influence of the presence of an out-of-plane carry-over brace member b on snf caused by reference effects is found to be negligible (differences within 5%). The snf results of the investigation on joints with braces perpendicular to the chord axis are summarized in table 38, whereas the sncf results for the cc;1,5 location in case of $F_{ch;ax}$ and the sncfs for the bs;3,7 location in case of $F_{br;ax;a}$ are shown in figure 80.
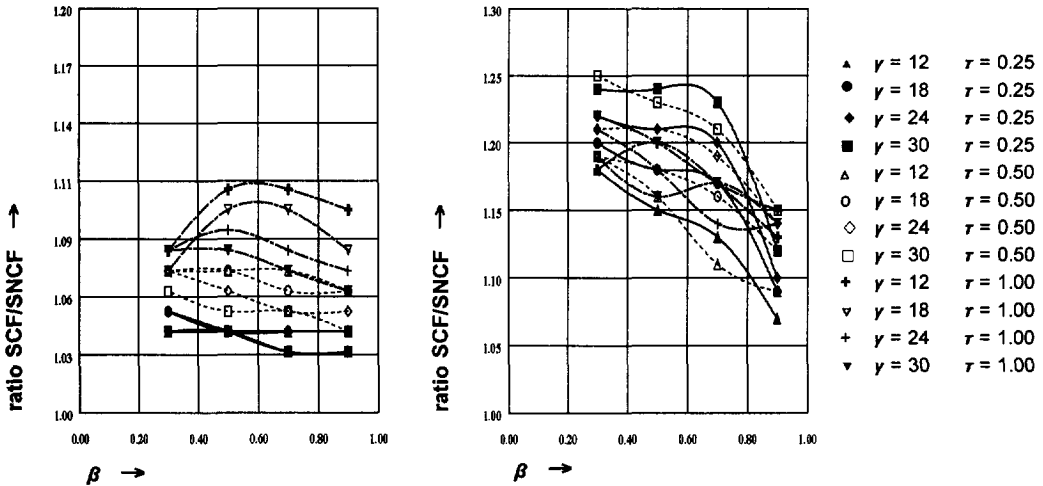
Figure 80. Ratio SCF/SNCF for the cc;1,5 location of a T joint loaded by $F_{ch;ax}$ (left figure) and for the bs;3,7 location of a T joint loaded by $F_{br;ax;a}$ (right figure).

119

Table 38. Results of the investigation on the relationship between SCFs and SNCFs.
(SNCF > 1.00).

Joint	Load case	Location	snf (=SCF/SNCF)		Influence of joint parameter		
			average	range	β	γ	τ
Reference loading							
T	$F_{br;ax;a}$	cs	1.16	1.12 < snf < 1.21	-	o	-
		bs	1.18	1.07 < snf < 1.25	-	+	- : β ≤ 0.70 + : β > 0.70
		cc	1.25	1.16 < snf < 1.33	o	-	- : β ≤ 0.70 + : β > 0.70
		bc	*	*			
	$M_{br;ip;a}$	cc	1.28	1.13 < snf < 1.35	o	o	-
		bc	1.27	1.18 < snf < 1.34	o	+	+
	$M_{br;op;a}$	cs	1.18	1.13 < snf < 1.21	-	o	-
		bs	1.20	1.11 < snf < 1.29	-	-	- : β ≤ 0.70 + : β > 0.70
	$F_{ch;ax}$	cc	1.05	1.02 < snf < 1.12	o	-	+
	$M_{ch;ip}$ **	cc	1.07	1.02 < snf < 1.15	o	o	+
Carry-over loading							
TT φ_{op}=90°	$F_{br;ax;b}$	cs;3	1.17	1.12 < snf < 1.19	-	o	-
		cs;7	1.19	1.11 < snf < 1.28	-	o	-
		bs;3	1.18	1.13 < snf < 1.23	-	+	-
		bs;7	1.22	1.09 < snf < 1.35	-	+	-
TT φ_{op}=135°	$F_{br;ax;b}$	cs;3	1.23	1.16 < snf < 1.26	-	o	-
		cs;7	1.26	1.22 < snf < 1.32	-	o	-
		bs;3	1.27	1.21 < snf < 1.33	-	o	-
		bs;7	1.31	1.22 < snf < 1.40	-	o	-
TT φ_{op}=180°	$F_{br;ax;b}$	cs	1.15	1.08 < snf < 1.21	-	o	- : β ≤ 0.70 + : β > 0.70
		bs	1.17	1.05 < snf < 1.27	-	o	- : β ≤ 0.70 + : β > 0.70

-   =   Increase of β, γ or τ results in a decrease of snf.
o   =   Influence of β, γ or τ on snf is negligible.
+   =   Increase of β, γ or τ results in an increase of snf.
*   =   SNCF < 1.00.
**   =   Causing a nominal bending stress of 1 N/mm² at the chord outer surface along the plane of the crown.

From the study on the relationship between SCF and SNCF, the following main conclusions are given:

-     Chord member loads give smaller *snfs* and a smaller range of variation

compared to brace member loads.
- For the reference effects as well as carry-over effects, the range of variation on *snfs* for the chord saddle locations is smaller than for the brace saddle locations.

7.6 Results of the investigation for joints with braces inclined to the chord axis

The main results and conclusions on the following subjects are summarized in this chapter.

- *Influence of φ_{ip} on SCFs caused by brace member loads.*
  (Loads considered are: $F_{br;ax;a}$, $M_{br;ip;a}$ and $M_{br;op;a}$).
- *Influence of φ_{ip} on SCFs caused by chord member loads.*
  (Loads considered are: $F_{ch;ax}$ and $M_{ch;ip}$).
- *Importance of in-plane carry-over effects on SCFs.*
  (Loads considered are: $F_{br;ax;c}$, $M_{br;ip;c}$ and $M_{br;op;c}$).
- *Influence of the presence of an in-plane carry-over brace member c on SCFs due to reference loadings.*
  (Loads considered are: $F_{br;ax;a}$, $M_{br;ip;a}$ and $M_{br;op;a}$).
- *Relationship between SCF and SNCF.*
  (Loads considered are: $F_{br;ax;a,c}$, $M_{br;ip;a,c}$, $M_{br;op;a,c}$, $F_{ch;ax}$ and $M_{ch;ip}$).

In an identical way as described for T joints, a comparison of Y, K and KK joint SCFs with available experimental work has been carried out.
The comparison results in the same conclusion as those found for T joints, namely a good agreement (differences within ±10%) exists between numerical results from the parameter study and the experimental results.

7.6.1 Influence of φ_{ip} on SCFs caused by brace member loads

Generally, for all brace member loads $F_{br;ax;a}$, $M_{br;ip;a}$ and $M_{br;op;a}$, larger SCFs are found with increasing φ_{ip}. This is because increasing φ_{ip} results in a smaller brace to chord intersection area and hence a smaller region for stress distribution. Also in case of $F_{br;ax;a}$, increase of φ_{ip} results in a larger component perpendicular to the chord axis.
A study on the SCFs for the chord crown and brace crown locations shows that the existing numerical work makes no distinction in toe and heel location. From the parameter study results however, it is found that the SCFs for those two locations entirely differ from each other.
Depending on the load case $F_{br;ax;a}$ or $M_{br;ip;a}$ and joint parameters β, γ, τ and φ_{ip} considered, the largest SCF occurs at the toe or heel location.
For Y joints with $\beta = 0.40$, $\gamma = 30$ and $\tau = 1.00$, as an example the influence of φ_{ip} on SCFs due to brace member loads $F_{br;ax;a}$, $M_{br;ip;a}$ and $M_{br;op;a}$ is shown in figures 81, 82 and 83.
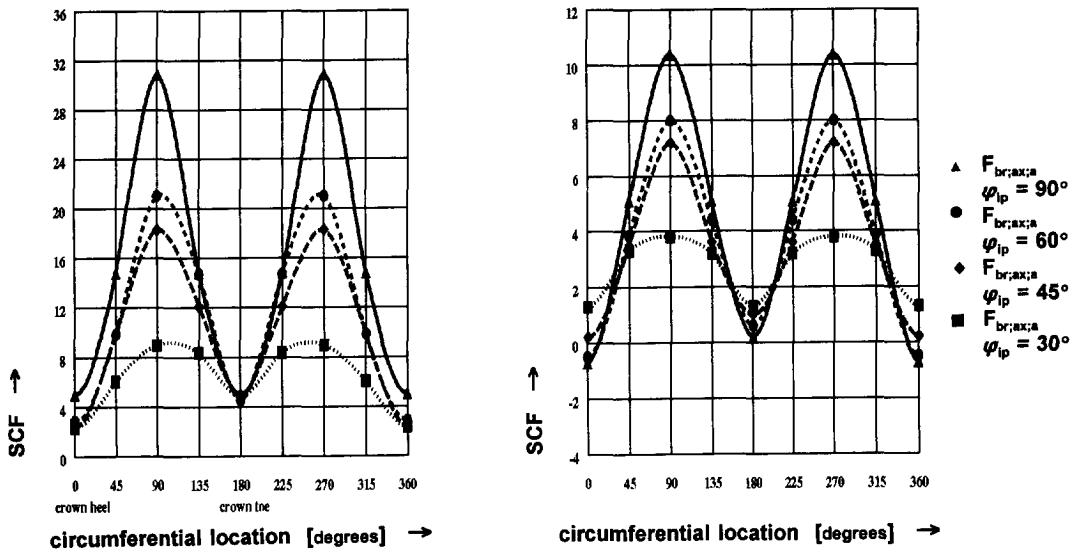
Figure 81. Influence of φ_{ip} on SCFs due to $F_{br;ax}$. Results shown for the chord member locations (left figure) and brace member locations (right figure) of a Y joint with $\beta = 0.40$, $\gamma = 30$ and $\tau = 1.00$.
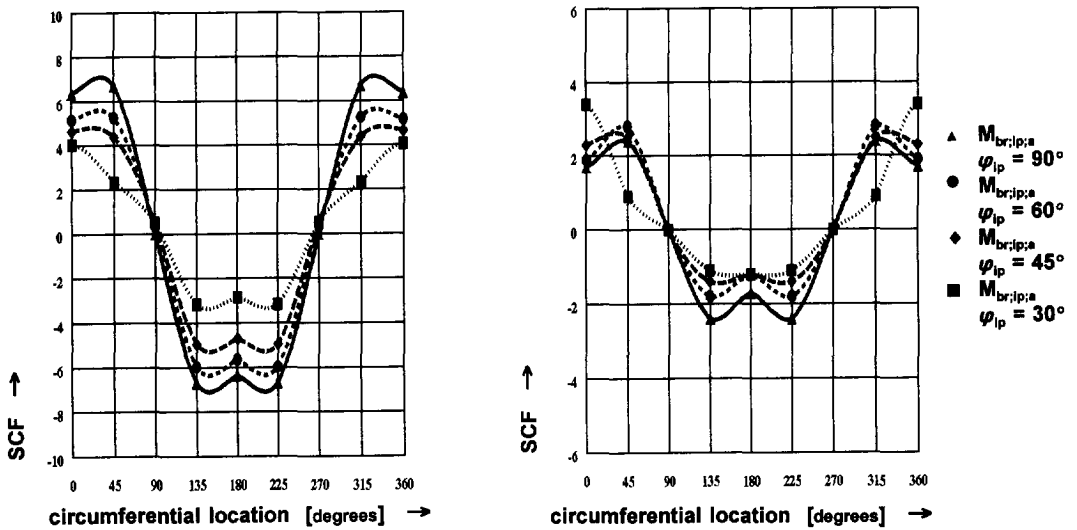
Figure 82. Influence of φ_{ip} on SCFs due to $M_{br;ip}$. Results shown for the chord member locations (left figure) and brace member locations (right figure) of a Y joint with $\beta = 0.40$, $\gamma = 30$ and $\tau = 1.00$.

122
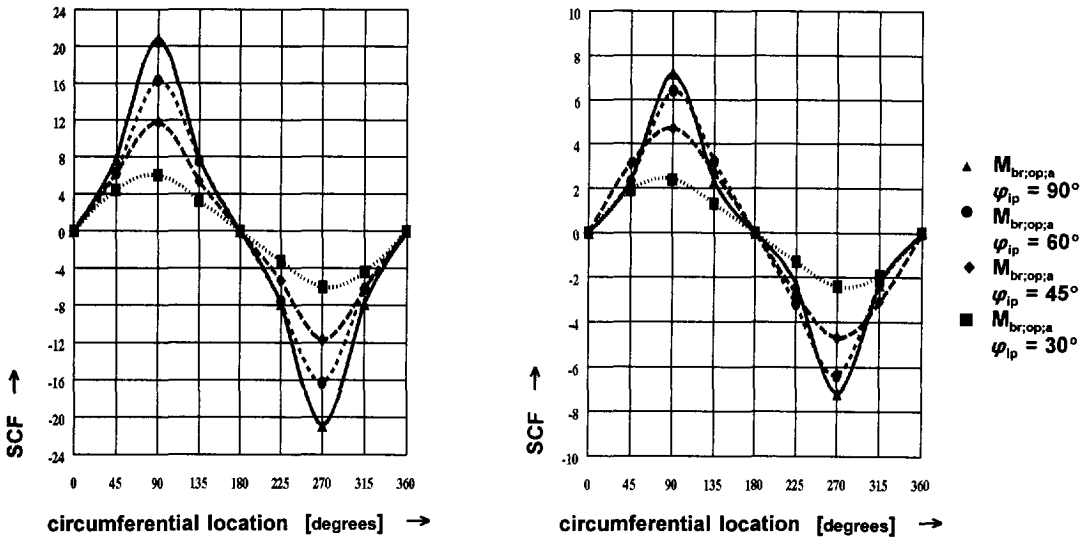
Figure 83. Influence of φ_{ip} on SCFs due to $M_{br;op}$. Results shown for the chord member locations (left figure) and brace member locations (right figure) of a Y joint with $\beta = 0.40$, $\gamma = 30$ and $\tau = 1.00$.

7.6.2 Influence of φ_{ip} on SCFs caused by chord member loads

The results of SCFs for the chord member loads on a Y joint are discussed only. This is because the influence of the presence of in-plane and out-of-plane carry-over brace members on SCFs caused by chord member loads is found to be negligible.

The range of SCFs obtained is given in table 39.

As an example, SCFs for the chord crown heel location (cc;1) caused by $F_{cb;ax}$ are shown in figure 84.

123

Table 39. Range of SCFs caused by chord member loads on Y joints.

Location		Range of SCFs	
		load case	
		$F_{ch;ax}$	$M_{ch;ip}$ [*]
		$\varphi_{ip} = 60°$	
chord crown	: heel	1.00 < SCF < 1.65	1.10 < SCF < 1.75
	: toe	1.00 < SCF < 1.60	1.05 < SCF < 1.70
brace crown	: heel	-0.25 < SCF < 0.15	-0.20 < SCF < 0.45
	: toe	-0.15 < SCF < 0.10	0.00 < SCF < 0.20
chord saddle		-0.20 < SCF < 0.05	-0.35 < SCF < 0.10
brace saddle		-0.10 < SCF < 1.20	-0.20 < SCF < 0.80
		$\varphi_{ip} = 45°$	
chord crown	: heel	1.05 < SCF < 2.00	1.20 < SCF < 2.20
	: toe	1.00 < SCF < 1.95	1.00 < SCF < 2.10
brace crown	: heel	-0.40 < SCF < 0.25	-0.30 < SCF < 0.60
	: toe	-0.20 < SCF < 0.15	0.00 < SCF < 0.25
chord saddle		-0.25 < SCF < 0.05	-0.30 < SCF < -0.05
brace saddle		0.20 < SCF < 1.20	0.10 < SCF < 0.90
		$\varphi_{ip} = 30°$	
chord crown	: heel	1.30 < SCF < 2.90	1.35 < SCF < 3.15
	: toe	1.00 < SCF < 2.35	1.20 < SCF < 2.40
brace crown	: heel	-0.50 < SCF < 0.45	-0.45 < SCF < 1.05
	: toe	-0.20 < SCF < 0.40	0.10 < SCF < 0.50
chord saddle		-0.40 < SCF < 0.00	-0.50 < SCF < -0.10
brace saddle		0.40 < SCF < 1.20	0.30 < SCF < 0.95

[*] Causing a nominal bending stress of 1 N/mm^2 at the chord outer surface along crown plane.

124

▲	$\gamma = 12$	$\tau = 0.25$
●	$\gamma = 18$	$\tau = 0.25$
◆	$\gamma = 24$	$\tau = 0.25$
■	$\gamma = 30$	$\tau = 0.25$
△	$\gamma = 12$	$\tau = 0.50$
o	$\gamma = 18$	$\tau = 0.50$
◇	$\gamma = 24$	$\tau = 0.50$
□	$\gamma = 30$	$\tau = 0.50$
+	$\gamma = 12$	$\tau = 1.00$
▽	$\gamma = 18$	$\tau = 1.00$
+	$\gamma = 24$	$\tau = 1.00$
▼	$\gamma = 30$	$\tau = 1.00$
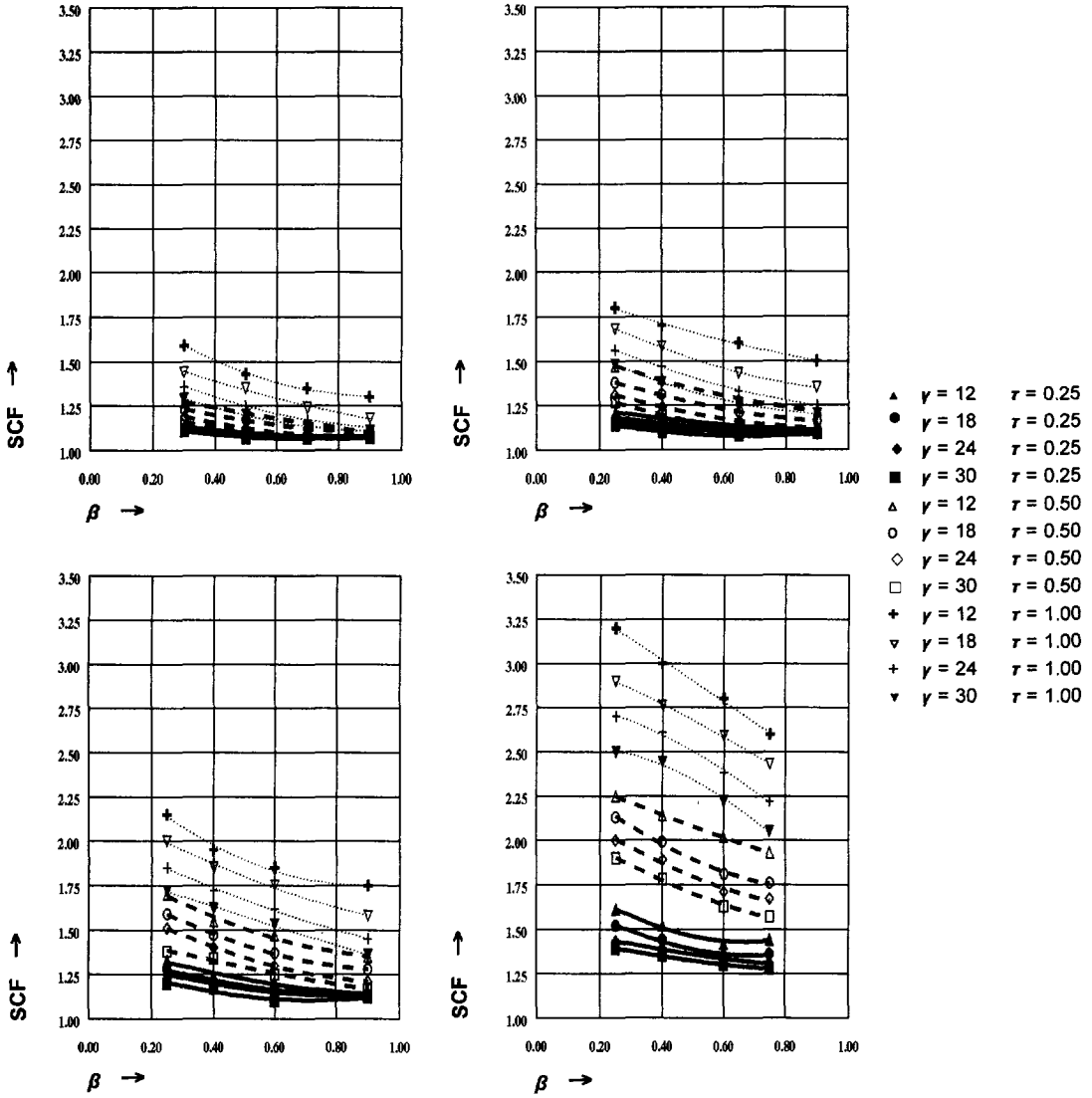
Figure 84. Y joint: SCFs for the chord crown heel location (cc;1) caused by $F_{ch;ax}$. Top left figure $\varphi_{ip} = 90°$ and top right figure $\varphi_{ip} = 60°$. Bottom left figure $\varphi_{ip} = 45°$ and bottom right figure $\varphi_{ip} = 30°$.

From the Y joint SCF results caused by chord member loads, the following conclusions are made.
- For the whole range of φ_{ip} investigated, the significant SCFs occur on the chord crown (heel + toe) and brace saddle locations.
- Decrease of φ_{ip} results in an increase of SCFs. This is especially the case for the chord crown locations, and so, Y joints give larger SCFs for chord loads compared to T joints.

125

- The SCFs for the toe locations (chord and brace member) are smaller than the SCFs for the heel locations, and the differences increase with decreasing φ_{ip}.
- Regarding the influence of joint parameters β, γ and τ on the SCFs and the difference in SCFs caused by $F_{ch;ax}$ and $M_{ch;ip}$, identical conclusions are made as given for T joints (see chapter 7.5.6).

7.6.3 Importance of in-plane carry-over effects on SCFs

In-plane carry-over effects on SCFs exist in case of brace member loads $F_{br;ax;c}$, $M_{br;ip;c}$ and $M_{br;op;c}$ of for example a K joint. The importance of SCFs due to in-plane carry-over effects of a K joint, is found to be as summarized in table 40. In this table, results of the importance of SCFs are given for $\gamma_{min};\tau_{min}$ (lower bound) and $\gamma_{max};\tau_{max}$ (upper bound). Figures 85 and 86 show some of the SCF results obtained.
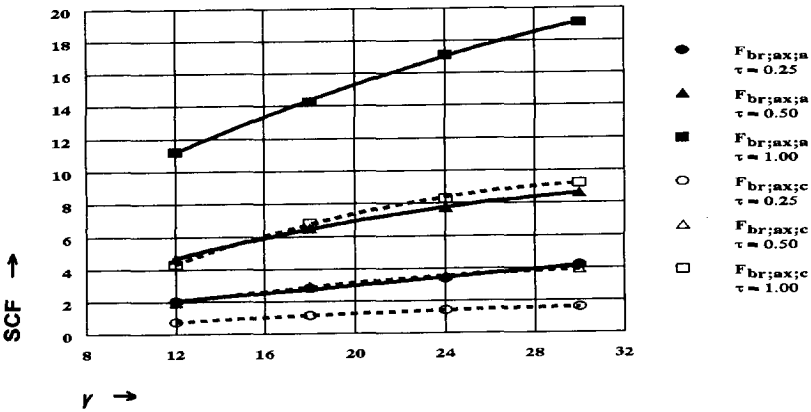
Figure 85. Influence of γ and τ on SCFs caused by in-plane carry-over loading $F_{br;ax;c}$ and reference loading $F_{br;ax;a}$ for the chord saddle location of a K joint with β=0.40 and φ_{ip}=60°.
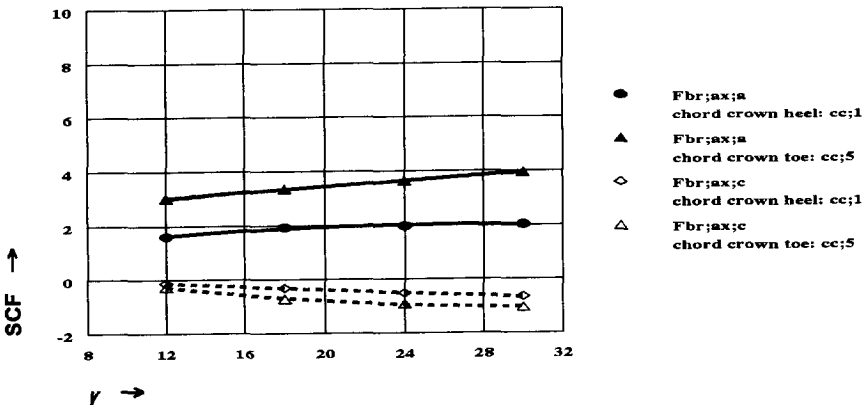
Figure 86. In-plane carry-over SCF results ($F_{br;ax;c}$) and reference SCF results ($F_{br;ax;a}$) for the two chord crown locations (toe and heel) of a K joint with β=0.40, τ=0.50 and φ_{ip}=60°.

Table 40. Importance of in-plane carry-over effects (SCFs caused by $F_{br;ax;c}$, $M_{br;ip;c}$ and $M_{br;op;c}$) related to SCFs due to reference effects (SCFs caused by $F_{br;ax;a}$, $M_{br;ip;a}$ and $M_{br;op;a}$) of a K joint.

φ_{ip}	γ	Load case	cc:1 (heel)		cc:5 (toe)		bc:1 (heel)		bc:5 (toe)		cs;3,7		bs;3,7	
			γ=12 r=0.25	γ=30 r=1.00	γ=12 r=0.25	γ=30 r=1.00	γ=12 r=0.25	γ=30 r=1.00	γ=12 r=0.25	γ=30 r=1.00	γ=12 r=0.25	γ=30 r=1.00	γ=12 r=0.25	γ=30 r=1.00
60°	0.25	$F_{br;ax;c}$	--	+	--	+	--	++	--	+	+	++	+	+
		$M_{br;ip;c}$	--	+	--	--	--	--	--	--	--	++	--	--
		$M_{br;op;c}$	--	--	--	--	--	--	--	--	--	+	--	--
	0.40	$F_{br;ax;c}$	--	+	--	+	--	+++	--	+	+	++	+	++
		$M_{br;ip;c}$	--	--	--	+	--	--	--	+	--	+++	--	++
		$M_{br;op;c}$	--	--	--	--	--	--	--	--	--	+	--	+
45°	0.25	$F_{br;ax;c}$	--	+	--	+	--	++	--	--	--	++	--	+
		$M_{br;ip;c}$	--	--	--	--	--	--	--	--	--	--	--	--
		$M_{br;op;c}$	--	--	--	--	--	--	--	--	--	+	--	--
	0.40	$F_{br;ax;c}$	--	++	--	+	--	++	--	--	--	+	--	+
		$M_{br;ip;c}$	--	--	--	--	--	--	--	--	--	+	--	--
		$M_{br;op;c}$	--	--	--	--	--	--	--	--	--	+	--	+
	0.60	$F_{br;ax;c}$	--	++	--	+	--	++	--	--	--	++	--	++
		$M_{br;ip;c}$	--	++	--	--	--	--	--	--	--	++	--	--
		$M_{br;op;c}$	--	--	--	--	--	--	--	--	--	+	--	+
30°	0.25	$F_{br;ax;c}$	--	+++	--	+	--	--	--	--	--	+	--	--
		$M_{br;ip;c}$	--	--	--	--	--	--	--	--	--	--	--	--
		$M_{br;op;c}$	--	--	--	--	--	--	--	--	--	--	--	--
	0.40	$F_{br;ax;c}$	--	+++	--	++	--	++	--	--	--	++	--	+
		$M_{br;ip;c}$	--	--	--	--	--	--	--	--	--	--	--	--
		$M_{br;op;c}$	--	--	--	--	--	--	--	--	--	--	--	--
	0.60	$F_{br;ax;c}$	--	+++	--	++	--	--	--	--	--	++	--	+
		$M_{br;ip;c}$	--	--	--	--	--	--	--	--	--	++	--	--
		$M_{br;op;c}$	--	--	--	--	--	--	--	--	--	++	--	--
	0.75	$F_{br;ax;c}$	--	++	--	++	--	--	--	+	--	++	--	+
		$M_{br;ip;c}$	--	--	--	--	--	--	--	--	--	--	--	--
		$M_{br;op;c}$	--	--	--	--	--	--	--	--	--	--	--	--

+++ = Very large SCFs due to carry-over effects (> 50 % of SCFs due to identical reference effects).

++ = Large SCFs due to carry-over effects (> 30 % of SCFs due to identical reference effects).

+ = Small SCFs due to carry-over effects (> 10 % of SCFs due to identical reference effects).

- = Negligible SCFs due to carry-over effects (SCF < 0.5).

-- = Approximately zero SCFs due to carry-over effects (SCF < 0.1).

About the importance of SCFs caused by in-plane carry-over effects it is conclu-
ded that:

-   The influence of changes in γ and τ on in-plane carry-over effects cannot
    be neglected.
-   For all locations, the load case $F_{br;ax;c}$ causes large in-plane carry-over
    effects. This is especially the case when increasing γ and τ. Figure 85
    shows for the chord saddle location of a K joint with $\varphi_{ip} = 60°$ and $\beta = 0.40$
    the influence of γ and τ on SCFs caused by in-plane carry-over loading
    $F_{br;ax;c}$ and reference loading $F_{br;ax;a}$.
-   As illustrated in figure 86, the in-plane carry-over SCF results for the two
    chord crown locations (toe and heel) might differ entirely. Existing formulae
    [*F13*, *F62*] makes no distinction on SCFs for the heel and toe locations.

7.6.4 Influence of the presence of an in-plane carry-over brace member on SCFs due to reference loading

The influence of the presence of the in-plane carry-over brace member c on SCFs
due to reference loadings $F_{br;ax;a}$, $M_{br;ip;a}$ and $M_{br;op;a}$ has been investigated by
comparison of SCF results from Y joints and K joints.
The results of comparison on SCFs between Y joints and K joints are summarized
in table 41.
This table shows the maximum range of the ratio *SCF Y joint / SCF K joint*, which
exists for the combination $\gamma_{min};\tau_{min}$ (lower bound) and $\gamma_{max};\tau_{max}$ (upper bound).

From the results given in table 41, the following conclusions are made:

-   The influence of the presence of the carry-over brace member c on SCFs
    due to reference loadings $F_{br;ax;a}$, $M_{br;ip;a}$ and $M_{br;op;a}$, mainly depends on γ
    and τ, the size of the smallest gap region (combination of β and φ_{ip}) and
    the load case considered.
    In general, for all locations considered, increase of γ and τ and decrease of
    the size of the gap region results in an increase of the influence of the
    presence of the carry-over brace member c on SCFs caused by the referen-
    ce loadings.

-   The influence of the presence of the in-plane carry-over brace member c on
    SCFs due to reference loading, which was ignored up to now, is found to be
    only negligible for the following situations (differences smaller than $\pm10\%$):
    -   The SCFs caused by reference loading $M_{br;op;a}$.
    -   For low values of γ and τ, the SCFs caused by reference loadings $F_{br;ax;a}$
        and $M_{br;ip;a}$.
    -   The SCFs caused by reference loadings $F_{br;ax;a}$, $M_{br;ip;a}$ for the chord
        saddle, brace saddle and brace crown heel locations.

128

As an example, for $F_{br;ax;a}$, due to the existence of an in-plane carry-over brace member c, a large influence on SCFs (differences with relation to Y joints up to 50%) is found for the chord crown toe location. Figure 87 illustrates the differences in SCFs.

Table 41. Influence of the presence of a carry-over brace member c on SCFs caused by reference loadings $F_{br;ax;a}$, $M_{br;ip;a}$ and $M_{br;op;a}$.
Maximum range of the ratio *SCF Y joint / SCF K joint* shown.

φ_{ip}	β	Load case	cc;1 (heel)		cc;5 (toe)		bc;1 (heel)		bc;5 (toe)		cs;3,7		bs;3,7	
			$\gamma=12$ $\tau=0.25$	$\gamma=30$ $\tau=1.0$	$\gamma=12$ $\tau=0.25$	$\gamma=30$ $\tau=1.0$	$\gamma=12$ $\tau=0.25$	$\gamma=30$ $\tau=1.0$	$\gamma=12$ $\tau=0.25$	$\gamma=30$ $\tau=1.0$	$\gamma=12$ $\tau=0.25$	$\gamma=30$ $\tau=1.0$	$\gamma=12$ $\tau=0.25$	$\gamma=30$ $\tau=1.0$
60°	0.25	$F_{br;ax;a}$	*	0.94	0.99	0.90	1.00	*	0.99	0.88	1.01	1.03	1.01	1.04
		$M_{br;ip;a}$	*	1.00	1.00	0.98	1.00	1.01	*	0.99	*	*	*	*
		$M_{br;op;a}$	*	*	*	*	*	*	*	*	1.00	1.01	1.00	1.01
	0.40	$F_{br;ax;a}$	*	0.77	0.93	0.51	0.96	*	0.95	*	1.03	1.10	1.02	1.09
		$M_{br;ip;a}$	*	1.03	0.98	0.82	1.01	1.04	0.98	0.77	*	*	*	*
		$M_{br;op;a}$	*	*	*	*	*	*	*	*	1.02	1.08	1.01	1.07
45°	0.25	$F_{br;ax;a}$ $M_{br;ip;a}$ $M_{br;op;a}$	all 1.00											
	0.40	$F_{br;ax;a}$	*	0.85	0.94	0.81	0.99	*	1.00	0.83	1.01	1.06	1.02	1.06
		$M_{br;ip;a}$	*	1.02	*	0.97	1.00	1.01	*	0.96	*	*	*	*
		$M_{br;op;a}$	*	*	*	*	*	*	*	*	1.00	1.02	1.00	1.02
	0.60	$F_{br;ax;a}$	*	0.74	0.92	0.50	0.97	*	0.98	*	1.03	1.09	1.00	1.01
		$M_{br;ip;a}$	*	1.04	0.98	0.80	1.01	1.06	0.99	*	*	*	*	*
		$M_{br;op;a}$	*	*	*	*	*	*	*	*	1.03	1.10	1.00	1.02
30°	0.25 and 0.40	$F_{br;ax;a}$ $M_{br;ip;a}$ $M_{br;op;a}$	all 1.00											
	0.60	$F_{br;ax;a}$	*	0.90	1.00	0.85	1.00	0.94	1.00	0.99	*	1.08	*	1.07
		$M_{br;ip;a}$	*	1.01	*	0.96	1.00	1.01	*	*	*	*	*	*
		$M_{br;op;a}$	*	*	*	*	*	*	*	*	*	1.02	*	1.02
	0.75	$F_{br;ax;a}$	*	0.98	0.97	0.58	0.99	*	1.01	*	*	1.09	*	1.09
		$M_{br;ip;a}$	*	1.02	*	0.88	1.00	1.02	*	*	*	*	*	*
		$M_{br;op;a}$	*	*	*	*	*	*	*	*	*	1.09	*	1.09

* = SCF < 1.00

129
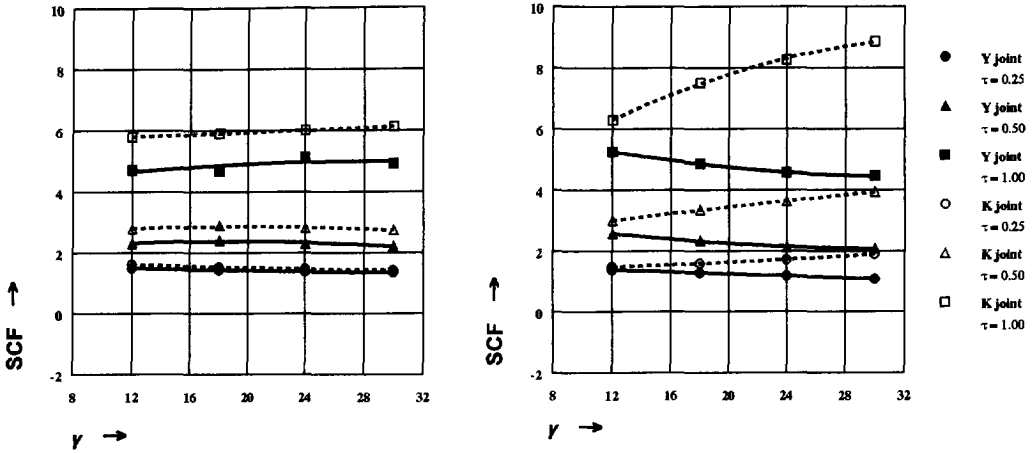
Figure 87. SCFs caused by $F_{br;ax;a}$ for the chord crown toe location of a Y joint and a K joint. Left figure φ_{ip} = 45°, and right figure φ_{ip} = 60°: β=0.40.

7.6.5 Results on the relationship between SCF and SNCF

In an identical way as described for joints with braces perpendicular to the chord axis (see chapter 7.5.7), the relationship between SCF and SNCF has been investigated for joints with braces inclined to the chord axis.

The relationship between SCF and SNCF has been investigated for reference member loads $F_{br;ax;a}$, $M_{br;ip;a}$ and $M_{br;op;a}$ and carry-over member loads $F_{br;ax;c}$, $M_{br;ip;c}$ and $M_{br;op;c}$.

The influence of the presence of an in-plane carry-over brace member 'c' on snf related to reference member loads is found to be negligible (differences within 5%).

The snf results of the investigation on joints with braces inclined to the chord axis are summarized in table 42.

In addition to the conclusions given on the relationship between SCF and SNCF for joints with braces perpendicular to the chord axis, for joints with braces inclined to the chord axis, it is concluded:

-    For the chord member loads, increase of φ_{ip} results in a decrease of the average snf.
-    For the reference brace loadings, increase of φ_{ip} generally results in an increase of average snf.
-    For the carry-over loadings, increase of φ_{ip} generally results in a decrease of the average snf.

130

Table 42.   Results of the investigation on the relationship between SCF and SNCF for joints with braces inclined to the chord axis.

Load case	Location	φ_{ip} = 30°		φ_{ip} = 45°		φ_{ip} = 60°		Influence of joint parameter		
		snf$_{average}$	range snf	snf$_{average}$	range snf	snf$_{average}$	range snf	β	γ	τ
				Reference loading : Y joint						
$F_{ch;ax}$	cc;1	1.16	1.12 < snf < 1.18	1.10	1.06 < snf < 1.14	1.08	1.04 < snf < 1.12	o	o	+
	cc;5	1.10	1.06 < snf < 1.15	1.09	1.03 < snf < 1.14	1.07	1.02 < snf < 1.12	o	o	+
$M_{ch;ip}$ [***]	cc;1	1.16	1.11 < snf < 1.20	1.13	1.08 < snf < 1.18	1.09	1.06 < snf < 1.15	o	o	+
	cc;5	1.13	1.08 < snf < 1.17	1.11	1.07 < snf < 1.15	1.08	1.05 < snf < 1.14	o	o	+
$F_{br;ax;a}$	cc;1	1.22	1.17 < snf < 1.25	1.21	1.13 < snf < 1.30	1.21	1.18 < snf < 1.29	o	-	+
	cc;5	1.28	1.24 < snf < 1.35	1.31	1.19 < snf < 1.43	1.30	1.21 < snf < 1.51	-	-	-
	bc;1	1.20	1.12 < snf < 1.25	1.25	1.17 < snf < 1.41	1.23	1.23 < snf < 1.33	o	+	-
	bc;5	1.32	1.22 < snf < 1.46	1.31	1.21 < snf < 1.43	1.34	1.23 < snf < 1.45	o	+	-
	cs;3,7	1.20	1.18 < snf < 1.22	1.19	1.15 < snf < 1.23	1.19	1.16 < snf < 1.23	o	o	-
	bs;3,7	1.39	1.10 < snf < 1.53	1.23	1.12 < snf < 1.40	1.18	1.13 < snf < 1.24	+ : φ_{ip} ≤ 45° - : φ_{ip} > 45°	o	+
$M_{br;op;a}$	cc;1	1.27	1.23 < snf < 1.32	1.28	1.23 < snf < 1.33	1.27	1.24 < snf < 1.32	-	-	-
	cc;5	1.23	1.21 < snf < 1.26	1.26	1.22 < snf < 1.37	1.27	1.21 < snf < 1.34	o	o	-
	bc;1	1.20	1.14 < snf < 1.26	1.21	1.17 < snf < 1.27	1.23	1.18 < snf < 1.31	o	o	+
	bc;5	**	**	**	**	1.23	1.19 < snf < 1.31	o	+	+
$M_{br;op;a}$	cs;3,7	1.20	1.18 < snf < 1.23	1.20	1.16 < snf < 1.25	1.19	1.17 < snf < 1.22	o	o	-
	bs;3,7	1.48	1.35 < snf < 1.56	1.25	1.12 < snf < 1.39	1.18	1.12 < snf < 1.24	+ : φ_{ip} ≤ 45° - : φ_{ip} > 45°	o	+ : φ_{ip} ≤ 45° - : φ_{ip} > 45°
				Carry-over loading : K joint						
$F_{br;ax;c}$	cc;1	**	**	1.25	1.24 < snf < 1.27	1.33	1.31 < snf < 1.35	+	+	+
	cc;5	1.14	1.12 < snf < 1.16	1.22	1.19 < snf < 1.25	1.30	1.26 < snf < 1.35	+	+	+
	cs;3,7	1.13	1.10 < snf < 1.16	1.15	1.14 < snf < 1.16	1.18	1.16 < snf < 1.19	o	-	o
	bs;3,7	**	**	1.34	1.33 < snf < 1.36	1.25	1.23 < snf < 1.27	o	+	o
$M_{br;op;c}$	cs;3,7	1.16	1.15 < snf < 1.16	**	**	1.15	1.14 < snf < 1.17	o	-	o

- = Increase of β, γ or τ results in a decrease of snf.
o = Influence of β, γ or τ on snf is negligible.
+ = Increase of β, γ or τ results in an increase of snf.
** = SNCF < 1.00.
*** = Causing a nominal bending stress of 1 N/mm² at the chord outer surface along the plane of the crown.

8. DESIGN RECOMMENDATIONS AND DESIGN GUIDANCE

Scope

The recommendations concern the linear-elastic analysis of lattice steel structures containing welded tubular joints and the fatigue design of these joints. They cover the use of tubular hollow sections, which may be either hot rolled or cold formed and having steel grades that complies with EN 10210 or equivalent.

Notation, Subscripts and Definitions

The notations and subscripts used in the design recommendations are identical to those used throughout this work. A summary of notations and subscripts used is given on pages 6 - 8. The definitions of stiffness and fatigue related terms used in this chapter are given in chapter 1.3.

8.1 *Design rules proposed*

Design rules are given on the following topics:

- *Numerical modelling of welded tubular joint flexibility and stress concentration factors.*
- *Linear elastic analysis of lattice structures containing welded tubular joints.*
- *Basics concerning fatigue analysis of welded tubular joints.*
- *Determination of stress concentration factors.*
- *Relationship between stress and strain concentration factor.*
- *Basic design fatigue resistance curve for welded multiplanar tubular joints.*
- *Fatigue design procedure of welded tubular joints.*

Numerical modelling of welded tubular joint flexibility and stress concentration factors

As concluded in chapter 3, results on joint flexibility and stress concentration factors based on numerical work using FE analyses largely depend on the type of element, mesh refinement, integration scheme and the weld shape considered. The following recommendations are given:

<u>Joint flexibility</u>

Element type:
- The use of shell or solid elements is recommended.
- For shell as well as solid elements, only elements having midside node(s) with a reduced integration scheme 2x2x2 are recommended.

132

Mesh refinement:
- For elements having a midside node, the length of the element measured along the weld toe should be approximately less than 1/12 of the total length around the perimeter of the brace to chord intersection.

Weld shape:
- Increasing the length of the weld footprint on the chord member surface results in a significant decrease of the joint flexibility (axial and bending). This is especially the case for joints having a small gap. For a tubular joint with a weld footprint on the chord member surface larger than $1.3 \cdot t_1$ and/or a gap region smaller than $5 \cdot t_o$, the real weld shape using 20-n solid elements should be included in the FE model.

Stress concentration factors

Element type:
- The use of 20-n solid elements with a reduced integration scheme 2x2x2 is recommended.

Mesh refinement:
- The length of the 20-n solid element measured along the weld toe should be approximately less than 1/16 of the total length around the perimeter of the brace to chord intersection.

Weld shape:
- The real weld shape using 20-n solid elements should be included in the FE model, and the SCFs should be determined at the weld toe location.

For both joint flexibility and stress concentration factors

- Near the weld toe location, the length of the elements measured perpendicular to the intersection area for the chord member and measured parallel to the brace axis for the brace member should be based on a convergence criteria. For that, the influence of at least three alternative mesh refinements on joint flexibility and stress concentration factors should be investigated.
- The use of transition elements is disadvised. Because these elements increase rather than decrease computer costs. Thus a combination of shell elements and solid elements should not be used.
- Regarding isolated joints, to avoid end effects, the length of the member parts outside the intersection area should be at least 3 times the diameter of the corresponding member.

Linear elastic analysis of lattice structures containing welded tubular joints

The flexibility of welded tubular joints affects the deflection and load distribution of lattice structures. The following recommendations are given:

<u>Numerical idealization of welded tubular joints</u>

Deflection:
- The use of a structure modelled with rigid ended beam elements (idealization M_1), or a structure modelled with beam elements, where braces are pin ended and the chords are continuous (idealization M_2), is recommended for analysing the initial deflection δ_i. The fictitious brace member parts inside the chord member should be taken infinitely stiff.
- The contribution of joint flexibility on the initial deflection δ_i can be taken into account by the use of a multiplication factor a_M, so that
$\delta_{tot} = a_M \cdot \delta_i$.
The limits of this factor are $1.05 < a_M < 1.20$.

The value of a_M depends on the stiffness ratio SR_{ax}, with $SR_{ax} = \dfrac{K_{ii;ax}}{K_{br;ax}}$.

Decrease of SR_{ax} results in an increase of a_M.
The value of $K_{ii;ax}$ depends on the type of joint (uniplanar-multiplanar; gap-overlap), the number of connecting braces and the joint parameters β, γ, τ, φ_{ip} and φ_{op}.
In general, a low number of connecting braces with uniplanar gap joints, a small β ratio, a large γ ratio and a large value of φ_{ip} results in a small value of $K_{ii;ax}$.
The value of $K_{br;ax}$ depends on the ratio A_{br} / I_{br}, and decrease of I_{br} results in an increase of $K_{br;ax}$.

Load distribution:

Fatigue design: axial forces:
- Axial forces can be obtained using idealization M_1 or M_2. In case of large axial carry-over effects $K_{ij;ax}$, which e.g. exists in case of multiplanar XX joints with carry-over brace members fixed against horizontal translation, the use of idealization M_5 (joints FE modelled) is recommended.

Fatigue design: secondary bending moments:
- For the chord as well as brace members, due to various influences such as joint flexibility and eccentricities in noding of the members, secondary bending moments occur, which have to be considered in fatigue design. The use of idealization M_1 or an alternative idealization M_5 with the joint under

134

consideration FE modelled and other joints of the structure modelled by rigid ended beam elements is recommended.
- For the brace members, the recommended idealizations might underestimate the bending stresses. Therefore, independent of the joint parameters considered, a minimum hot spot stress caused by brace member loads equal to 1.5 times the hot spot stress obtained from axial brace member loadings should be used.

Basics concerning fatigue analysis of welded tubular joints

From the research results described in chapter 7.2, based on the use of the hot spot approach, the following basics concerning fatigue analysis of welded tubular joints are recommended:

Stresses (strains) to be considered

- Stresses should be used in a direction perpendicular to the weld toe for the chord member locations and in a direction parallel to the axis of the brace member for the brace member locations (this direction mostly differs from the direction perpendicular to the weld toe) should be used.

Extrapolation region

- For the chord and brace member locations, the following extrapolation region measured in a direction equal to the direction of stresses considered is preferred:
  - chord member (crown, inbetween and saddle):
    $l_{r,min} = 0.4 \cdot t_0$ and $l_{r,max} = 1.4 \cdot t_0$
  - brace member (crown, inbetween and saddle):
    $l_{r,min} = 0.4 \cdot t_1$ and $l_{r,max} = 1.4 \cdot t_1$

Method of extrapolation

- A parabolic quadratic curve fitting through all the data points in and around the extrapolation region and determining the stresses at $l_{r,min}$ and $l_{r,max}$ using the obtained curve should be carried out firstly.
  Secondly, for determining the hot spot stress, using the two determined coordinates $l_{r,min}, \sigma_{l_{r,min}}$ and $l_{r,max}, \sigma_{l_{r,max}}$, a linear extrapolation to the weld toe should take place.

Locations around the reference brace where the hot spot stress is determined

- The fixed weld toe locations of interest for both chord and brace member are crown, saddle and inbetween. This results, when analysing one load case, into eight hot spot stresses for the chord member and eight hot spot stresses for the

brace member.

- Hot spot stresses at other weld toe locations can be determined from polynomial curve fitting through the hot spot stresses of the eight fixed weld toe locations around the intersection area along the member surface.

Boundary conditions

- The stress concentration factors analysed should be independent of boundary conditions used. Therefore, in case of brace member loads which causes bending in the chord member, to obtain the effect of brace member load only, compensating moment(s) on the chord member end(s) needs to be incorporated.

Nominal stress: isolated joints

- The nominal stress σ_{nom} should be defined as the maximum stress (linear-elastic behaviour) in a cross section of a loaded brace or chord member according to the equations:

$$\sigma_{axial;nom} = \frac{F_{axial}}{A_x} \qquad \sigma_{ipb;nom} = \frac{M_{ipb}}{W_y} \qquad \text{and} \qquad \sigma_{opb;nom} = \frac{M_{opb}}{W_z} \; .$$

Nominal stress: joints located inside a structure

- For the joints located inside a structure, extrapolated nominal stresses for the braces under axial tension loading should be used, for which:

$$\sigma_{extrap;nom} = \sigma_{axial;nom} + \sqrt{\sigma^2_{extrap;ipb} + \sigma^2_{extrap;opb}}$$

- Extrapolation of stresses to the intersection of the brace center-line and chord outer wall surface is recommended.

Stress concentration factor: isolated joints

- The stress concentration factor (SCF) for an isolated joint loaded individually by separate chord member loads $F_{ch;ax}$, $M_{ch;ip}$ and $M_{ch;op}$ and separate brace member loads $F_{br;ax}$, $M_{br;ip}$ and $M_{br;op}$ should be defined as:

for the chord member loads:

$$SCF_{m.n.o} = \frac{\sigma_{h.s.;m.n.o}}{\sigma_{ch;nom;o}} \qquad\qquad \text{and}$$

for the brace member loads:

136

$$SCF_{m.n.o} = \frac{\sigma_{h.s.;m.n.o}}{\sigma_{br;nom;o}} \qquad \text{with:}$$

m   =   Chord member at the connection of brace 'a', or brace 'a' member.

n   =   Location around the perimeter of the brace 'a' to chord intersection, e.g. crown, saddle or inbetween.

o   =   Type of loading (axial, in plane bending or out of plane bending).

<u>Stress concentration factor:</u> joints located inside a structure

- For joints located inside a structure, the stress concentration factor (SCF) includes the influence of all chord and brace member loads as follows:

$$SCF_{m.n.o} = \frac{\sigma_{h.s.;m.n.o}}{\sigma_{extrap;nom}} \qquad \text{with:}$$

m   =   Chord member or a brace member.

n   =   Location around the perimeter of a brace to chord intersection, e.g. crown, saddle or inbetween.

o   =   Combination of all chord and brace member loads.

$\sigma_{extrap.;nom}$ =   Extrapolated nominal stress of the in-plane axial tensile loaded brace member.

<u>Total hot spot stress:</u> isolated joints

- The total hot spot stress $\sigma_{h.s.;m.n\,total}$ for an isolated joint under combined loads at a particular location around the brace to chord connection is defined as the superposition of the individual hot spot stress components $\sigma_{h.s.}$ according to the following equations:

$$\sigma_{h.s.;m.n\,total} = \sigma_{h.s.;m.n\,chord\ loads} + \sigma_{h.s.;m.n\,brace\ loads}$$

with for the chord member loads (reference loads exist <u>only</u>):

$$\sigma_{h.s.;m.n\,chord\ loads} = SCF_{m.n;F_{ch;ax}} \cdot \sigma_{nom;F_{ch;ax}} + SCF_{m.n;M_{ch;ip}} \cdot \sigma_{nom;M_{ch;ip}} +$$
$$SCF_{m.n;M_{ch;op}} \cdot \sigma_{nom;M_{ch;op}}$$

and for the brace member loads (reference loads and carry-over loads exist):

$$\sigma_{h.s.;m.n\,brace\ loads} = \sum_{i=1}^{p} SCF_{m.n;F_{br;ax;i}} \cdot \sigma_{nom;F_{br;ax;i}} +$$
$$SCF_{m.n;M_{br;ip;i}} \cdot \sigma_{nom;M_{br;ip;i}} + SCF_{m.n;M_{br;op;i}} \cdot \sigma_{nom;M_{br;op;i}}$$

with: i =   The brace number.
              p =   The total number of connecting braces.

- Hot spot stresses caused by a torsion brace moment can be determined by resolving the torsion brace moment into an out-of-plane bending component and considering the hot spot stress due to this component only.

Determination of stress concentration factors

The stress concentration factors can be determined in three ways, namely:

- *Through experimental model studies.*
  Information on the test method used for the development of the fatigue resistance curve for welded multiplanar joints is given in [F23].

- *Through numerical model studies.*
  Recommendations on numerical modelling of welded tubular joint stress concentration factors are given on page 133, and basics concerning fatigue analysis of welded tubular joints are given on pages 135-138.

- *Data files and parametric formulae.*
  Stress concentration factors are determined for several common types of welded uniplanar and multiplanar tubular joints. Because of the enormous data obtained, the results are stored in data files, from which e.g. by the use of an input-file and a program-file the SCFs (SNCFs) and hot spot stresses (strains) can be obtained automatically.
  In addition to the data files, for multiplanar XX joints parametric formulae are developed.

By means of tables, conclusions are made on:

- *The importance of SCFs due to in-plane carry-over effects (see table 40).*
- *The importance of SCFs due to out-of-plane carry-over effects (see table 33).*
- *The influence of the presence of an in-plane carry-over brace member on SCFs due to reference loading (see table 41).*
- *The influence of the presence of an out-of-plane carry-over brace member on SCFs due to reference loading (see table 34).*

The information given in tables 33, 34, 40 and 41 are assumed to be helpful when analysing SCFs for any type of welded tubular joint. This because, in many cases the SCFs caused by carry-over loading are found to be negligible. Also, in many cases, the influence of the presence of a carry-over member on the SCFs due to reference loading is found to be negligible.

138

Relationship between stress and strain concentration factor

When assuming a plane-stress condition and a fully isotropic behaviour of steel with $E = 2.068 \cdot 10^5 N/mm^2$ and $v=0.30$, the relationship between SCF and SNCF can be written as:

$$snf = \frac{SCF}{SNCF} = 1.10 + 0.33 \cdot \frac{\epsilon_y}{\epsilon_{x;h.s.}}$$

The parameter study results show the existence of a large variation on *snf*.

Related to the joint parameters β, γ, τ, φ_{ip} and φ_{op} and to the type of joint, for the relevant reference as well as carry-over effects, values of *snfs* are stored in data files. These *snfs* are recommended when converting hot spot strains into hot spot stresses.
A summary of *snf* results is given in tables 38 and 42.

Basic design fatigue resistance curve for welded multiplanar tubular joints

There is sufficient evidence from de DEn design fatigue resistance curve for welded uniplanar tubular joints (see figure 48). This curve relies on an empirically derived relationship between the applied stress ranges and the fatigue life (**S-N** approach), based on a large amount of test data from simple tubular joints.
The characteristic DEn design curve for uniplanar tubular joints based upon the mean line minus two standard deviation (2σ) and a wall thickness of 16 mm is

for: $10^3 < N_f < 5 \cdot 10^6$: $\log N_f = 12.4756 - 3 \cdot \log (S_{r_{h.s.}})$

For wall thicknesses larger than 16 mm, a thickness correction of

$S_{r_{h.s.;t \geq 16}} = S_{r_{h.s.;t = 16}} \cdot (16/t)^{0.30}$ is applied for the whole curve.

The fatigue data based on first through-thickness cracking from the tested multiplanar KK joints with wall thicknesses of 4, 8 and 16 mm are in good agreement with the proposed DEn design curve for uniplanar tubular joints.
Because of this agreement, for welded multiplanar KK joints with wall thicknesses between 4 and 16 mm, the use of the DEn design curve for welded uniplanar joints with a wall thickness of 16 mm is recommended.
For multiplanar joints in a non-corrosive environment and those in a corrosive environment which are adequately protected, a fatigue cut-off limit is adopted at $N=5 \cdot 10^6$ cycles for constant amplitude loading in accordance with EC3 [F12].
For variable amplitude loading, a slope of m=-5 is used between $5 \cdot 10^6$ and the cut-off limit $1 \cdot 10^8$.

Fatigue design procedure of welded tubular joints

The fatigue design life N_f of each joint should be at least the intended service life of the structure.

An additional factor on design life may be included if appropriate, for instance, in case of critical joints whose sole failure may induce a catastrophic failure of the structure. In EC3 [*F12*], instead of factors on life, partial safety factors γ_m have to be applied to the hot spot stress range. The partial safety factors are given in table 42.

Table 42.   Partial safety factor γ_m according to EC3 on the hot spot stress range.

Inspection and access	"Fail-safe" structure	Non "fail-safe" structure
Period inspection and maintenance. Accessible joint detail.	$\gamma_m = 1.00$	$\gamma_m = 1.25$
Periodic inspection and maintenance. Poor accessibility.	$\gamma_m = 1.15$	$\gamma_m = 1.35$

For each potential crack location, the long term distribution of relevant stress ranges should be established and the probable fatigue life based on first through-thickness cracking should satisfy the Palmgren-Miner linear cumulative damage rule.

$$D_d = \sum_1^I \frac{n_i}{N_i} \leq 1.0$$

The fatigue design procedure for a potential crack location of a welded tubular joint placed inside a lattice structure is given below.

Fatigue Design Procedure

1.   Replace the structure into an acceptable numerical model.

2.   Determine the load distribution by means of nominal stresses.

-    This needs to be done for the brace and chord members of the joint(s) under consideration only.
-    Relevant member loads are:
    -    Chord member: $F_{ch;ax}$, $M_{ch;ip}$ and $M_{ch;op}$;
    -    Brace member: $F_{br;ax}$, $M_{br;ip}$ and $M_{br;op}$ (incl. $M_{br;t}$) .

140

3. *Determine the extrapolated nominal stresses.*

- The stresses should be extrapolated to the intersection of the brace centre-line and the outerwall surface of the continuous member.

4. *Determine the stress concentration factors using SCF formulae, graphs or data files.*

For SCF results by means of formulae, graphs and/or data files, reference is made to chapter 7, in which the parameter study SCF results for T, Y, K, TT, XX and KK joints are discussed.

- Based on information given in tables 33 and 40, decide whether SCFs caused by carry-over effects can be neglected.
- Based on information given in tables 34 and 41, decide whether SCFs caused by reference effects are influenced by the presence of a carry-over brace member.

5. *Determine the total hot spot stress (range) $(\Delta)\sigma_{h.s.;tot}$ for the potential crack location(s).*

- For the contribution of secondary bending moments, independent of the method of numerical idealization and independent of the location (crown, saddle and inbetween) considered, a minimum of

$$\sigma_{h.s;br_{tot}} = 1.5 \cdot \sum_{i=1}^{n} SCF_{br_i;axial} \cdot \sigma_{br_i;axial}$$

should be used in case of lattice structures.
- Depending upon the code of practice, a safety factor γ_m should be applied.
- For wall thicknesses larger than 16 mm, a thickness correction should be applied.

6. *Determine the Palmgren-Miner cumulative damage factor*

$$D_d = \sum_{1}^{i} \frac{n_I}{N_i} \leq 1.0 \ .$$

- Use a design fatigue resistance curve.
- The damage factor D_d should not exceed 1.0.

8.2 Design example

Given:
A welded multiplanar joint is subjected to a fatigue loading.
- Joint geometry: TT (90°) joint:
                                 chord ∅ 500 x 20.8 : braces ∅ 325 x 10.4.

141

- Joint parameters: $\beta = 0.65$, $\gamma = 12$, $\tau = 0.50$, $\varphi_{op} = 90°$ and $t_0 = 20.8$ mm.
- Member forces:

  Figure 88 shows the direction of the extrapolated nominal force ranges. Forces are obtained from a numerical model using rigid ended beam elements.

  Extrapolated nominal forces and stresses for a load spectrum $1.00 \cdot \sigma_{max}$ are:

    - Chord member (both member ends):

      $F_{ch;ax} = 2481$ kN $\Rightarrow 80$ N/mm² ;

      $M_{ch;ip} = 71$ kNm $\Rightarrow 20$ N/mm² ;

      $M_{ch;op} = 36$ kNm $\Rightarrow 10$ N/mm².

    - Brace member 'a':

      $F_{br;ax;a} = 412$ kN $\Rightarrow 40$ N/mm² ;

      $M_{br;ip;a} = 11.7$ kNm $\Rightarrow 15$ N/mm² ;

      $M_{br;op;a} = 7.8$ kNm $\Rightarrow 10$ N/mm².

    - Brace member b:

      $F_{br;ax;b} = 155$ kN $\Rightarrow 15$ N/mm² ;

      $M_{br;ip;b} = 3.9$ kNm $\Rightarrow 5$ N/mm² ;

      $M_{br;op;b} = 3.1$ kNm $\Rightarrow 4$ N/mm².

- Partial safety factor: 1.15.
- Weld: A butt weld shape according to AWS-code is been used.
- Loading: Variable amplitude loading with $N_{tot} = 1 \cdot 10^6$ cycles.

  The load spectrum for the combination of stress range is:

    $1.00 \, \sigma_{max} = 0$ cycles

    $0.90 \, \sigma_{max} = 1150$ cycles

    $0.70 \, \sigma_{max} = 9850$ cycles

    $0.50 \, \sigma_{max} = 190000$ cycles

    $0.25 \, \sigma_{max} = 799000$ cycles

Requested: Check the TT joint on fatigue.

The results on hot spot stresses and fatigue damage factor are shown in tables 43 and 44.
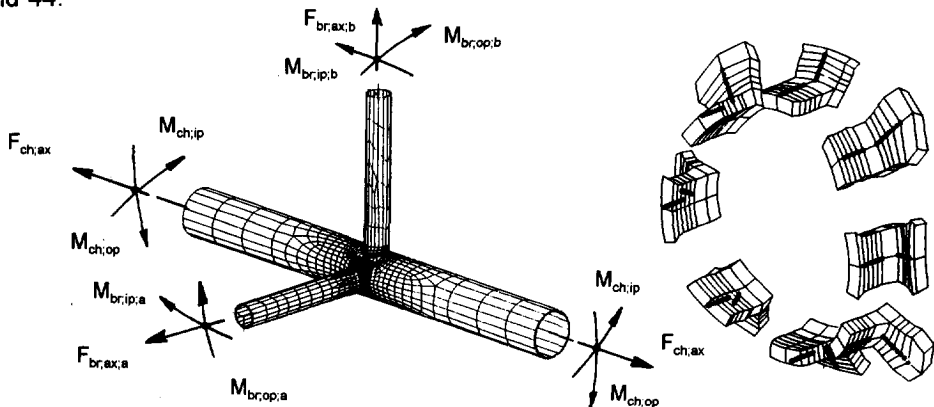

Figure 88.   Direction of extrapolated nominal force ranges and fixed weld toe locations.

Table 43.   Determination of the maximum hot spot stress range for the fixed weld toe locations of the chord and brace member of a TT joint.

Fixed weld toe location	SCFs from parameter study (chapter 7): TT joint; $\beta = 0.65$, $\gamma = 12$, $\tau = 0.50$, $\varphi_{op} = 90°$									Hot spot stress range $S_{h.s.}$ (load spectrum $1.00 \cdot \sigma_{max}$)					
	Reference loading						Carry-over loading			Chord $S_{h.s.}$	Brace 'a' $S_{h.s.}$	Brace b $S_{h.s.}$	$S_{h.s.}$	$S_{h.s.;br,ax_a}$ + $S_{h.s.;br,ax_b}$	$1.5 \cdot (4)$
	Chord member			Brace 'a' member			Brace 'b' member						(1)+(2)+(3)		(1)+
	$F_{ch;ax}$	$M_{ch;ip}$	$M_{ch;op}$	$F_{br;ax,a}$	$M_{br;ip,a}$	$M_{br;op,a}$	$F_{br;ax,b}$	$M_{br;ip,b}$	$M_{br;op,b}$	(1)	(2)	(3)	(1)+(2)+(3)	(4)	(1)+1.5·(4)
cc;1	1.17	1.29	0.00	1.53	2.08	0.04	0.26	-0.31	0.17	119	93	3	215	64	215
ci;2	0.85	0.77	-0.44	3.46	1.85	2.27	-0.73	-0.39	-0.56	79	189	-15	253	127	270
cs;3	-0.01	-0.13	0.04	6.58	0.00	5.99	-2.65	0.00	-1.90	-3	323	-47	273	223	331*
ci;4	0.85	0.77	-0.44	3.46	-1.85	2.27	-0.73	0.39	-0.55	79	134	-11	202	127	270
cc;5	1.17	1.29	0.00	1.53	-2.08	0.04	0.26	0.31	0.17	119	31	6	156	65	217
ci;6	0.85	0.76	0.42	2.98	1.85	-2.08	-0.67	0.03	0.49	87	126	-8	205	109	251
cs;7	0.07	-0.09	-0.02	4.54	0.00	-5.57	-2.35	0.00	1.35	4	126	-30	100	146	223
ci;8	0.85	0.76	0.42	2.98	-1.85	-2.08	-0.67	-0.03	0.49	87	71	-8	150	109	250
bc;1	0.06	0.21	0.01	1.48	1.71	-0.03	-0.21	-0.11	-0.15	9	85	-1	93	57	94
bi;2	0.18	0.25	-0.08	2.77	1.71	1.73	-1.03	-0.22	-0.51	19	154	-19	154	95	161
bs;3	0.41	0.33	-0.17	4.69	0.00	4.33	-2.21	0.02	-1.50	38	231	-39	230	154	269**
bi;4	0.18	0.25	-0.08	2.77	-1.71	1.73	-1.03	0.22	-0.51	19	103	-16	106	95	162
bc;5	0.06	0.21	0.01	1.47	-1.71	-0.03	-0.21	0.11	-0.15	9	33	-3	39	55	92
bi;6	0.18	0.25	0.09	2.55	1.70	-1.70	-0.90	-0.02	-0.16	21	111	-14	118	89	154
bs;7	0.45	0.36	0.22	4.03	0.00	-4.29	-3.58	-0.02	-0.42	45	118	-56	107	108	207
bi;8	0.18	0.25	0.09	2.54	-1.71	-1.70	-0.90	0.02	-0.16	21	59	-14	66	88	153
Extrapolated nominal stress range [N/mm²] : load spectrum $1.00 \cdot \sigma_{max}$	80	20	10	40	15	10	15	5	4						

*   Maximum hot spot stress range for the chord member is 331 N/mm².
** Maximum hot spot stress range for the brace member is 269 N/mm².

Including the partial safety factor and the wall thickness correction results in:

$$S_{r_{h.s.}} = 1.15 \cdot S_{r_{h.s.;\ t>16}} \cdot (t/16)^{0.30} = 1.15 \cdot 331 \cdot (20.8/16)^{0.30} = 412 \text{ N/mm}^2.$$

As summarized in table 44, using the fatigue design curve, the linear damage calculation by "Palmgren-Miner" summation and the load spectrum, the fatigue damage by summation is 0.95 which satisfy the Palmgren-Miners rule.

Table 44.　Check on damage: $D_d = \sum_1^j \dfrac{n_i}{N_i} \leq 1.0$

Load spectrum [factor] $\cdot S_{r_{h.s.;16}}$	n_i	$S_{r_{h.s.;i}}$	$N_i \cdot 10^6$	$\dfrac{n_i}{N_i}$
0.90	1150	371	0.06	0.02
0.70	9850	289	0.12	0.08
0.50	190000	207	0.34	0.56
0.25	799000	103	2.73	0.29
	1000000			0.95

9. SUMMARY AND CONCLUSIONS

9.1 *General conclusions*

Numerical modelling of welded tubular joints

The use of a combination of element type, mesh refinement and integration scheme results into a certain accuracy on analytical results.
Including a weld shape in the FE model can significantly affects the analytical results.
Depending on the problem to be solved (joint flexibility, joint stress concentration factor), a correct choice of these aspects is found to be important.
A standard for modelling of tubular joint flexibility and tubular joint stress concentration factor has been developed.

Numerical idealization of multiplanar lattice tubular structures

Deflection:
The contribution of joint flexibility on the total deflection varies up to approximate 20%. Therefore, when analysing lattice tubular structures the effect of joint flexibility should be taken into account when analysing the deflection.
A multiplication factor to account for the influence of joint flexibility on the deflection when using beam elements only, is proposed.

Fatigue design: load distribution; axial forces
In general, a numerical idealization using beam elements only can be used when analysing axial forces. However, depending on the type of structure and the type of joint, the axial joint flexibility can significantly affect the axial load distribution, which puts restrictions on the use of a numerical idealization using beam elements.

Fatigue design: load distribution; secondary bending moments
For both the chord and brace members, in many cases a large contribution of (secondary) bending moment strains on the total strains is found, which should be taken into account when analysing the hot spot strains for fatigue design.
For practical reasons, the use of a numerical idealization with beam elements only, is preferred above more complicated idealizations like including the joint flexibility by modelling the joints with FE models. In addition, for the brace members, a multiplication factor taking into account the influence of joint behaviour on the load distribution is proposed.

Development of a standard for determining stress concentration factors

Results of tubular joint SCFs are found to be dependent on type of stress, extrapolation region, method of extrapolation and boundary condition used.
Based on numerical results and calibration with experimental results, a standard for determining stress concentration factors have been developed (isolated joints as well as joints located inside a structure), which results in a consistent method of stress concentration factor analysis.

Stress and strain concentration factors

Stress and strain concentration factors have been analysed for T, Y, K, TT, XX and KK joints. A complete range of joint parameters β, γ, τ, φ_{ip} and φ_{op} is considered.
The stress and strain concentration factors are analysed at crown (heel and toe), saddle and inbetween locations of both the chord member and brace member(s).
The load cases on the chord and brace member(s) considered (reference as well as carry-over effects) are axial forces, in-plane bending moments, out-of-plane bending moments and torsion moments.
The results allow the determination of hot spot stresses for uniplanar and multiplanar welded tubular joints under combined loadings.
By means of tables, the importance of the presence of unloaded in-plane and out-of-plane carry-over brace members on stress concentration factors caused by reference loadings and the importance of stress concentration factors caused by in-plane and out-of-plane carry-over loadings is explained.
Numerical models for the determination of stress concentration factors are consequently calibrated with experimental results. In general a good agreement is obtained between numerical and experimental results.

Relationship between stress and strain concentration factors

The results of the parameter study on stress and strain concentration factors show the existence of a large scatter on the conversion factor, and the main influences are discussed. When converting experimentally measured hot spot strains into hot spot stresses, the use of analysed conversion factors instead of a constant value of scf/sncf = 1.2 is proposed.

Basic design fatigue resistance curve for welded multiplanar tubular joints

The obtained fatigue data, based on first through-thickness cracking from tested multiplanar KK joints placed inside lattice girders and having wall thicknesses of 4, 8 and 16 mm, are in good agreement with the fatigue design curve for uniplanar joints for t=16 mm.
Therefore, for multiplanar KK joints with wall thicknesses up to 16 mm, the use of

146

the fatigue design curve for uniplanar tubular joints with a wall thickness of 16 mm is recommended.

9.2   Recommendations for future work

Weld size effect on fatigue behaviour of tubular joints

Hot spot stresses are found to be influenced considerably by the type of weld.
As an example, increasing the length of the weld footprint on the chord member results into a decrease of hot spot stresses for the chord member locations and into an increase of hot spot stresses for the brace member locations.
Correction factors should be established, allowing the designer to take advantage of the size effect on the fatigue behaviour of tubular joints.

Design guidelines for multiplanar tubular joints: thickness effect

The establishment of design guidelines for multiplanar tubular joints requires data on fatigue strength for joints having a wall thickness larger than 16 mm.

Secondary bending moments

Due to the non-uniform stiffness around the perimeter of the brace to chord intersection, secondary bending moments in the members occur, which need to be taken into account in fatigue design. To avoid a complicated numerical idealization, multiplication factors on axial stresses which take into account these secondary bending moments are recommended. Regarding these multiplication factors, limited experimental as well as numerical information is available.

Expert system

The development of an expert system for the design of welded tubular joints subjected to fatigue loading.
Information should be given on:

- *Multiplication factors taking into account secondary bending moments;*
- *SCFs (and hot spot stresses) around the perimeter of the brace to chord intersection;*
- *Fatigue life;*
- *Economical aspects (optimization in design of joints).*

The information on fatigue strength given by international codes like API, IIW, EC3, DEn, AWS, etc. should be incorporated in the expert system.
It is recommended to develop and maintain the expert system at one central place.

SCF data for alternative tubular joints

Up to now, SCF (and fatigue life) data exist mainly for gap joints having no eccentricity.
For frequently used alternative tubular joints however, like overlap joints, joints with gusset plates, stiffened joints, composite steel-concrete joints and cast joints, limited information on SCFs (and fatigue life) exist.

Influence of gradient of stress field near the weld toe on fatigue strength

The gradient of the stress field near the weld toe depends on several aspects like:
- the joint geometry;
- the joint parameters β, γ, τ, φ_{ip} and φ_{op};
- the external diameter of the chord member d_o;
- load case.

It is expected that some scatter on fatigue data results (like thickness effect) is caused by the gradient of the stress field near the weld toe. Using the combination of data on hot spot stress and data on gradient of stress field near the weld toe might be a more accurate method when determining the fatigue strength.

10.   REFERENCES

10.1   *Numerical aspects of the analysis of welded tubular joints*

[N1]	Blaauwendraad, J. Kok, A.W.M.	Elementenmethode voor constructeurs. Part 1 and 2. ISBN 90 10 10440 0 1973. Elsevier Science publishers ltd. Amsterdam, The Netherlands.
[N2]	Bathe, K.J.	Finite element procedures in engineering analysis. ISBN 0-13-317305-4. Prentice-Hall, Inc., Englewood Cliffs, New Jersey, USA.
[N3]	Kok, A.W.M.	Numerical Mechanics. 104041-B18. Delft University of Technology, The Netherlands.
[N4]	NAFEMS	National Agency for Finite Element Methods and Standards. A finite element primer. ISBN 0 903640 17 1. 1986. Published by Department of Trade and Industry, National Engineering Laboratory, East Kilbride, Glasgow G75 0QU, UK.
[N5]	Romeijn, A. Puthli, R.S. Wardenier, J.	"Finite element modelling of multiplanar joints in tubular structures". 2nd INTERNATIONAL OFFSHORE AND POLAR ENGINEERING CONFERENCE. International Society of Offshore and Polar Engineers, P.O. Box 1107 Golden, Colorado, U.S.A. San Francisco, U.S.A., June 1992.

10.2   *Flexibility (stiffness) behaviour of welded tubular joints*

[S1]	Buitrago, J. Healy, B.E. Chang, T.Y.	"Local joint flexibility of tubular joints". INTERNATIONAL OFFSHORE MECHANICS AND ARCTIC ENGINEERING SYMPOSIUM, Glasgow 1993.
[S2]	Chen, B. Hu, Y. Xu, H.	"Theoretical and experimental study on the local flexibility of tubular joints and its effect on the structural analysis of offshore platforms". 5th INTERNATIONAL SYMPOSIUM ON TUBULAR STRUCTURES, p. 543-550.
[S3]	Dumonteil, P.	"In-plane buckling of trusses". Canadian journal civil engineering volume 16. 1989. p. 504-518.
[S4]	Efthymiou, M.	Local rotational stiffness of unstiffened tubular joints. Koninklijke Shell Exploitatie en Produktie Laboratorium, Report RKER.85.199.
[S5]	Fessler, H.	"Experimental determination of stiffness of

tubular joints". 2nd INTERNATIONAL CONFERENCE ON INTEGRITY OF OFFSHORE STRUCTURES, paper 28.

[S6] Fessler, H. "Parametric equations for the flexibility matri-
      Mockford, P.B. ces of single brace tubular joints in offshore
      Webster, J.J. structures". Institute of civil engineers.
                     Part 2.81. 1986.

[S7] Frater, G.S. "Performance of welded rectangular hollow
      Packer, A. structural section trusses". IASS - CSCE INTERNA-
                  TIONAL CONGRESS ON INNOVATIVE LARGE SPAN
                  STRUCTURES, Toronto, Ontario, Canada, July
                  1992.

[S8] Hu, Y. "Structural analysis of offshore platforms con-
      Zhu, J. sidering local joint flexibility". INTERNATIONAL
      Chen, B. OFFSHORE MECHANICS AND ARCTIC ENGINEERING
              SYMPOSIUM. Volume III-B, Materials Enginee-
              ring ASME 1993.

[S9] Jong, H. de The effect of joint rigidity on the buckling be-
                  haviour of a member in compression. Stevinre-
                  port 6-86-6. Delft University of Technology,
                  The Netherlands.

[S10] Nakacho, K. "Stiffness and yield strength of simple V-joint
      Ueda, Y. of offshore structures". 3th INTERNATIONAL OFF-
                SHORE AND POLAR ENGINEERING CONFERENCE.
                p. 175-182.

[S11] Romeijn, A. "Flexibility of uniplanar and multiplanar joints
      Puthli, R.S. made of circular hollow sections".
      Wardenier, J. 1th INTERNATIONAL OFFSHORE AND POLAR ENGINE-
                    ERING CONFERENCE. International Society of
                    Offshore and Polar Engineers, P.O. Box 1107
                    Golden, Colorado, U.S.A. San Francisco,
                    U.S.A., June 1991.

[S12] Packer, J.A. On the use and calibration of design standards
      Davies, G. for SHS joints. The structural engineer. Volu-
                  me 67. No.21/7, november 1989.

[S13] Ueda, Y. An improved joint model and equations for
      Rashed, S.M.H. flexibility of tubular joints. Journal of offshore
      Nakacho, K. mechanics and arctic engineering, Volume
                   112, p. 157-168.

[S14] Underwater Node flexibility and its effect on jacket structu-
      Engineering res. UEG Publication, UR 22.
      Group

10.3   *Fatigue behaviour of welded tubular joints*

[F1]	American Petroleum Institute	Recommended practice for planning, designing and constructing fixed offshore platforms, API RP2A-LRFD, API RP2A-WSD, July 1, 1993.
[F2]	American Welding Society	Structural welding code - Steel. ANSI/AWS D1.1-94, 14th edition, Miami, USA, 1994.
[F3]	Back, J. de Vaessen, G.H.G.	Fatigue behaviour and corrosion fatigue behaviour of offshore structures. Final report ECSC Convention 7210-KB/6/602 (J.7. 1 f/76). Foundation for Materials Research in the Sea. Delft/Apeldoorn, April 1981. The Netherlands.
[F4]	Back, J. de	"Size effect and weld profile effect on fatigue of tubular joints". IIW - AIJ CONFERENCE SAFETY CRITERIA IN DESIGN OF TUBULAR STRUCTURES. February 1987, Tokyo, Japan. p. 331-341.
[F5]	Back, J. de	"Strength of tubular joints". INTERNATIONAL CONFERENCE ON STEEL IN MARINE STRUCTURES. 1981. France.
[F6]	Back, J. de	"The design aspects and fatigue behaviour of tubular joints". INTERNATIONAL CONFERENCE ON STEEL IN MARINE STRUCTURES. 1987. The Netherlands.
[F7]	Berge, S.	"Fatigue strength of tubular joints: some unresolved problems". 1993.
[F8]	Delft, D.R.V. van Noordhoek, C. Da Re, M.L.	"The results of the European fatigue tests on welded tubular joints compared with SCF formulas and design lines". INTERNATIONAL CONFERENCE ON STEEL IN MARINE STRUCTURES. 1987. The Netherlands.
[F9]	Department of Energy	Department of Energy, 1984, Offshore installation guidance on design and construction, UK.
[F10]	Dijkstra, O.D. Back, J. de	"Fatigue strength of tubular T and X joints". INTERNATIONAL CONFERENCE ON STEEL IN MARINE STRUCTURES. 1981. France.
[F11]	Dijkstra, O.D. Puthli, R.S. Snijder, H.H.	"Stress concentration factors in T and KT tubular joints using finite element analysis". Journal of Energy Resources Technology, december, 1988.
[F12]	EC	European Committee for Standardization, Eurocode 3: Design of steel structures - Part 1.1: General rules and rules for buildings. ENV 1993-1-1: 1992E, British Standards Institution, London, UK 1992.

[F13]	Efthymiou, M.	Development of SCF formulae and generalized functions for use in fatigue analysis. Report published by Shell International Petroleum Maatschappij B.V, September 1988. The Netherlands.
[F14]	European Committee for Standardization	Eurocode 3: design of steel structure - Part 1.1: General rules and rules for building. ENV 1993-1-1: 1992E, British Standards Institution of Welding Annual Assembly, The Hague, The Netherlands, 1991.
[F15]	Gibstein, M.B. Moe, M.T.	"Numerical and experimental stress analysis of tubular joints with inclined braces". INTERNATIONAL CONFERENCE ON STEEL IN MARINE STRUCTURES. 1981. France.
[F16]	Gibstein, M.B.	"Parametrical stress analysis of T joints". European Offshore Steels Research Preprints Volume 2. Paper 26. UK Department of Energy. Abington Hall, Cambridge, UK November 1978.
[F17]	Gibstein, M.B.	"Fatigue strength of welded tubular joints tested at Det Norske Veritas Laboratories". INTERNATIONAL CONFERENCE ON STEEL IN MARINE STRUCTURES. 1981. France.
[F18]	Harrison, J.D.	"The significance of welded defects with regard to fatigue behaviour". Fatigue aspects in structural design. ISBN 90-6275-560-7. Delft University Press. The Netherlands.
[F19]	Hirt, M.	"Interaction between research, standardization and design". Fatigue aspects in structural design. ISBN 90-6275-560-7. Delft University Press. The Netherlands.
[F20]	Irvine, N.M.	"Stress analysis of tubular joints: safety and reliability". Fatigue in offshore steel, ICE, London, 1981.
[F21]	Irvine, N.M.	"Comparison of the Performance of modern semi-empirical parametric equations for Tubular Joint Stress Concentration Factors". INTERNATIONAL CONFERENCE ON STEEL IN MARINE STRUCTURES. 1981. France.
[F22]	International Institute of Welding	Subcommission XV-E. Recommended fatigue design procedure for hollow section joints. Part 1 - Hot spot stress method for nodal joints. IIW Doc. XIII-1158-85, XV-582-85, International Institute of Welding Annual Assembly. France, 1985.
[F23]	Koning, C.H.M. de et al	Fatigue behaviour of multiplanar welded hollow section joints and reinforcement measures

152

for repair. TNO-Building and Construction Research, Rijswijk, The Netherlands. Report BI-92-0079/21.4.6394. Delft University of Technology. The Netherlands. Report 6.92.17/A1/1-2.06. 1992. Stevinweg 1, 2628 CN Delft, The Netherlands.

[F24]   Kuang, J.G.
Potvin, A.B.
Leick, R.D.

"Stress concentration in tubular joint". OFFSHORE TECHNOLOGY CONFERENCE (OTC '75). paper 2205. P.O. Box 833868, Richardson. 1975. USA.

[F25]   Kurobane, Y.

Recent developments in the fatigue design rules in Japan. Fatigue aspects in structural design. ISBN 90-6275-560-7. Delft University Press. The Netherlands.

[F26]   Lalani, M.

"Developments in tubular joints technology for offshore structures". 2nd INTERNATIONAL OFFSHORE AND POLAR ENGINEERING CONFERENCE. International Society of Offshore and Polar Engineers, P.O. Box 1107 Golden, Colorado, U.S.A. San Francisco, U.S.A., June 1992.

[F27]   Lalani, M.
Tebbet, I.E.
Choo, B.S.

"Improved fatigue life estimation of tubular joints" 18th OFFSHORE TECHNOLOGY CONFERENCE OTC 5306. Houston, Texas, 1986.

[F28]   Lieurade, H.P.
Gerald, J.

"Results of static tests on ten full scale X joints. INTERNATIONAL CONFERENCE IN STEEL MARINE STRUCTURES. 1981. France.

[F29]   Ma, S.Y.
Tebbet, I.E.

"Estimations of stress concentration factor for fatigue design of welded tubular connections". OFFSHORE TECHNOLOGY CONFERENCE OTC 5666. Houston, Texas, 1986.

[F30]   Marshall, P.W.

Report "Design of welded tubular connections: basis and use of AWS code provisions". 1989. U.S.A. Civil Engineering Consultant. Shell Oil Company, Houston, Texas. U.S.A.

[F31]   Marshall, P.W.

Recent developments in the fatigue design rules in the USA. Fatigue aspects in structural design. ISBN 90-6275-560-7. Delft University Press. The Netherlands.

[F32]   Marshall, P.W.

"Design of welded tubular connections: Basis and use of AWS code provisions" Shell Oil Company, Houston, U.S.A. Developments in Civil Engineering, Volume 37. Elsevier applied science publishers ltd. Amsterdam / London / New York / Tokio.

[F33]   Niemi, E.

"Determination of stresses for fatigue analysis of welded components". Engineering design in welded constructions. Published on behalf of

153

		the International Institute of Welding 1992. ISBN 0 08 041910 0.
[F34]	Niemi, E.	Recommendations concerning stress determination for fatigue analysis of welded components. IIW Doc. XIII-1458-92 XV-797. 1992.
[F35]	Packer, J.A. Henderson, J.E.	Design guide for hollow structural section connections. ISBN 0-88811-076-6, July 1992. Canadian Institute of Steel Construction.
[F36]	Puthli, R.S.	"Geometrical non-linearity in collapse analysis of thick walled shells, with application to tubular steel joints". HERON, TU-Delft, TNO-IBBC, Volume 26, No. 1, 1981.
[F37]	Radenkovic, D.	"Stress analysis in tubular joints". INTERNATIONAL CONFERENCE ON STEEL IN MARINE STRUCTURES. 1981. France.
[F38]	Reynolds, A.G.	"The fatigue performance of tubular joints". An overview of recent work to revise Department of Energy guidance, 4th INTERNATIONAL SYMPOSIUM ON INTEGRITY OF OFFSHORE STRUCTURES, Glasgow, UK, July 1990.
[F39]	Romeijn, A. Puthli, R.S. Wardenier, J. Koning, C.H.M. de Dutta, D.	"Fatigue behaviour of multiplanar welded hollow section joints and reinforcement measures for repair". TNO-Building and Construction Research, Rijswijk, The Netherlands. Report BI-92- 0064/21.4.6394. Delft University of Technology, The Netherlands. Report 6.92.-09/A1/12.08. 1992.
[F40]	Romeijn, A. Panjeh Shahi, E. Puthli, R.S. Wardenier, J.	"Fatigue strength of multiplanar welded, unstiffened hollow section joints and reinforcement measures for in-plane and multiplanar joints in repair". Stevin report 25.6.89.40/A1. Delft University of Technology. The Netherlands.
[F41]	Romeijn, A.	"Stress and strain concentration factors for T joints in circular hollow sections". STW project: DCT 80-1457 "Numerical and Experimental Investigation for the Stress Concentration Factors in Multiplanar Joints". Delft University of Technology. The Netherlands. Report 6.93.35-/12.07. 1993.
[F42]	Romeijn, A.	"Stress and strain concentration factors for TT (180°) joints in circular hollow sections. STW project: DCT 80-1457 "Numerical and Experimental Investigation for the Stress Concentration Factors in Multiplanar Joints". Delft University of Technology. The Netherlands. Report 6.93.37/12.07. 1993.

154

[F43]	Romeijn, A.	"Stress and strain concentration factors for TT(90°) joints in circular hollow sections". STW project: DCT 80-1457 "Numerical and Experimental Investigation for the Stress Concentration Factors in Multiplanar Joints". Delft University of Technology. The Netherlands. Report 6.93.38/12.07. 1993.
[F44]	Romeijn, A.	"Stress and strain concentration factors for TT(135°) joints in circular hollow sections". STW project: DCT 80-1457 "Numerical and Experimental Investigation for the Stress Concentration Factors in Multiplanar Joints". Delft University of Technology. The Netherlands. Report 6.93.40/12.07. 1993.
[F45]	Romeijn, A.	"Stress and strain concentration factors for TT joints in circular hollow sections". STW project: DCT 80-1457 "Numerical and Experimental Investigation for the Stress Concentration Factors in Multiplanar Joints". Delft University of Technology. The Netherlands. Report 6.93.41-/12.07. 1993.
[F46]	Romeijn, A. Puthli, R.S. Wardenier, J.	"Guidelines on the numerical determination of SCFs of Tubular Joints". 5th ISTS INTERNATIONAL SYMPOSIUM ON TUBULAR STRUCTURES, Nottingham, 1993 UK. University of Nottingham, NG7 2RD United Kingdom.
[F47]	Romeijn, A. Puthli, R.S. Koning, C. de Wardenier, J.	"Stress and strain concentration factors of multiplanar joints made of circular hollow sections". 2nd INTERNATIONAL OFFSHORE AND ENGINEERING CONFERENCE. International Society of Offshore and Polar Engineers, P.O. Box 1107 Golden, Colorado, U.S.A. San Francisco, U.S.A., June 1992.
[F48]	Romeijn, A. Puthli, R.S. Koning, C. de Wardenier, J. Dutta, D.	"Fatigue behaviour and influence of repair on multiplanar K joints made of circular hollow sections". 3th INTERNATIONAL OFFSHORE AND ENGINEERING CONFERENCE. International Society of Offshore and Polar Engineers, P.O. Box 1107 Golden, Colorado, U.S.A. Singapore, Japan, June 1993.
[F49]	Romeijn, A. Wardenier, J.	"Stress concentration factors of welded tubular joints". 6th INTERNATIONAL SYMPOSIUM ON TUBULAR STRUCTURES. 1994. Australia.
[F50]	Ship Structure Committee 1993	Report SSC-367 "Fatigue Technology assesment and strategies for fatigue avoidance in Marine Structures". Executive Director Ship Structure Committee. U.S. Coast Guard.

155

		2100 Second Street, S.W. Washington, D.C. 20593-0001.
[F51]	Smedley, P.	"Stress concentration factors for ring-stiffened tubular joints". Lloyd's Register of Shipping, London, UK. 4th INTERNATIONAL SYMPOSIUM TUBULAR STRUCTURES. 1991. The Netherlands.
[F52]	Smedley, P. Fisher, P.	"Stress concentration factors for simple tubular joints". 1th INTERNATIONAL OFFSHORE AND POLAR ENGINEERING CONFERENCE. International Society of Offshore and Polar Engineers, P.O. Box 1107 Golden, Colorado, U.S.A. Edinburgh, Scotland. June 1991.
[F53]	Tebbet, I.E. Lalani, M.	"A new approach to stress concentration factor for tubular joint design". 16th OFFSHORE TECHNOLOGY CONFERENCE, Houston, Texas, 1984.
[F54]	Tebbett, I.E. Ma, S.A.	"Estimations of stress concentration for fatigue design of welded tubular connections". 20th OFFSHORE TECHNOLOGY CONFERENCE, Houston, Texas, 1988.
[F55]	Tolloczko, J.A. Lalani, M.	"The implication of new data on the fatigue life assessment of tubular joints". 20th OFFSHORE TECHNOLOGY CONFERENCE, Houston, Texas, 1988.
[F56]	UEG	Offshore Research: Publication UR 33, 1985. Design of Tubular Joints for Offshore Structures, Volume 2. ISBN 0 86017 231 7. UEG 6 Storey's Gate Westminster London SW1P 3AU. United Kingdom.
[F57]	UKOSRPII	Summary and Task Reports. HMSO, London 1987. United Kingdom.
[F58]	Wardenier, J.	Hollow section joints. Delft University Press. 1982. The Netherlands.
[F59]	Wardenier, J. Kurobane, Y. Packer, J. Dutta, D. Yeomans, N.	Design guide for circular hollow section joints under predominantly static loading. CIDECT. ISBN 3885859750. Köln, Germany, 1991.
[F60]	Wingerde, A.M. van Wardenier, J. Puthli, R.S. Dutta, D. Packer, J.A.	"Design recommendations and commentary regarding the fatigue behaviour of hollow section joints. 2nd INTERNATIONAL OFFSHORE AND POLAR ENGINEERING CONFERENCE. International Offshore and Polar Engineers, P.O. Box 1107 Golden, Colorado, U.S.A. San Francisco, U.S.A., June 1992.
[F61]	Wingerde, A.M. van	The fatigue behaviour of T- and X-joints made of square hollow sections. Heron, 37(2)(1992)

1-180.

[*F62*]   Wordsworth, A.C.   "Stress Concentrations at unstiffened tubular
                     Smedley, G.P.   joints". European Offshore Steels Research
Preprints. Volume 2. Paper   31. UK Department of Energy. Abington Hall, Cambridge, UK 1978.

[*F63*]   Wordsworth, A.C.   Lloyd's Register of Shipping Research Laboratory, UK. Paper "Stress concentration factors at K and KT tubular joints".
CONFERENCE FATIGUE IN OFFSHORE STRUCTURAL STEEL, ICE, London, 1981. UK.

[*F64*]   Wordsworth, A.C.   Lloyd's Register of Shipping Research Laboratory, UK. Paper "Stress Concentration Factors
                     Smedley, P.   at K and KT tubular Joints". CONFERENCE FATIGUE IN OFFSHORE STRUCTURAL STEEL, ICE, London 1981. UK.

[*F65*]   Wordsworth, A.C.   Aspects of the stress concentration factors at tubular joints. 3th INTERNATIONAL OFFSHORE CONFERENCE ON STEEL IN MARINE STRUCTURES. Delft, The Netherlands. 1987.

157

SAMENVATTING

Spannings- en rekconcentratiefactoren van gelaste
ruimtelijke verbindingen van ronde buisprofielen

De toepassing van gelaste ruimtelijke verbindingen van ronde buisprofielen neemt een enorme vlucht.

Een kenmerkende eigenschap van een rechtstreeks gelaste buisverbinding is, dat de stijfheid bij de aansluiting van twee buisprofielen niet uniform is, waardoor bij belasting spanningspieken ontstaan.
Ingeval van op vermoeiing belast zijn - hierbij kan gedacht worden aan constructies zoals bruggen, kranen en booreilanden - is het nodig de grootte van deze spanningspiek te weten. Immers, laatstgenoemde bepaalt in sterke mate de vermoeiingslevensduur van de constructie.

In dit proefschrift worden de resultaten gegeven van een experimenteel en numeriek onderzoek naar spannings- en rekconcentratiefactoren van gelaste verbindingen, samengesteld uit ronde buispofielen.

Voor het experimenteel onderzoek zijn proeven uitgevoerd op ruimtelijke vakwerkliggers, waarbij is gekeken naar de spanningspieken en de vermoeiingslevensduur van KK verbindingen. Op grond van de verkregen resultaten is een S-N lijn bepaald voor gelaste ruimtelijke verbindingen van ronde buisprofielen.

Voor het numeriek onderzoek zijn allereerst numerieke modellen gecalibreerd met experimentele onderzoeksresultaten van buisverbindingen. Tevens is de invloed van de verbindingsstijfheid op o.a. de krachtsverdeling binnen ruimtelijke vakwerkconstructies onderzocht. Vervolgens is met gebruikmaking van de internationaal aanvaarde zogeheten "hot spot" spanningsmethode een consistente manier van spanningsconcentratiefactor bepaling gedefinieerd. Met het verkregen inzicht in numeriek modelleren en de "hot spot" spanningsmethode is voor verschillende soorten verbindingen een parameterstudie naar spannings- en rekconcentratiefactoren uitgevoerd. De onderzochte typen betreffen K, T, X, Y, KK, TT en XX verbindingen met variatie in verbindingsparameters.

Met de experimenteel en numeriek verkregen resultaten is het voor op vermoeiing belaste gelaste ruimtelijke verbindingen van ronde buisprofielen mogelijk geworden een gefundeerd ontwerp uit te voeren.
De resultaten kunnen worden opgenomen in internationale normen zoals bijvoorbeeld Eurocode 3.

CURRICULUM VITAE

Naam	Arie Romeijn
Geboren	21 januari 1958 te Hardinxveld-Giessendam
1976-1980	HTS te Dordrecht (met lof)
1981-1982	Dienstplicht als reserve officier
1982-1985	Werkzaam bij Ingenieursbureau Veth te Dordrecht
1985-1988	Werkzaam bij Mercon Steel Structures b.v. te Gorinchem
1988-1989	Werkzaam aan de TU-Delft, faculteit der Civiele Techniek
1989-1993	Werkzaam aan de TU-Delft, faculteit der Civiele Techniek voor onderzoek van de Stichting voor de Technische Wetenschappen (STW)
1993-1994	Werkzaam bij respectievelijk Nederlandse Spoorwegen te Utrecht, Gemeentewerken Rotterdam en Bouwdienst Rijkswaterstaat te Zoetermeer
1982-1994	Periodiek werkzaam bij Koninklijke Landmacht

1. Voor buisverbindingen bestaat slechts één consistente methode van spanningspiek-bepaling gebaseerd, op primaire spanningen met een extrapolatie in een richting loodrecht op de lasteen voor de randstaaflocaties en in een richting evenwijdig aan de hartlijn van de wandstaaf voor de bijbehorende wandstaaflocaties.

2. Het gegeven dat bij buisverbindingen de scheurvorming veroorzaakt door wisselende belasting voornamelijk optreedt ter plaatse van een lasteenlocatie, betekent dat een spanningspiek ook uitsluitend voor die locatie moet zijn gedefinieerd.

3. Bij buisverbindingen varieert de verhouding tussen spanningsconcentratiefactor en rekconcentratiefactor in die mate dat geen constante waarde kan worden aangehouden, maar een waarde die afhankelijk is van de geometrie, belasting en lasteenlocatie.

4. Ook al vindt extrapolatie van spanningen naar de lasteen plaats, dan nog is er een invloed van de vorm van de las op de grootte van de spanningspiek, welke in de huidige richtlijnen niet opgenomen is.

5. Bij het ontwerp van een op vermoeiing belaste verbinding van ronde buisprofielen moeten niet alleen de spanningspieken op de kruin- en zadellocaties beschouwd worden, maar ook de locaties gelegen tussen de kruin en het zadel.

6. Het samenspel tussen industrie en universiteit is het hart van de economie. De rechterkamer als industrie voedt de linkerkamer en raakt daarmee ontlast. De linkerkamer als onderwijsfabriek en wetenschappelijk bedrijf levert af met een te slappe spierwand, veroorzaakt door bezuinigingen.

7. Met het uithoudingsvermogen en de doelgerichtheid van een marathonloper, slechts omringd door een handvol waterdragers, legt een promovendus zijn traject af in grote eenzaamheid.

8. Beantwoorden aan het door het Vaticaan opgelegde verbod op gebruik van voorbehoedsmiddelen leidt tot scheppingvernietigende groei van de wereldbevolking.

9. Het aantal stellingen bij promoties staat in geen verhouding tot het aantal stellingen in de bouw.

10. Terwille van bedrijfspolitiek bestaat de kans dat een promotor een stelling afkeurt.

11. Oorlog is als voetbal.
    In tenue wordt aangevallen, verdedigd, geschoten en gevlucht met de media, die van succes verzekerd zijn door het strijdtoneel.